SEDIMENTOLOGICAL CONSTRAINTS ON PRECAMBRIAN CRUSTAL EVOLUTION IN NORTHERN NEW MEXICO

by

Kristian Soegaard

Dissertation submitted to the Faculty of the

Virginia Polytechnic Institute and State University

in partial fulfillment of the requirements for the degree of

DOCTOR OF PHILOSOPHY

in

Geology

APPROVED:

K. A. Eriksson

R. K. Bambach

J. F. Read

C. Simpson

A. K. Sinha

August, 1984
Blacksburg, Virginia

SEDIMENTOLOGICAL CONSTRAINTS ON PRECAMBRIAN CRUSTAL EVOLUTION IN NORTHERN NEW MEXICO

by

Kristian Soegaard

(ABSTRACT)

The Precambrian of northern New Mexico is part of an extensive 1,800 to 1,500 m.y. terrane stretching from Colorado through northern New Mexico into central Arizona. Three lithostratigraphic sequences are present in New Mexico. The oldest consists of 1,760 to 1,720 m.y. metamorphosed bimodal volcanic and volcaniclastic rocks to which no basement has been recognized. This juvenile crust developed as a magmatic arc complex and represents an early period of crustal instability. Between 1,755 and 1,700 m.y., the volcanogenic sequence was intruded by voluminous, coeval granodiorites and tonalites which stabilized the early crust. Unconformably overlying the volcano-plutonic terrane is a thick sequence of metamorphosed quartz arenites and subordinate argillites, the Ortega Group, which accumulated on a stable continental shelf. The inner shelf was dominated by tidal processes with subordinate reworking by storm and fair-weather waves. Storm

processes were responsible for deposition on the outer shelf. The Ortega shelf sloped gently to the south and experienced an overall transgression which culminated in drowning of the outer shelf with onlap of black basinal muds from the south. Stable shelf sedimentation resulted from prolonged thermal subsidence following cratonization of the juvenile volcanogenic crust by intrusion of granitoid plutons.

The third lithostratigraphic sequence, the Marquenas Quartzite, consists of polymictic metaconglomerates and texturally-immature metasandstones deposited in a braided-alluvial environment. These terrigeneous sediments were supplied from the south and pebble compositions indicate derivation from the underlying volcanogenic and shelf sequences. The Marquenas Quartzite signifies cannibalization of the underlying magmatic arc and shelf succession in response to deformation of the cratonic margin to the south.

The transition from arc volcanism to stable-shelf sedimentation and subsequent deformation of the craton margin in northern New Mexico has been recognized in central Arizona and southern Wisconsin between 1,800 and 1,630 m.y. This common crustal evolution suggests that a proto-North American craton margin opening to the south existed from central Arizona and northern New Mexico into southern Wisconsin at ca. 1,700 m.y. and was destroyed between 1,660 m.y. and 1,630 m.y.

ACKNOWLEDGMENTS

I wish to thank my principal advisor Kenneth A. Eriksson who not only provided the stimulus for this study and invaluable support during the course of the project, but also became a very close friend. The support, advice and critical reviews of my examining committee (Drs. Richard Bambach, Dave Grey, Fred Read, Carol Simpson, and Krishna Sinha) are gratefully acknowledged. Appreciation is also expressed to Drs. Kent Nielsen and Jeff Grambling for introducing me to the Precambrian terranes in northern New Mexico and for their generous assistance throughout the course of the study. Bud Wobus and Kim Manley provided geological maps for portions of the Tusas mountains. Drs. Leon T. Silver and Sam Bowring are acknowledged for providing unpublished radiometric dates from Precambrian rocks in New Mexico. Appreciation is also expressed to Drs. David Hewitt and Mike Holdaway for assistance in interpreting metamorphic textures in the Study area. Facilities at the Southern Methodist University Fort Burgwin Research Center were used during the summers of 1981-1983. The Picuris Pueblo is acknowledged for providing access to the southern Picuris range. Llyn Sharp and Sharon Chiang generously shared their photographic and drafting expertise, respectively. A very special thanks is expressed to David Guido for his assistance during the 1981 field season.

Financial support was provided by National Science Foundation Grants EAR-8107523 and EAR-8118235, both to Kenneth A. Eriksson.

Finally, I wish to thank my parents Daks and Peter Soegaard for their support and encouragement throughout my academic pursuits.

TABLE OF CONTENTS

Appendix

LIST OF FIGURES

TRANSITION FROM ARC VOLCANISM TO STABLE SHELF AND SUBSEQUENT CONVERGENT-MARGIN SEDIMENTATION IN NORTHERN NEW MEXICO

Abstract

The Precambrian of northern New Mexico is part of an extensive 1,800 to 1,500 m.y. terrane stretching from Colorado through northern New Mexico into central Arizona. Three lithostratigraphic sequences are present in New Mexico. The oldest consists of 1,760 to 1,720 m.y. metamorphosed bimodal volcanic and volcaniclastic rocks to which no basement has been recognized. This juvenile crust developed as a magmatic arc complex and represents an early period of crustal instability. Between 1,755 and 1,700 m.y., the volcanogenic sequence was intruded by voluminous, coeval granodiorites and tonalites which stabilized the early crust. Unconformably overlying the volcano-plutonic terrane is a thick sequence of metamorphosed quartz arenites and subordinate argillites, the Ortega Group, which accumulated on a stable continental shelf. The inner shelf was dominated by tidal processes with subordinate reworking by storm and fair-weather waves. Storm processes were responsible for deposition on the outer shelf. The Ortega shelf sloped gently to the south and experienced an overall transgression which culminated in drowning of the outer shelf with onlap of black basinal muds from the south. Stable shelf sedimentation

resulted from prolonged thermal subsidence following cratonization of the juvenile volcanogenic crust by intrusion of granitoid plutons.

The third lithostratigraphic sequence, the Marquenas Quartzite, consists of polymictic metaconglomerates and texturally-immature metasandstones deposited in a braided-alluvial environment. These terrigeneous sediments were supplied from the south and pebble compositions indicate derivation from the underlying volcanogenic and shelf sequences. The Marquenas Quartzite signifies cannibalization of the underlying magmatic arc and shelf succession in response to deformation of the cratonic margin to the south.

The transition from arc volcanism to stable-shelf sedimentation and subsequent deformation of the craton margin in northern New Mexico has been recognized in central Arizona and southern Wisconsin between 1,800 and 1,630 m.y. This common crustal evolution suggests that a proto-North American craton margin opening to the south existed from central Arizona and northern New Mexico into southern Wisconsin at ca. 1,700 m.y. and was destroyed between 1,660 m.y. and 1,630 m.y.

Introduction

Several Precambrian basement age provinces are present in the United States stretching from the Great Lakes in the northeast to Colorado, New Mexico and Arizona in the southwest (van Schmus and Bickford, 1982). These basement age provinces display a progressive younging to the south away from the Archean Wyoming and Superior

Provinces (Silver et al., 1977). This progressive decrease in age of Precambrian basement away from cratonic nucleii was first recognized be Engel (1963) and spawned ideas of crustal accretion to account for Precambrian crustal evolution in the western part of the United States (Condie, 1982). Although a unifying model for development of the entire Precambrian crust in the southwest may be premature, it is possible to evaluate early crustal evolution in more restricted areas. In this paper the evolution of four separate but related Precambrian basement uplifts in northern New Mexico are investigted. These uplifts are the Tusas mountains, the Picuris and Truchas ranges and the Pecos belt, all of which are situated in the Sangre de Cristo Mountains (Fig. 1). These terranes are located along the southern margin of the 1,800 to 1,700 m.y.-old basement age province of van Schmus and Bickford (1981).

Based on geochemical studies of metavolcanic rocks, several tectonic models have been presented for the Precambrian succession in northern New Mexico. These models include an (unspecified) extensional environment to accommodate bimodal volcanic rocks in the Pecos "Greenstone" Belt (Robertson and Moench, 1979), a magmatic arc for the coeval Taos belt northeast of the Picuris range (Condie and McCrink, 1982) and a back-arc basin for the Pecos belt (Fig. 1; Klich and Robertson, 1983). However, in all studies sedimentary successions and their relationship to the volcanogenic unit have not been emphasized, and the importance of voluminous plutonic rocks disregarded. The objective of this paper is to place further constraints on existing tectonic models for Precambrian crustal evolution in

Figure 1: Distribution of Precambrian rocks in northern New Mexico. Inset illustrates Precambrian rocks in southwestern United States (Compiled from Bingler, 1968; Robertson and Moench, 1979; Condie, 1982).

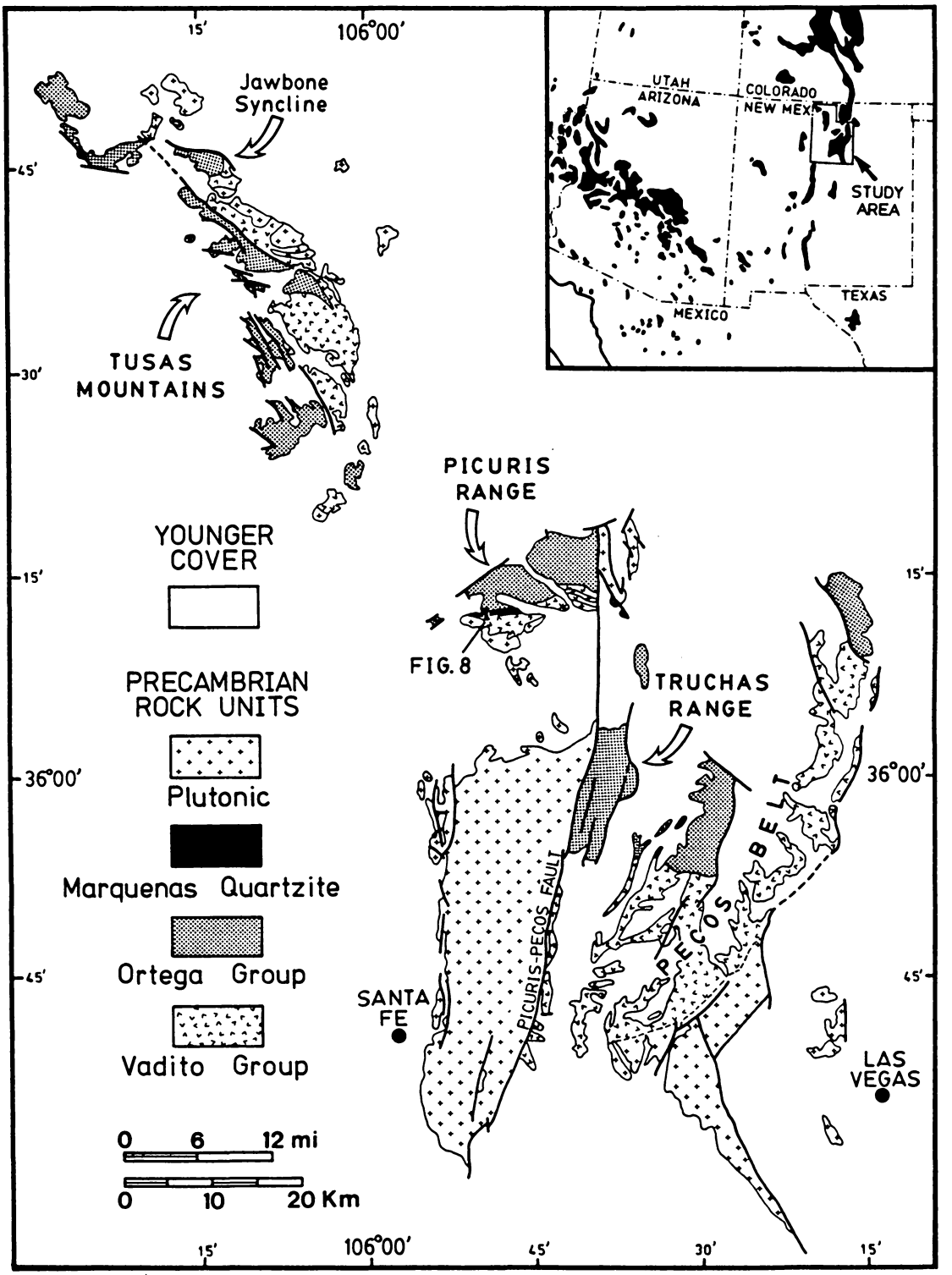
15'
106°00'
Jawbone
Syncline
45'
TUSAS
MOUNTAINS
30'
UTAH
ARIZONA
COLORADO
NEW MEX
STUDY
AREA
TEXAS
MEXICO
PICURIS
RANGE
YOUNGER
COVER
15'
FIG. 8
TRUCHAS
RANGE
PRECAMBRIAN
ROCK UNITS
36°00'
Plutonic
Marquenas Quartzite
Ortega Group
45'
Vadito Group
SANTA
FE
PICURIS-PECOS FAULT
PECOS BELT
LAS
VEGAS
0 6 12 mi
0 10 20 Km
15'
106°00'
45'
30'
15'

northern New Mexico based on a detailed sedimentologic investigation of an extensive quartz arenite-mudstone succession (now quartzite-schist) and immature conglomeratic metasediments in the area.

Stratigraphy

Stratified Precambrian rocks in northern New Mexico are subdivided into three distinct lithostratigraphic units. Two of the three units are laterally extensive and occur across the entire area investigated. These are a heterogeneous succession of amphibolites, felsites, quartzites and minor orthochemical sediments, collectively referred to as the Vadito Group, and a thick sequence of quartzites and subordinate metapelites termed the Ortega Group (Montgomery, 1963). The third lithostratigraphic unit, the Marquenas Quartzite, consists of metaconglomerates and quartzites and is restricted to the southern Picuris range (Nielsen and Scott, 1979; Fig. 1). The entire succession has been subjected to Precambrian ductile polyphase deformation (Nielsen and Scott, 1979; Grambling and Codding, 1982) and lower amphibolite grade metamorphism (Holdaway, 1978; Grambling, 1979a, 1981 and 1984). Table 1 lists the dominant rock types in each of the three lithostratigraphic units.

The Precambrian stratigraphy in northern New Mexico was initially developed by Montgomery (1953) in the southern Picuris range (Fig. 2). However, relationships between rock units in the Picuris range are unclear due to structural complexities discussed above and consequently the stratigraphy has been reinterpreted by later workers in both the

Table 1: Rock types present within Precambrian lithostratigraphic units in northern New Mexico.

MARQUENAS QUARTZITE

- chlorite-epidote-biotite-muscovite quartzite (a)
- polymictic metaconglomerate (a)

ORTEGA GROUP

- calc-silicate (with chlorite, epidote, calcite, garnet, hornblende, muscovite and/or plagioclase) (r)
- slate (c)
- pelitic schist (with muscovite, biotite, quartz, garnet, staurolite, kyanite and/or andalusite) (a)
- black quartzite (with disseminated hematite) (r)
- garnet-biotite quartzite (r)
- metaquartzite (a)

VADITO GROUP

- biotite-quartz-muscovite schist (a)
- sericite schist (a)
- amphibolite (with retrograde chlorite) (c)
- porphyritic metarhyolite (c)
- metaconglomerate (c)
- metaquartzite (c)
- feldspathic metasandstone (c)
- sericitic metagreywacke (c)
- iron formation (r)

(a) = abundant

(c) = common

(r) = rare

Figure 2: Previously proposed stratigraphic relationships for Precambrian stratified rocks in northern New Mexico.

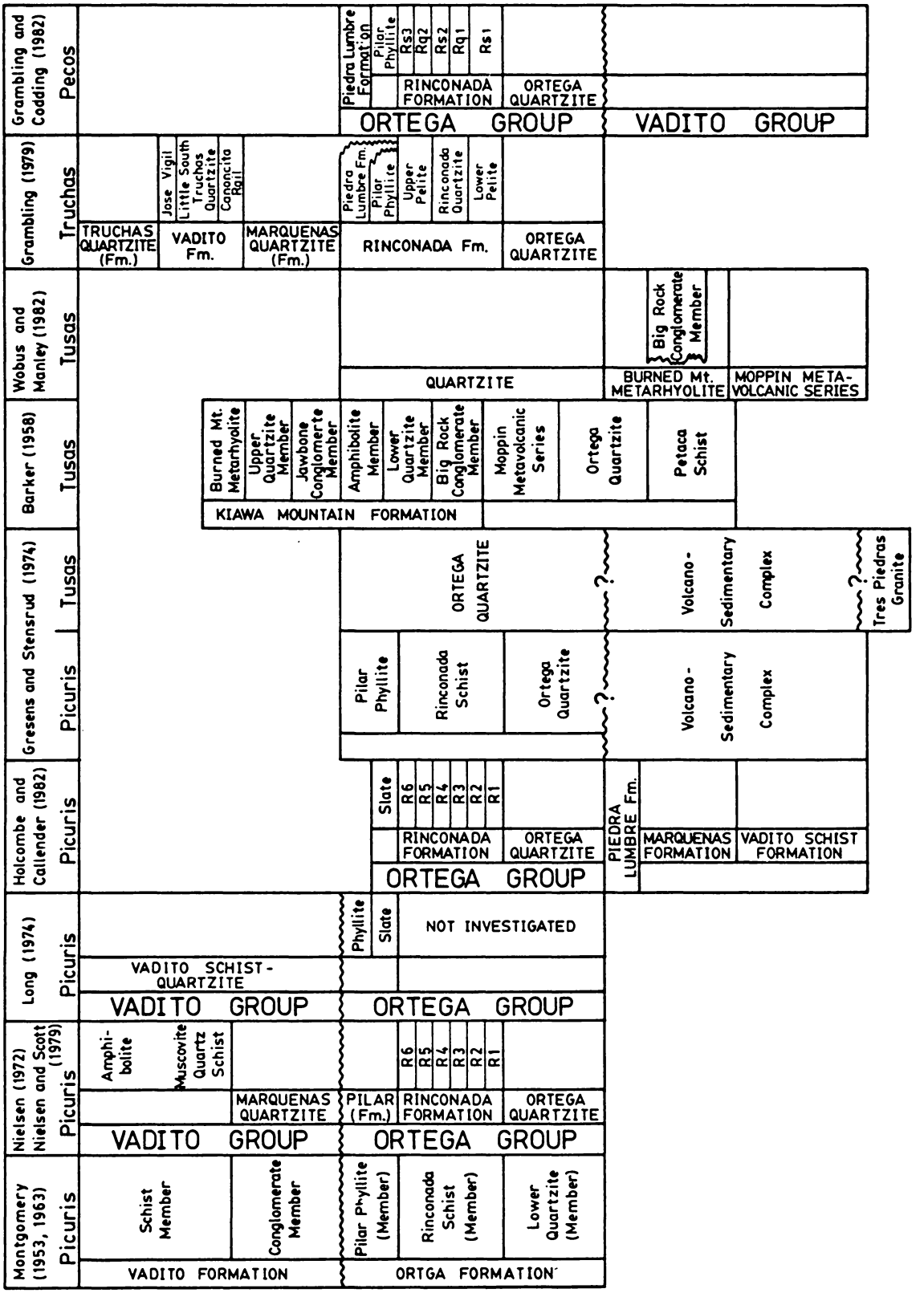
Grambling and Codding (1982) Pecos
Piedra Lumbre Formation
Pilar Phyllite
Rs3
Rq2
Rs2
Rq1
Rs1
RINCONADA FORMATION
ORTEGA QUARTZITE
ORTEGA GROUP
VADITO GROUP
Grambling (1979) Truchas
Jose Vigil
Little South Truchas Quartzite
Canoncita Rgll
Piedra Lumbre Fm.
Pilar Phyllite
Upper Pelite
Rinconada Quartzite
Lower Pelite
TRUCHAS QUARTZITE (Fm.)
VADITO Fm.
MARQUENAS QUARTZITE (Fm.)
RINCONADA Fm.
ORTEGA QUARTZITE
Wobus and Manley (1982) Tusas
Big Rock Conglomerate Member
QUARTZITE
BURNED Mt. METARHYOLITE
MOPPIN META-VOLCANIC SERIES
Barker (1958) Tusas
Burned Mt. Metarhyolite
Upper Quartzite Member
Jawbone Conglomerate Member
Amphibolite Member
Lower Quartzite Member
Big Rock Conglomerate Member
Moppin Metavolcanic Series
Ortega Quartzite
Petaca Schist
KIAWA MOUNTAIN FORMATION
Gresens and Stensrud (1974) Tusas
ORTEGA QUARTZITE
?
Volcano-Sedimentary Complex
?
Tres Piedras Granite
Gresens and Stensrud (1974) Picuris
Pilar Phyllite
Rinconada Schist
Ortega Quartzite
?
Volcano-Sedimentary Complex
Holcombe and Callender (1982) Picuris
Slate
R6
R5
R4
R3
R2
R1
RINCONADA FORMATION
ORTEGA QUARTZITE
ORTEGA GROUP
PIEDRA LUMBRE Fm.
MARQUENAS FORMATION
VADITO SCHIST FORMATION
Long (1974) Picuris
Phyllite
Slate
NOT INVESTIGATED
VADITO SCHIST-QUARTZITE
VADITO GROUP
ORTEGA GROUP
Nielsen (1972) Nielsen and Scott (1979) Picuris
Amphibolite
Muscovite Quartz Schist
R6
R5
R4
R3
R2
R1
MARQUENAS QUARTZITE
PILAR (Fm.)
RINCONADA FORMATION
ORTEGA QUARTZITE
VADITO GROUP
ORTEGA GROUP
Montgomery (1953, 1963) Picuris
Schist Member
Conglomerate Member
Pilar Phyllite (Member)
Rinconada Schist (Member)
Lower Quartzite (Member)
VADITO FORMATION
ORTGA FORMATION

Picuris range and adjacent areas (Fig. 2). To establish the relative age between the Vadito and Ortega Groups, evidence should not be drawn from a single area, as done in the past, but rather from all four outcrop belts containing the two rock units.

In the Jawbone Syncline, Tusas mountains (Fig. 1), a simple relationship exists between the Ortega Quartzite and amphibolites of the Vadito Group (Fig. 3). The older Vadito Group developed between 1,760-1,730 m.y. (U-Pb; Silver, 1984; Fig. 4) and was intruded by the coeval Marquinita Granodiorite with a U-Pb zircon age of 1,755±5 m.y. (L.T. Silver, personal communication 1984; Figs. 3 and 4). Unconformably overlying the amphibolites and granodiorite is a thin discontinous layer of flow-banded metarhyolite with quartz phenocrysts correlative with the Burned Mountain Metarhyolite which has a U-Pb zircon age of 1,700±5 m.y. (L.T. Silver, personal communication 1984). The metarhyolite is unconformably overlain by the Ortega Group (Fig. 3). Abundant cross bedding in the Ortega Group shows that the quartzites young away from the Vadito amphibolites indicating the Ortega Quartzite as the youngest in the sequence. A similar relationship in which the Ortega succession overlies older Vadito Group has been recognized by Burns and Wobus (1983) in the central Tusas mountains and by Grambling and Codding (1982) in the Pecos belt. Although lithostratigraphic correlation in the Vadito Group is not possible between separate basement uplifts, due to the lack of laterally extensive marker beds, the common stratigraphic position below the Ortega Group across the study area, and similar isotopic ages of about 1,760-1,720

Figure 3: Geologic map of the Jawbone Syncline, northern Tusas mountains (Fig. 1). Inset shows proposed relationship between Vadito metavolcanic section, Marquinita Granodiorite, Burned Mountain Metarhyolite and Ortega Quartzite in the nose of the Jawbone Syncline southeast of Jawbone Mountain.

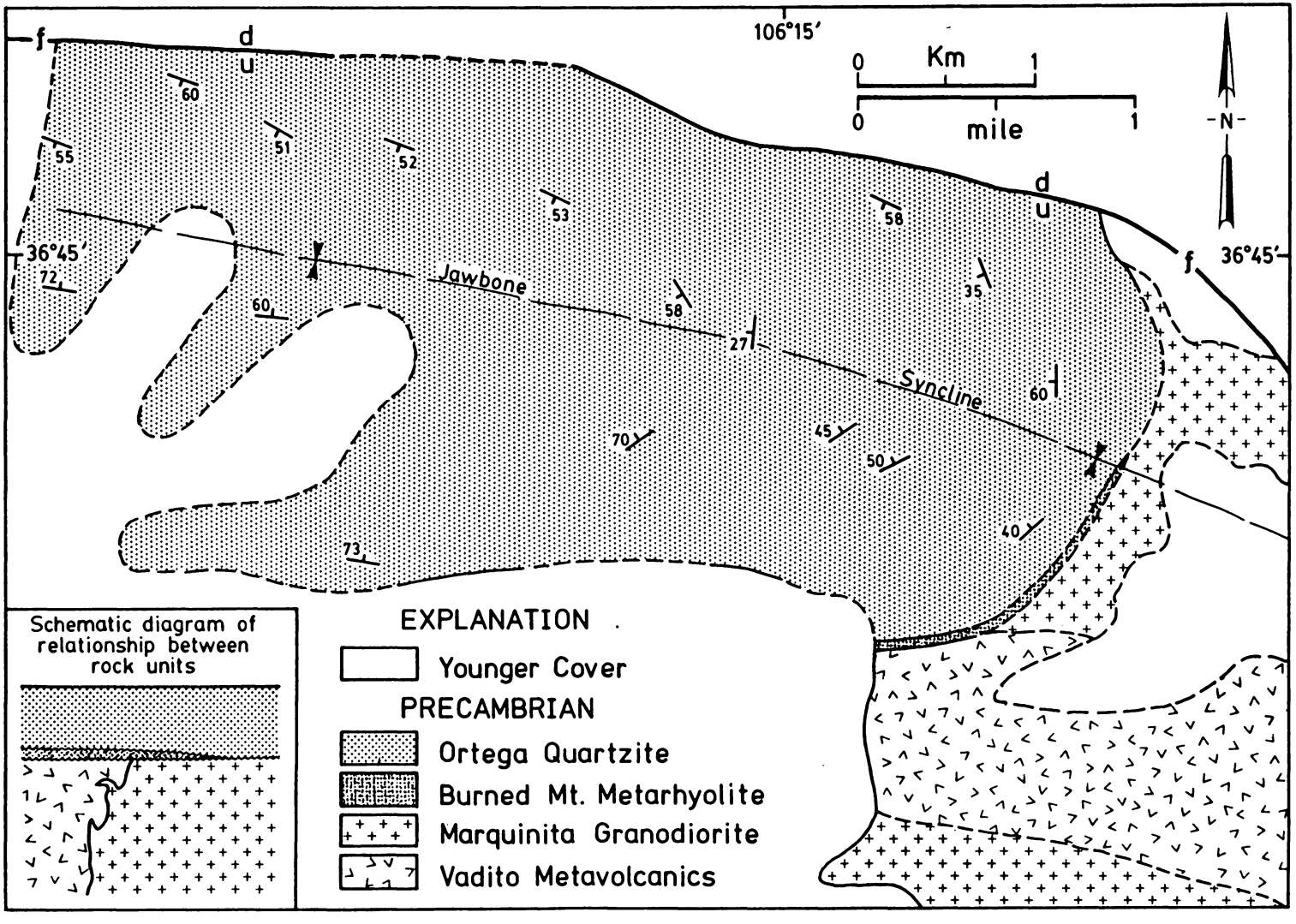
106°15'
0 Km 1
0 mile 1
-N-
f
d
u
60
55
51
52
53
58
35
72
60
58
27
45
70
50
40
73
60
Jawbone
Syncline
36°45'
36°45'
Schematic diagram of relationship between rock units
EXPLANATION
Younger Cover
PRECAMBRIAN
Ortega Quartzite
Burned Mt. Metarhyolite
Marquinita Granodiorite
Vadito Metavolcanics

Figure 4: Summary of isotopic ages for important intrusive and extrusive rocks in northern New Mexico, and the time constraints they place on stratified rocks.

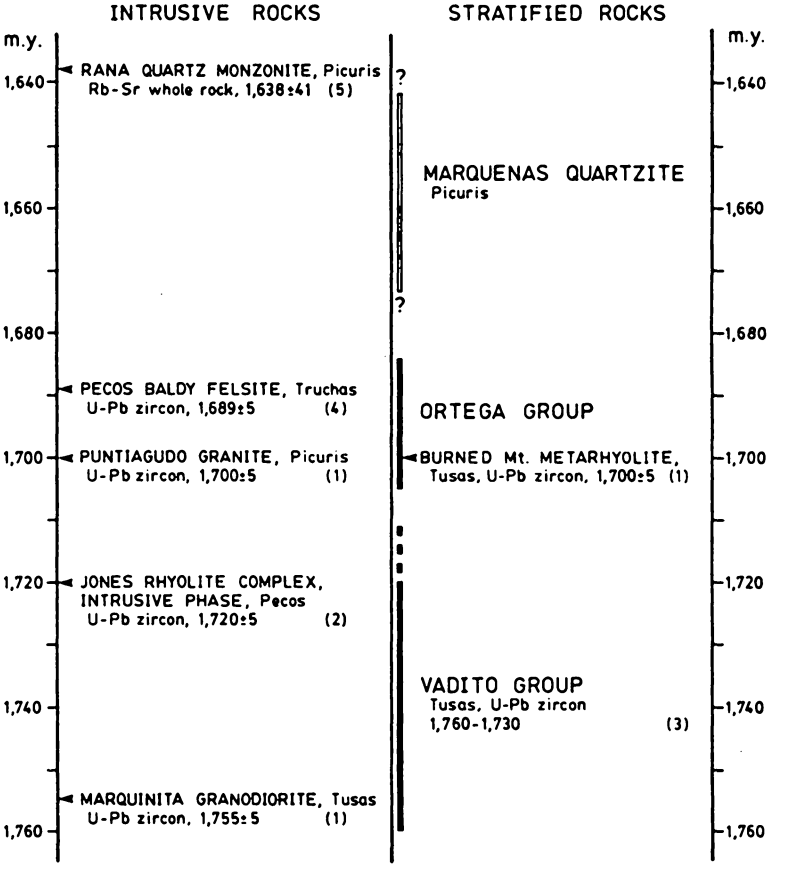

(1) L.T. Silver, pers. comm. (1984)
(2) Bowring and Condie (1982)
(3) Silver (1984)
(4) S.A. Bowring and J.A. Grambling, pers. comm. (1983)
(5) Fullager and Shiver (1973) using revised Rb^{87} decay const. of $1,42 \times 10^{-11} yr^{-1}$

m.y., implies that the unit can be considered as a single lithostratigraphic sequence (Fig. 5).

Nowhere in the Tusas, Picuris or Pecos belts do plutonic rocks intrude the Ortega Group and consequently a minimum age for the quartzite-metapelite succession is not available. However, circumstantial evidence of post-Ortega plutonism may be inferred in the southern Picuris range (Long, 1974; 1976). In the southern Picuris range the Cerro Alto Metadacite was intruded by the Puntiagudo Granite Porphyry. Both pre-date the Rana Quartz Monzonite which has a Rb-Sr whole-rock age of 1,638±41 m.y. (Fullager and Shiver, 1973; Figs. 4 and 5). The Cerro Alto Metadacite was intruded at less than 2 Km depth and the Puntiagudo pluton was emplaced between 1 and 4 Km depth (Long, 1974). Zircons from the Puntiagudo Granite have yielded a U-Pb age of 1,700±5 m.y. (L.T. Silver, personal communication 1984). This granite is thus coeval with the 1,700±5 m.y. Burned Mountain Metarhyolite in the Tusas mountains and must predate deposition of the Ortega Group (Fig. 4). The Rana Quartz Monzonite, which intrudes the Puntiagudo Granite Porphyry, was emplaced at depths of 3 to 6 Km (Long, 1974). Deposition of the 1 to 2 Km of Ortega Group subsequent to intrusion of the Puntiagudo Granite but prior to emplacement of the Rana Quartz Monzonite therefore could account for the increase in depth of emplacement with time observed by Long (1974) in the southern Picuris Range. If this relationship is correct a minimum age of 1,638 m.y. is placed on the Ortega Group by the Rana Quartz Monzonite (Fig. 4). In the southern Truchas range, the Ortega Group was

Figure 5: Genetic stratigraphic cross section of Ortega Group adopted for lithostratigraphic correlation between separate outcrop belts. Relationship between Ortega Group and underlying volcano-plutonic basement complex is illustrated. Position of Truchas range and Pecos belt relative to Picuris range corrected for right-lateral strike-slip displacement along Picuris-Pecos Fault according to Montgommery (1963). Horizontal and vertical scales are approximate.

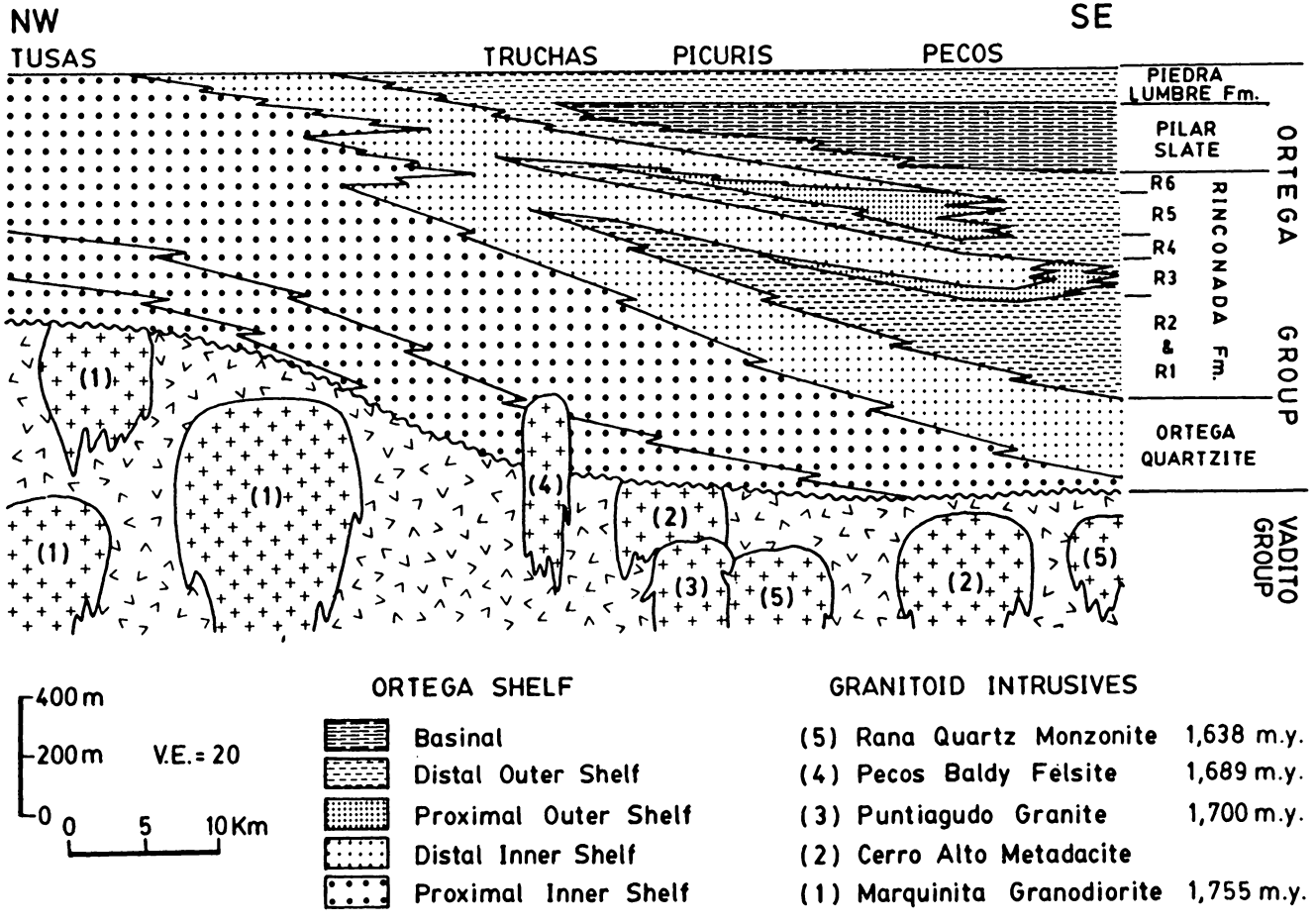
NW
SE
TUSAS
TRUCHAS
PICURIS
PECOS
PIEDRA LUMBRE Fm.
PILAR SLATE
R6
R5
R4
R3
R2 & R1
RINCONADA Fm.
ORTEGA GROUP
ORTEGA QUARTZITE
VADITO GROUP
(1)
(2)
(3)
(4)
(5)
400 m
200 m
V.E. = 20
0
0 5 10 Km
ORTEGA SHELF
Basinal
Distal Outer Shelf
Proximal Outer Shelf
Distal Inner Shelf
Proximal Inner Shelf
GRANITOID INTRUSIVES
(5) Rana Quartz Monzonite 1,638 m.y.
(4) Pecos Baldy Felsite 1,689 m.y.
(3) Puntiagudo Granite 1,700 m.y.
(2) Cerro Alto Metadacite
(1) Marquinita Granodiorite 1,755 m.y.

intruded by the Pecos Baldy Felsite (Grambling, 1979a). The felsite occurs as a small stock and has a provisional U-Pb zircon date of 1,689±5 m.y. (S.A. Bowring and J.A. Grambling, personal communication 1984). Plutonic rocks thus bracket the age of the Ortega Group between 1,705 and 1,684 m.y. indicating that the thick quartzite-metapelite succession was deposited in less than 21 million years and possibly in an even shorter time period (Fig. 4).

Vadito Volcanogenic Unit

Information from previous studies on the Vadito Group are utilized here to resolve the earliest history of the crust in northern New Mexico. Well-preserved pillows lavas, pillow breccias and relict vesicles in amphibolites in the Pecos belt (Robertson, 1984) and Picuris range (Long, 1974) imply that protoliths to the amphibolites were mafic volcanic rocks. Megabreccias containing large blocks of metavolcanics and metasediments within a structureless siltstone in association with metacherts and metabasalts in the southern Picuris range are considered to be analogous to melanges within Paleozoic subduction complexes (Shore and Duncan, 1983). Felsites dominate the upper Vadito stratigraphy. Quartz and feldspar phenocrysts, flow banding and relict pyroclastic fragments support a volcanic origin for the felsites (Barker, 1958; Gresens and Stensrud, 1974; Robertson and Moench, 1979). Felsic volcanic rocks comprise 10 to 20 percent of the total volcanic pile in the Pecos belt and occur in several central volcanic complexes cored by subvolcanic intrusives (Robertson and Moench, 1979). Gresens and

Stensrud (1974) predict a greater proportion of felsic volcanic rocks in the Tusas and Picuris mountains than envisaged previously. They argue that metarhyolites have been mistaken for pelitic metasediments due to hydrogen metasomatic alteration of rhyolites to quartz muscovite schists. However, subordinate polymictic metaconglomerates, metamorphosed feldspathic arenites containing ab turbidite divisions (cf. Bouma, 1962), and orthochemical sediments in the Tusas and southern Picuris mountains imply that sedimentation was active during deposition of the Vadito Group.

No field evidence exists of pre-1,900 m.y.-old basement below the volcanogenic unit. Although Gresens and Stensrud (1974) proposed that the Tres Piedras granite in the Tusas mountains may be unconformably overlain by a volcanosedimentary complex (Fig. 2), Wobus and Manley (1983) interpret the granites as younger intrusives on the basis of field relationships. Isotopic evidence supports the field observations. A Sr^{87}/Sr^{86} initial ratio of 0.7012 for the Rana Quartz Monzonite in the southern Picuris range indicates a mantle derivation for the original magma with no contamination by significantly-older crust (Fullager and Shiver, 1973). Nd^{143}/Nd^{144} ratios for a wide range of volcanic and plutonic rocks across Colorado and northern New Mexico coincide with Nd mantle growth curve at 1,800 m.y., likewise implying that no significantly older basement contaminated the volcanic and plutonic rocks during their emplacement (DePaolo, 1981). Nd-Sm data for the volcanic and plutonic rocks define a single isochron suggesting that the early volcanogenic crust developed rapidly over a large area around

1,800±100 m.y. (DePaolo, 1981). Lead isotope data from New Mexico, Arizona, southern Colorado and Utah substantiate the Nd evidence, suggesting that juvenile volcanic crust developed across the entire southwestern U.S.A. around 1,750 m.y. (Stacey and Hedlund, 1983).

The bimodal volcanic suite accumulated in an extensional environment (Robertson and Moench, 1979). Absence of significantly-older basement below the Vadito Group and lack of extrabasinal detritus refutes incipient rifting of significantly older sialic crust. A back-arc setting has been proposed for the volcanic succession in the Pecos belt and satisfies geochemical constraints for the volcanogenic succession in the Tusas, Picuris and Pecos belts (Klich and Robertson, 1983). Bimodal volcanic suites also comprise the oldest stratified units in southern Colorado and are likewise interpreted as back-arc volcanics (Condie and Nuter, 1981; Bickford and Boardman, in review). However, the absence of orogenic volcanic suites in New Mexico and southern Colorado presents an unrealistic case in which extensive back-arc volcanism occurred with no indiction of an actual arc. Possible evidence of an arc assemblage has been proposed by Condie and McCrink (1982) in the Taos range, immediately north of the Picuris range. Here 1,750 m.y. old bimodal metavolcanic rocks display calcalkaline affinities. Amphibolites have similar Ti, Zr, Cr, Ni and REE contents to immature arc basalts whereas felsic metavolcanic rocks resemble rhyolites from mature arc systems based on immobile-element contents (Condie and McCrink, 1982). Robertson (1984) has equated subalkaline, mainly low K-tholeiites from the Pecos belt with modern arc tholeiites and calc

alkaline basalts, further supporting an orogenic origin for the volcanic suite.

Regardless of the tectonic setting in which the Vadito Group developed, this early sequence of volcanic and volcaniclastic rocks signifies a period of crustal instability and represents the juvenile lithosphere in northern New Mexico.

Ortega Group

Unconformably overlying the Vadito Group in the Tusas and Pecos belts, and present in the Picuris and Truchas ranges is a thick sequence of quartzites and metapelites constituting the Ortega Group. Apart from rare amphibolites in the central Truchas range and Pecos belt, which have bulk composition similar to tholeiitic basalts (Grambling 1979b), a sedimentary origin is invoked for the Ortega Group by virtue of the abundant primary sedimentary structures present.

In the Jawbone Syncline, the Ortega Group is more than 850 m thick and contains horizons of mature, quartz-pebble conglomerates in the lower third of the succession. To the south, in the Picuris, Truchas and Pecos belts, the Ortega Group is in excess of 1000 m thick and exhibits a general decrease in grain size upwards through the section from quartz arenite to mudstone (Fig. 5). In the Picuris range, Nielsen (1972) subdivided the Ortega Group into the Ortega Quartzite, Rinconada Formation and Pilar Formation (Fig. 5). In the Pecos belt a similar stratigraphy is recognized (Grambling and Codding, 1982; Fig. 2).

A detailed sedimentary facies analysis has shown that the entire Ortega Group accumulated on a broad continental shelf on which tide, storm and wave processes operated (Soegaard and Eriksson, submitted). The shelf is subdivided into inner- and outer-shelf environments based on inferred depositional processes active within each zone (Fig. 5). The inner shelf facies are characterized by quartz arenites structured by large- and medium-scale tabular-planar cross beds. Reactivation surfaces (Fig. 6) and mudstone drapes, herringbone cross stratification and bimodal-bipolar paleocurrent trends imply that tidal processes dominated on the inner shelf (cf. Klein, 1970b). Symmetrical ripples preserved on upper surfaces of tidal sandstone beds indicate that subordinate fair-weather wave processes were active on the distal inner shelf during slack periods within the tidal rhythm. On the proximal inner shelf in the Tusas mountains (Fig. 5), a significant storm overprint is indicated by winnowed pebble lags at the top of tabular, tidal sandstone bodies (cf. Anderton, 1976). A storm overprint is also recognized on the distal inner shelf and is represented by tabular, horizontally-stratified and lenticular, trough cross-bedded sandstone bodies deposited by offshore-directed gradient currents (cf. Aigner and Reineck, 1982). The outer shelf was dominated by storm processes with no evidence of tides. The outer shelf facies are characterized by upward-thickening sequences of planar-laminated quartz arenites in 1 to 11 m-thick genetic packages. Proximal outer-shelf packages consist of single or amalgamated, 2 to 55 cm-thick depositional units with frequent wave-reworked tops (Fig. 7). The uppermost sandstones in the

Figure 6: Reactivation surface (arrow) in medium-scale, tabular-planar cross beds. R3 Member, Rinconada Formation, southern Picuris range.

Figure 7: Planar-laminated siltstone deposited by storm-generated gradient currents on proximal outer shelf. Subsequent scouring by oscillatory wave currents and draping by form-concordant, parallel-laminated siltstone. Lower R3 Member, Rinconada Formation, Pecos belt.

sequences often contain shallow, scour channels occupied by small-scale, trough cross beds (cf. Anderton, 1976). Distal outer-shelf sediments are characterized by discrete depositional units and an absence of wave ripples. The planar-laminated sandstones resulted from suspension transport onto the outer shelf by storm-induced gradient currents (cf. Reineck and Singh, 1972). The upward-thickening genetic packages, coupled with the distribution of wave ripples, indicate that storm sands were deposited on progradational outer-shelf sand lobes both above and below storm wave base. The absence of storm-generated turbidites below storm wave base reflects very gentle gradients on the Ortega shelf.

The distribution of sedimentary facies coupled with paleocurrent data from storm-generated, offshore-directed trough cross beds indicate that the Ortega shelf sloped to the south. The overall Ortega succession is transgressive culminating in drowning of the outer shelf with onlap of black basinal mudstones from the south (Fig. 5).

Detrital zircons near the base of the Ortega Group in the Tusas mountains have yielded a U-Pb zircon age of ca. 1,755 m.y. suggesting that the source to the Ortega Group was Marquinita-age granodiorites intrusive into the Vadito Group (Fig. 4; Silver, 1984). This source, according to paleocurrent data and facies patterns lay to the north of the present outcrop belt of the Ortega Group (Soegaard and Eriksson, submitted), although sediment dispersal by tidal currents on the inner shelf could have transported sand considerable distances along the strike of the shelf.

Phanerozoic analogues of thick transgressive quartz arenite sequences have been described by Banks (1973), Anderton (1976), Hobday and Tankard (1978) and Hiscott (1982). All successions accumulated within tectonically stable, shallow marine environments. Thick quartz arenite successions are also characteristic of the latest Archean and Proterozoic where they developed following cratonization (see for example Button, 1973; Hoffman et al., 1974; von Brunn and Hobday, 1979; Trevena, 1979; Eriksson, et al., 1981; Tankard et al., 1982; Dott, 1983). It follows, therefore, that the thick Ortega quartz arenite sequence accumulated within a tectonically stable environment analogous to that of shelf sediments along Holocene passive continental margins.

Transition from Vadito to Ortega Group

The transition from back-arc and/or arc volcanism in the Vadito Group to shelf sedimentation for the Ortega Group signifies a change from a tectonically active environment to prolonged stable conditions. Development of thick, mature shelf sediments above an active arc sequence contrasts with passive margin sequences in the Phanerozoic which develop subsequent to rifting of stable continental crust (Bally, 1981). Two criteria are fundamental to developing passive-margin sequences:

(1) A stable tectonic environment with no significant volcanic or seismic activity (Bally, 1981); and,

(2) Significant subsidence to accommodate the thick sedimentary prism (Beaumont et al., 1982; Bond and Kominz, 1984).

Beaumont et al. (1982) and Bond and Kominz (1984) have shown that in addition to gravity induced passive subsidence caused by eustatic sea level rise and sediment loading (cf. Vail et al., 1977; Pittman, 1978), thermal contraction of the crust is the active driving mechanism mechanism in passive margin subsidence. During initial thermal doming and rifting, heating of continental crust causes reduction in density of lithosphere by thermal expansion and phase transitions with resulting isostatic uplift (Bott, 1979). This thermally elevated crust is subjected to substantial erosion and has a high subsidence potential. As the crust cools with time, deposition of thick sedimentary sequences takes place in response to thermal contraction of the lithosphere (Sleep, 1976, and Beaumont et al., 1982).

Prior to deposition of the Ortega shelf sediments in northern New Mexico, the Vadito volcanogenic unit was intruded extensively by granitoid plutons between 1,755 and 1,700 m.y., including the Cerro Alto Metadacite and the Puntiagudo Quartz Monzonite (Fig. 5). Intrusion by these granitoid bodies served to cratonize and heat the juvenile volcanogenic crust, causing reduction in density of the early lithosphere by thermal expansion and subsequent isostatic uplift. Uplift caused erosion and possible dissection of plutons, such as the Marquinita Granodiorite, and resulted in development of a regional unconformity. Crustal thinning by erosion, thermal bouyancy and stable cratonized lithosphere provided a crust with high subsidence potential.

As cooling of the Vadito volcano-plutonic complex proceeded, sustained subsidence promoted deposition of the thick, stable-shelf sediments of the Ortega Group.

According to geochronologic constraints on the Ortega Group, the shelf succession was deposited within a maximum of 21 m.y. years. The drift phase along Phanerozoic trailing continental margins generally lasts considerably longer. The early Paleozoic passive margin along western North America lasted from 600-650 m.y. (Bond and Kominz, 1984) until its destruction by the Antler Orogeny at ca. 380 m.y. (Lanphere et al., 1968; Burchfiel and Davis, 1975), thus spanning more than 200 m.y. The passive margin along the present east coast of the United States has lasted 180 m.y. (Bally, 1982). In the Early-Proterozoic Coronation Geosyncline in northern Canada, however, the passive-margin phase lasted less than 15 m.y. and a change in polarity of plate motion, from divergence to convergence, took place over less than 20 m.y. (Hoffman and Bowring, 1984). Bickle (1978) argues that plate tectonic processes in the early Precambrian operated significantly faster than at present, and that passive margins would not have resisted collision for more than 40 m.y. Although the absolute age of the Ortega Group needs verification by further high-resolution geochronology, the apparent short life span of the Ortega shelf is consistent with shelf sequences of similar age in other parts of the world.

Marquenas Quartzite

Stratigraphic Position of Marquenas Quartzite

The third lithostratigraphic sequence in northern New Mexico is the Marquenas Quartzite (Montgomery, 1963; Figs. 1 and 2) which consists of boulder-size, polymictic metaconglomerates and texturally immature metasandstones. Unlike the Vadito and Ortega Groups which have a regional distribution, the Marquenas Quartzite is confined to the southern Picuris range where it is sandwiched between the Ortega shelf sediments to the north and the Vadito volcanogenic sequence to the south (Fig. 8).

Cross bedding in the Ortega Group indicates stratigraphic younging to the south (Fig. 8). The Vadito Group, in contrast, contains no conclusive stratigraphic indicators in the southern Picuris range. Montgomery (1953 and 1963) did not identify younging directions in the Marquenas Quartzite and therefore assumed a simple stratigraphy with the Ortega Group at the base overlain by the Marquenas Quartzite and Vadito Group (Fig. 2). This stratigraphic interpretation was supported by Nielsen (1972), Long (1974) and Nielsen and Scott (1979), again with no stratigraphic indicators in the Marquenas Quartzite or Vadito Group (Fig. 2). As shown earlier, however, the Vadito Group is the oldest unit in the Precambrian section in northern New Mexico. In addition, trough cross bedding in the southern half of the Marquenas Quartzite indicates younging to the north (Fig. 9),

Figure 8: Cross section from the southern Picuris range illustrating relationship between the Marquenas Quartzite and Ortega and Vadito Groups.

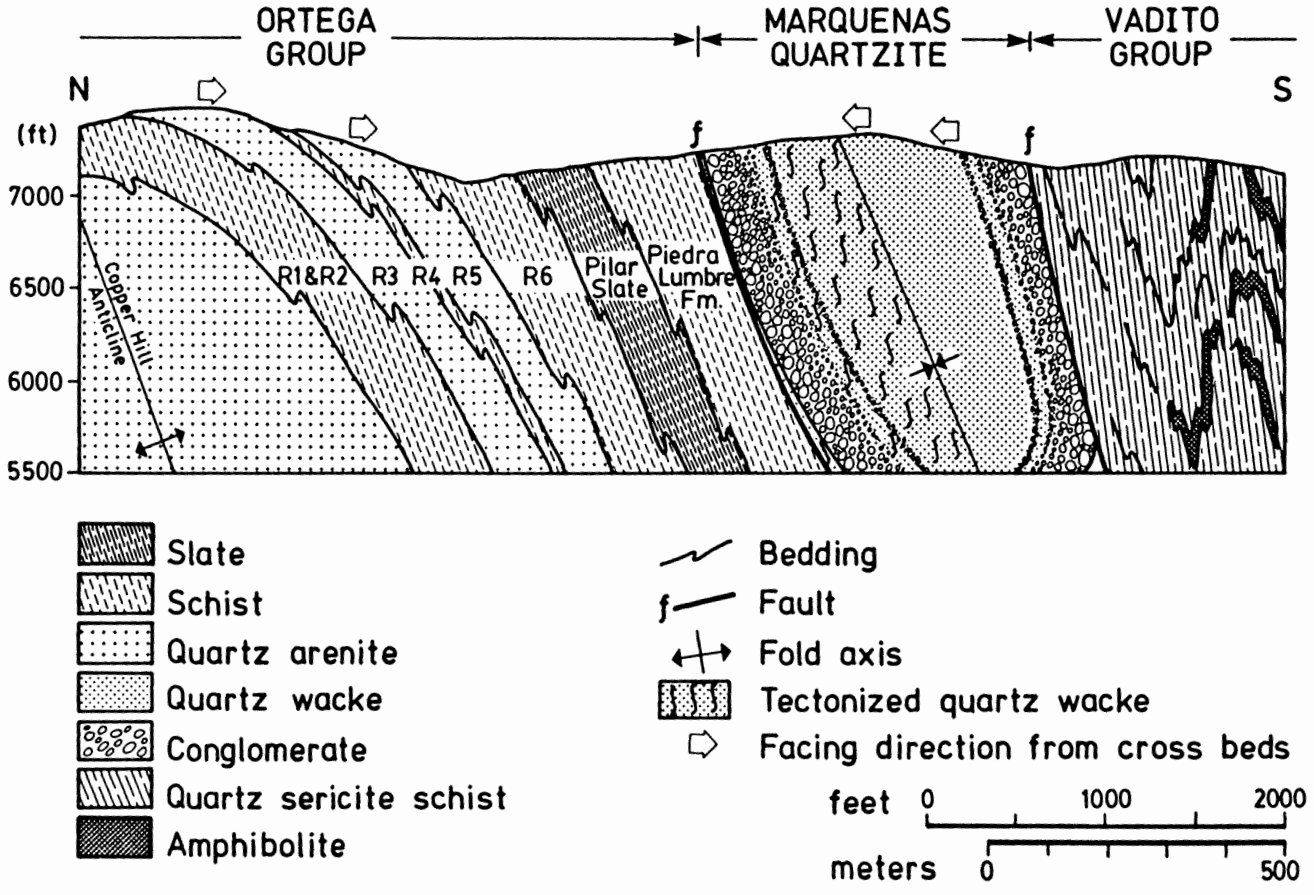
ORTEGA GROUP
MARQUENAS QUARTZITE
VADITO GROUP
N
S
(ft)
7000
6500
6000
5500
R1&R2
R3
R4
R5
R6
Pilar Slate
Piedra Lumbre Fm.
Copper Hill Anticline
f
f
Slate
Schist
Quartz arenite
Quartz wacke
Conglomerate
Quartz sericite schist
Amphibolite
Bedding
Fault
Fold axis
Tectonized quartz wacke
Facing direction from cross beds
feet 0 1000 2000
meters 0 500

Figure 9: Trough cross bed indicating younging to the north to the left (north; see Fig. 1), overlain by planar-laminated sandstone in upper sandstone lithofacies in the Marquenas Quartzite, southern Picuris range.

opposite to that in the Ortega Group and thus negating a simple stratigraphy in the southern Picuris range (Fig. 8). Holcombe and Callender (1982) proposed a fault north of the Marquenas Quartzite between the Piedra Lumbre Formation and the Pilar Slate in the Ortega Group based on spatial variation in structural fabric across the boundary separating the two units. They placed the Vadito Group at the base of the section, overlain by the Marquenas Quartzite and Piedra Lumbre Formation with the remaining Ortega Group at the top of the succession (Fig. 2). However, the Piedra Lumbre Formation consistently occurs at the top of the Ortega Group in both the Picuris range (Montgomery, 1963, and Nielsen, 1972) and Pecos belt (Grambling and Codding, 1982) and sedimentological characteristics of the Piedra Lumbre Formation are comparable with the upper Ortega Group but different from both the Marquenas Quartzite and lower Ortega Group. The original Ortega Group stratigraphy of Montgomery (1963) therefore is retained here.

Conglomerates in the Marquenas Quartzite exhibit perfect symmetry across the outcrop belt suggesting that the unit may be duplicated by isoclinal folding with a fold axial surface dipping to the south (Fig. 8). In the northern half of the Marquenas Quartzite, cross beds are not present as the metasandstones are highly tectonized and have undergone pressure solution which has obliterated primary depositional structures (Fig. 10). Cleavage-to-bedding relationships likewise are not clear due to transposition of bedding, and can therefore not be used to substantiate the synclinal structure. To

Figure 10: Tectonized sandstone in northern half of Marquenas Quarztite. Simple-shear rotation of laminated sandstone results in cross-bedded appearance yielding a pressure-solution fabric.

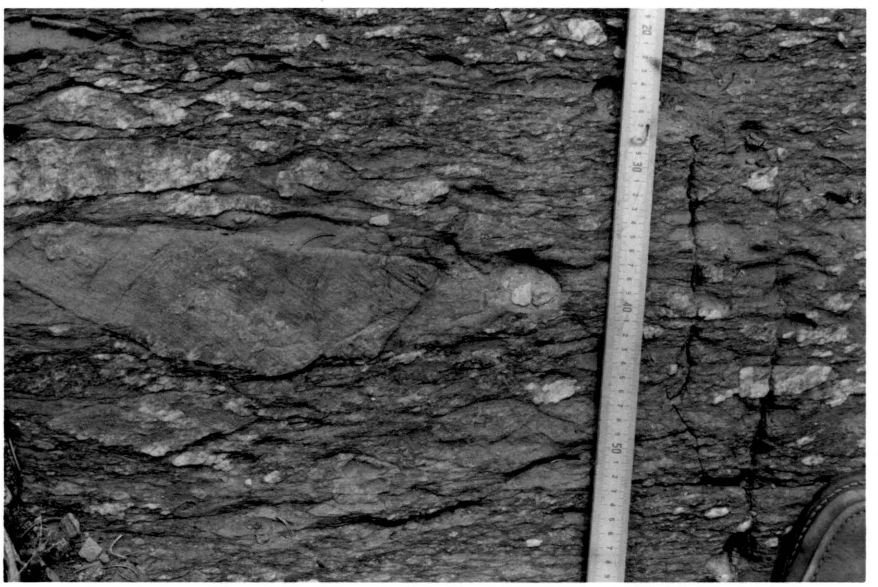

resolve the stratigraphic controversy of the Marquenas Quartzite, a detailed examination of the sedimentological attributes of the succession has been undertaken.

Sedimentology of the Marquenas Quartzite

The Marquenas Quartzite is 330 m thick and consists of two major lithofacies; a conglomeratic lithofacies occupies the lower 100 m and texturally immature sandstones comprise the upper 230 m of the succession (Fig. 11). A detailed facies analysis has shown that the Marquenas Quartzite was deposited on an alluvial plain by a variety of braided-alluvial processes.

The conglomeratic lithofacies is upward fining with boulder-size clasts attaining more than 35 cm in diameter. The conglomerate is very-poorly sorted and generally is clast supported with a sandstone matrix. Bedding is discernable where thin, discontinous sandstone layers are present (Figs. 11a and 12). These sandstone lenses are either planar laminated or have rare wedge-planar cross bedding (Fig. 12). The lithologies and primary sedimentary structures in the conglomeratic lithofacies are comparable to proximal alluvial-plain deposits such as the Holocene Scott River in Alaska (cf. Miall, 1977). Sedimentation occurred during waning flood stages and was characterized by development of longitudinal, conglomeratic bar deposits which occasionally were capped by planar-laminated sandstones. During late stages in flood cycles, bar-edge accretion resulted in the wedge-planar, cross-bedded sandstones.

Figure 11: Measured stratigraphic column through Marquenas braided-alluvial facies in southern Picuris range (see text for explanation).

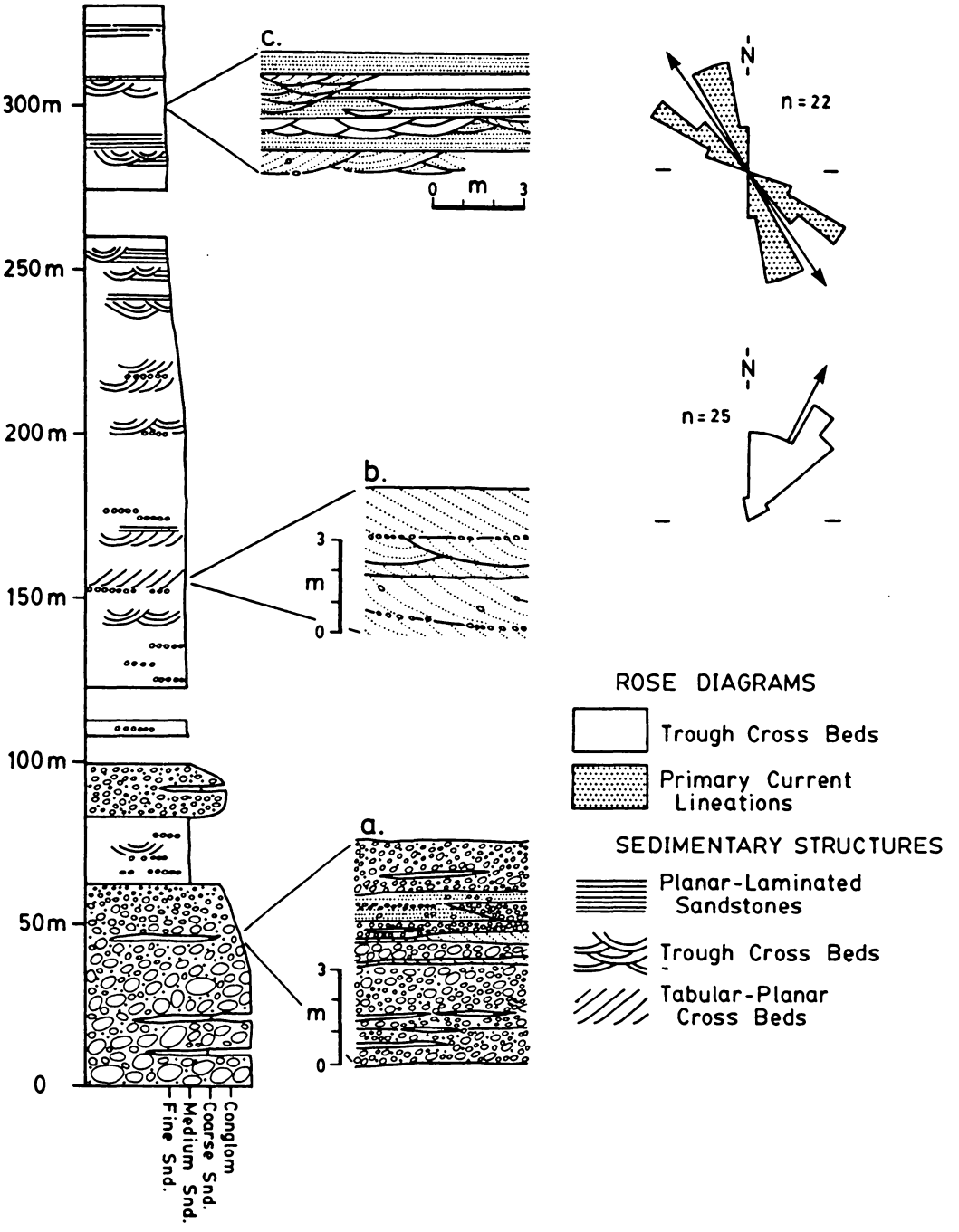
300m
250m
200m
150m
100m
50m
0
c.
0 m 3
b.
3
m
0
a.
3
m
0
Fine Snd.
Medium Snd.
Coarse Snd.
Conglom
N
n = 22
N
n = 25
ROSE DIAGRAMS
Trough Cross Beds
Primary Current Lineations
SEDIMENTARY STRUCTURES
Planar-Laminated Sandstones
Trough Cross Beds
Tabular-Planar Cross Beds

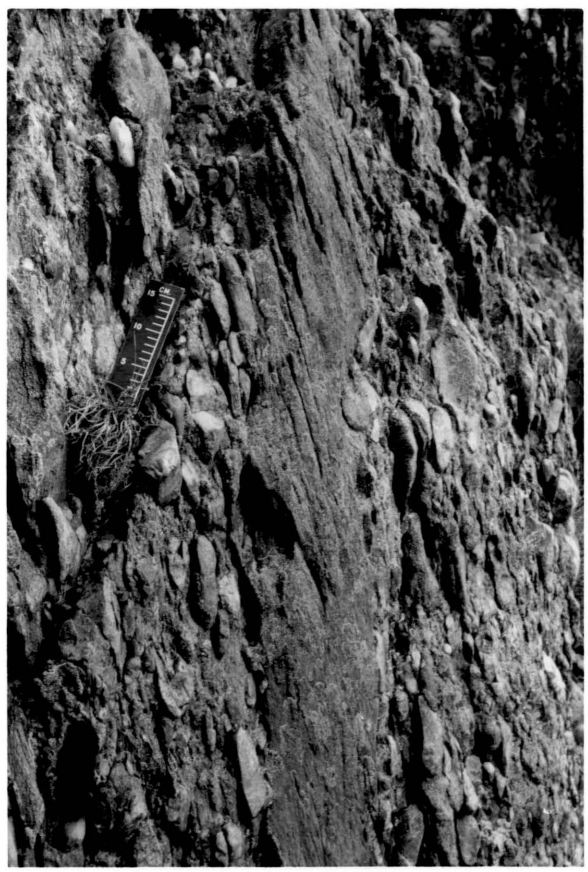

Figure 12: Wedge-planar cross-bed set within lower Marquenas conglomerate lithofacies in the southern Picuris range.

The sandstone lithofacies in the Marquenas Quartzite displays a progressive change in sedimentary strutures upwards through the section. Abundant trough cross beds up to 1.3 m thick and rare tabular-planar cross beds dominate the lower 90 m (Fig 11b). Single layer pebble lags commonly define the base of large cross-bed sets and solitary pebbles are often scattered along foresets. This association is analogous to that present in the South Saskatchewan River in Canada (Cant, 1978). Minimum flow depths of 8 m are inferred from trough cross beds (cf. Allen, 1982) implying that large channels existed on a perennial braided-alluvial plain. The dominant trough cross beds are interpreted as mid-channel bar deposits formed by aggradation during the initial waning of discharge. Accretion off mid-channel bars produced large-scale, tabular-planar cross beds. Absence of mudstones and small-scale structures in the Marquenas Quartzite contrasts with the depositional sequence developed for the South Saskatchewan River and may reflect either erosion of bar-top deposits or absence of fine-grained material available during deposition of the Marquenas alluvial facies.

The upper 140 m of the sandstone lithofacies is dominated by planar laminations with subordinate 20 to 60 cm-thick trough cross-bed cosets (Fig. 11c). This facies association is similar to braided ephemeral river deposits such as the present Bijou Creek in Colorado (cf. McKee et al., 1967). Trough cross beds and planar-laminated sandstones are considered to represent stream-flood deposits within shallow, poorly-developed channels (Turnbridge, 1981; Sneh, 1983). Thick planar-laminated sandstones, in contrast, are attributed to overbank sheet-

Figure 13: Primary current lineations on upper surface of planar-laminated sandstone in upper sandstone lithofacies of Marquenas Quartzite.

flood processes (Fig. 13). Paleocurrent trends of primary current lineations on the upper surface of planar-laminated sandstones deviate from northerly modes of trough cross-bedded, stream-flood deposits (Fig. 11), suggesting that sheet flooding resulted from channel breaching.

The upward transition from Scott- to South Saskatchewan-type braided-alluvial sediments in the lower two-thirds of the Marquenas Quartzite reflects a temporal decrease in competency of perennial streams. This decrease in competency is controlled by diminution of source area relief and/or backstepping of faults within the provenance causing successively distal braided alluvial facies to overlie more proximal facies (cf. Heward, 1978). The lower Marquenas Quartzite therefore represents a retrogradational sequence in which stacking of coexisting braided-alluvial facies was controlled by extrabasinal processes. In contrast, ephemeral fluvial sediments in the upper Marquenas Quartzite cannot be related in space to the underlying South Saskatchewan-type alluvial facies. Rather, the upper and lower sandstone lithofacies are separated in time and reflect a decrease in water discharge with time (Schumm, 1968), a phenomenon also governed by extrabasinal processes.

Source to Marquenas Quartzite

Trough cross beds such as present in the Marquenas braided-alluvial deposits, and which form by downstream dune migration, may be oriented either at right angles or parallel to tectonic highlands.

Examples of these two situations are respectively, the Kosi River which flows southwards from the Himalayan Mountain Belt and the Ganges River which drains from west to east parallel to the orogen and reworks sediment introduced by the Kosi River (Gole and Chitale, 1966). The Scott- and South Saskatchewan-type braided-alluvial deposits in the Marquenas Quartzite are more analogous in grain size to sediments of the Kosi River; boulders, cobbles and pebbles do not reach the Ganges River which is mainly a sandy system. Thus, the northward-oriented trough cross beds in the Marquenas Quartzite are considered to be oriented perpendicular to the source, placing the provenance to the Marquenas Quartzite south of the present outcrop belt (Fig. 11).

The composition of this southerly provenance is reflected in the composition of pebbles within the lower Marquenas conglomerates. Over 90 percent of the pebbles are grey quartzite. Well-rounded, detrital tourmaline with authigenic overgrowths, and detrital zircon indicate a sedimentary origin for the grey quartzite pebbles which had a quartz arenite protolith. These quartz arenite pebbles with high ZTR indices (cf. Hubert, 1962) are identical to the texturally and minerallogically mature quartz arenites within the Ortega Group. Several other more exotic pebble types are also present in the Marquenas Conglomerate (Table 2). Calc-silicate pebbles containing metamorphic mineral assemblages of garnet, hornblende, calcite and dominated by microcrystalline quartz are paired with identical calc-silicate lithologies in the Piedra Lumbre Formation in the upper Ortega Group (Fig. 5). Black quartzite pebbles match similar black quartzites at the top of the

Table 2: Pebbles in Marquenas conglomerate paired with lithologies in Ortega shelf sediments and Vadito volcanogenic unit.

ORTEGA GROUP - MARQUENAS CONGLOMERATE

- quartz arenite (a)
- quartz arenite with heavy mineral banding (r)
- quartz arenite with primary sedimentary laminations (r)
- calc-silicate (c)
- black quartzite (c)
- garnet-biotite-quartzite (r)
- biotite-garnet-quartz-muscovite-schist (r)

VADITO GROUP - MARQUENAS CONGLOMERATE

- porphyritic rhyolite (c)
- amphibolite (r)

(a) = abundant
(c) = common
(r) = rare

R5 and R6 members in the Ortega Group (Fig. 5). In addition, quartz arenite pebbles with hematite banding are similar to quartz arenites in the Ortega Quartzite. Porphyritic rhyolite pebbles with large quartz phenocrysts, and amphibolite pebbles from the Marquenas are comparable, respectively, to felsic and mafic metavolcanic rocks in the Vadito Group.

To the south of the study area basement rocks are younger than 1,700 m.y. (van Schmus and Bickford, 1981) and could not have supplied the voluminous quartz arenite pebbles found in the Marquenas Quartzite. Instead, it is concluded that the Vadito and Ortega Groups served as the provenance to the Marquenas succession. This not only implies that the Marquenas Quartzite postdates the Vadito and Ortega Groups, but also that the Marquenas alluvial succession was deposited in response to deformation and uplift of the Vadito-Ortega cratonic margin to the south. Northward vergence of F1 recumbent folds in the Picuris range (Nielsen and Scott, 1979) and Pecos belt (Grambling and Codding, 1982) is consistent with compression from the south.

Stratigraphic Evolution: A Model

The three lithostratigraphic units comprising the Precambrian section in northern New Mexico were formed in different tectonic environments. The Vadito volcanogenic unit suggests a period of crustal instability during which the juvenile crust developed. Based on geochemical studies, the Vadito Group evolved as an extensive magmatic arc complex (Fig. 14a). Voluminous granitoid bodies intruded the

Figure 14: Schematic illustration of tectonic evolution of Precambrian crust in northern New Mexico between 1,800 m.y. and 1,500 m.y.

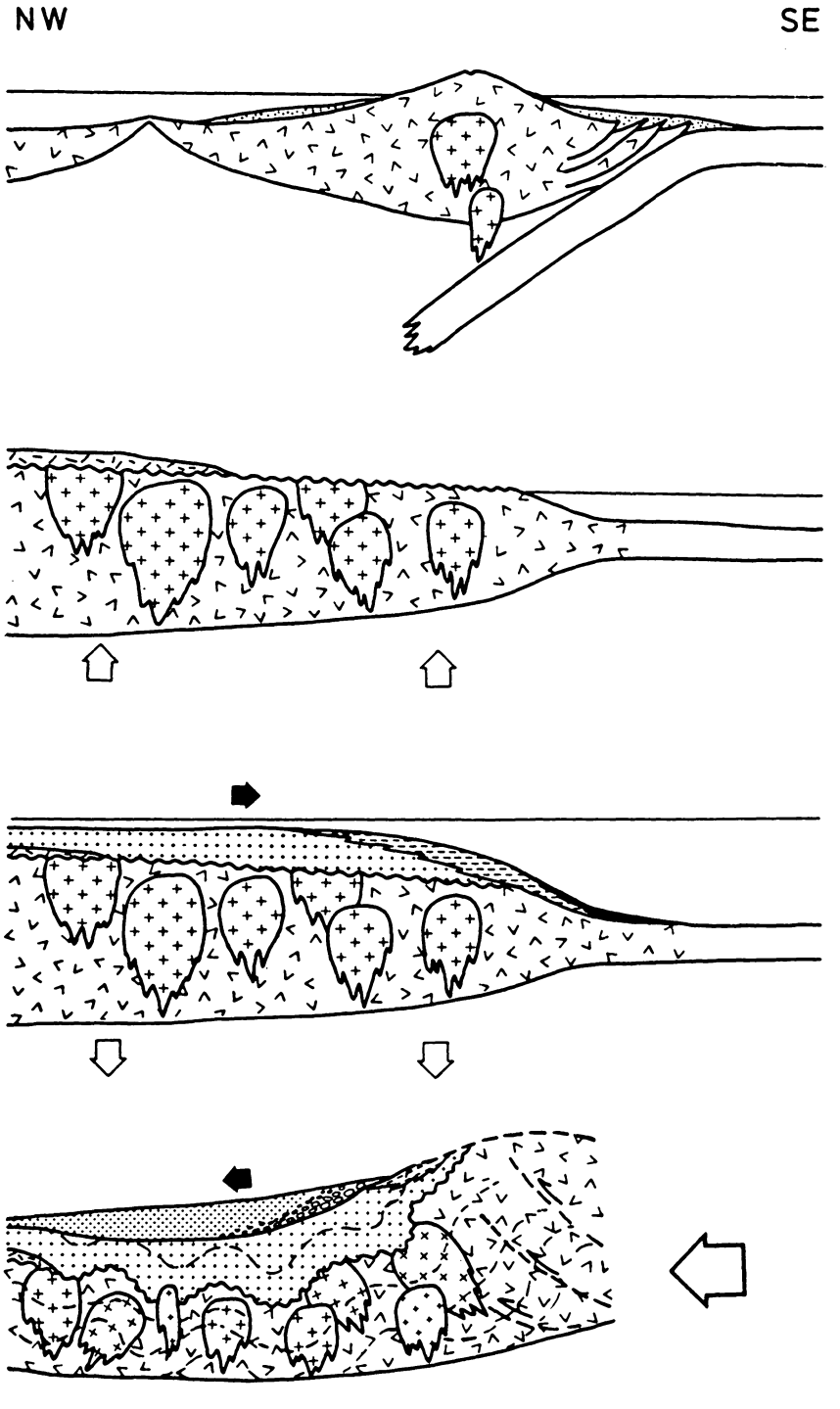

a.
1,760-1,720 m.y.
Unstable juvenile volcanogenic crust.

b.
>1,700 m.y.
Cratonization by intrusion of granitoid plutons. Local extrusion of felsic volcanics.

c.
1,705-1,684 m.y.
Deposition of Ortega shelf sediments.

d.
Pre-metamorphic compression of craton margin and deposition of Marquenas Quartzite in foreland basin? Intrusion by later granitoid bodies.

Vadito Group at shallow levels between 1,755 and 1,700 m.y. and were in part cogenetic with felsic volcanic complexes. Intrusion by granitoid bodies served to stabilize the juvenile crust and resulted in thermal uplift and subsequent erosion of the crust (Fig. 14b). As this bouyant crust cooled, prolonged thermal subsidence enabled the Ortega Group to accumulate on a shelf sloping gently to the south and southeast (Fig. 14c). Distal-outer shelf facies in the Ortega Group coincide with the margin of the 1,800 to 1,700 m.y.-old basement age province defined by van Schmus and Bickford (1981), suggesting that a cratonic margin may have existed to the south of the study area during deposition of the Ortega Group (Fig. 14c). Deformation of the cratonic margin resulted in cannibalization of the shelf sediments and underlying Vadito volcanogenic basement into the Marquenas braided-alluvial sequence, which was derived from the newly-formed highlands to the south (Fig. 14d). Development of this highland resulted in a dramatic switch in depositional slope from a southward orientation during Ortega times to a northerly-dipping paleoslope during deposition of the Marquenas Quartzite.

Evidence presented by previous workers for the Vadito Group representing a magmatic arc complex suggests that plate tectonic processes were operative during development of the juvenile crust in northern New Mexico. The early granitoid plutons, which served to stabilize the crust, can then be interpreted as subvolcanic plutons. In the absence of recognizable rift volcanics and sediments between the Vadito and Ortega Groups, the role of plate tectonics in promoting shelf

subsidence is uncertain and a passive margin cannot be invoked for the Ortega Group. Such a rift-drift margin may have existed to the south of the study area. Destruction of the cratonic margin during deposition of the Marquenas Quartzite may have resulted from subduction-related orogenesis. The attitude of a possible subduction zone cannot be resolved on the basis of the sedimentological evidence presented here. Rather, a subduction model can only be verified following a detailed petrogenetic study of the ca. 1,650 m.y. post-Ortega granites. Timing of granite emplacement relative to early deformation and metamorphism is not known, and is fundamental to understanding the post-Ortega tectonic framework.

Regional Implications

The 1,800 to 1,700 m.y.-old basement age province in northern New Mexico extends to the southwest into central Arizona and northeast into the Great Lakes area (van Schmus and Bickford, 1981). Within both these regions, thick quartz arenite sequences of similar age to the Ortega Group are developed and likewise accumulated along a cratonic margin opening to the southeast (Trevena, 1979; Dott, 1983).

In central Arizona a greater than 1,775±10 m.y. volcanogenic sequence (Anderson et al., 1971) was cratonized by granitoid emplacement between 1,760 and 1,720 m.y. (Silver, 1968; Anderton et al, 1971). Rhyolites dated at 1,715±15 m.y. were extruded following cratonization and occur at a similar stratigraphic position to those in the Tusas mountains in New Mexico (Fig. 4). Overlying quartz arenites

of the Mazatzal Group are in excess of 1200 m thick. Braided-alluvial deposits are recognized in the north and interfinger with shallow-marine sediments to the south with an inferred coastline trending southwest-northeast (Trevena, 1979). Destruction of the cratonic margin in central Arizona occurred during the Mazatzal orogeny with the development of northward-verging recumbent folds and imbricate thrusts (Wilson, 1939). The orogeny predated intrusion of 1,660±15 m.y.-old granites (Silver, 1965). Unlike northern New Mexico no sedimentary response to the destruction of the cratonic margin is recognized in central Arizona.

Rhyolites with an age of 1,760±10 m.y. comprise the oldest rocks in southern Wisconsin and are situated immediately south of the Penokean Fold Belt (van Schmus, 1980). Unconformably overlying the rhyolites is the Baraboo Quartzite which is a 1500 m thick quartz arenite sequence (Dott, 1983). The depositional setting of the Baraboo Quartzite is equivocal. Dott (1983) argues for braided alluvial and/or shallow marine processes during deposition of the quartz arenites. Overlying the Baraboo Quartzite is a 100 m thick slate similar to the Pilar Slate in the Ortega Group. Unlike the Ortega Group, however, the slate in Wisconsin is capped by 300 m of dolomite and iron-formation of shallow-marine origin (Dott, 1983). Deformation of the Baraboo interval is considered to have reset the Rb-Sr system between 1,630-1615 m.y. (van Schmus et al., 1975). This deformation is approximately coeval with the Mazatzal orogeny in Arizona and is of similar age to plutonic rocks in northern New Mexico. As in Arizona, no sedimentary response to the deformation is recognized in southern Wisconsin.

The ca. 1,700 m.y.-old shelf sequences, overlying the 1,800-1,700 m.y. basement age province (van Schmus and Bickford, 1981) in central Arizona, northern New Mexico and Wisconsin, are thought to define the southern margin of the proto-North American continent. Destruction of this continental margin took place between 1,660 and 1,630 m.y. during the regional orogenic event proposed by Wilson (1939) and van Schmus and Bickford (1981).

Conclusion

Three Precambrian lithostratigraphic units exist in northern New Mexico. Each unit is a response to different tectonic environments attesting to the fact that the early crust evolved through a complex sequence of events:

(1) The juvenile crust developed as an unstable volcanogenic terrane between 1,760-1,720 m.y. and has been interpreted by other workers as a magmatic-arc complex.

(2) This juvenile crust was intruded extensively by granitoid plutons until 1,700 m.y., resulting in cratonization of the early unstable crust.

(3) Thermal subsidence of the volcano-plutonic crust between 1,705-1684 m.y. promoted accumulation of a ca. 2 Km thick sequence of cratonic shelf sediments.

(4) Deformation and destruction of the cratonic margin to the south resulted in cannibalization of the shelf sediments and underlying volcanogenic basement.

(5) A similar crustal evolution is recognized in central Arizona and southern Wisconsin between 1,760-1,630 m.y. along the southern margin of the proto North American continent.

EVIDENCE OF TIDE, STORM AND WAVE INTERACTION ON A PRECAMBRIAN CLASTIC SHELF: THE 1,700 M.Y. ORTEGA GROUP, NEW MEXICO

Abstract

The 1,700 m.y. Ortega Group in northern New Mexico is a sequence of quartz arenites and subordinate mudstones in excess of 1000 m thick. Sedimentation took place in diverse shallow-shelf environments under the influence of tidal, wave and storm processes. Time-velocity asymmetry of tidal flow on the inner shelf produced large-scale trough cross beds and tabular-planar cross beds with multiple reactivation surfaces. In contrast, tabular cosets structured internally by small-scale trough cross beds and herringbone cross beds resulted from time symmetrical tidal flow on the inner shelf. Fair-weather waves reworked the upper surface of tidal sand bodies on the inner shelf during quiet periods within the tidal rhythm. During storms, sand was entrained into the water column on the proximal inner shelf leaving winnowed pebble lags at the top of tidal sand bodies. Sand transported by storm-induced gradient currents was deposited on the outer shelf as discrete lobes. Progradation of sand lobes produced 1-to-11 m thick, upward-thickening genetic packages capped by cosets of tabular, planar-laminated sandstones. On the proximal outer shelf storm sands were reworked by wave processes whereas storm-deposited sands on the

distal outer shelf remained unmodified. No evidence of tidal processes exists on the outer shelf.

Distribution of facies and paleocurrent patterns indicate that the shelf sloped to the south, and experienced an overall transgression which culminated in drowning of the outer shelf with onlap of black basinal muds. Absence of shallow water turbidites below storm wave base reflects low gradients on the shelf. Vertical transition from tide- to storm-dominated sedimentation in the Ortega Group does not represent a change in depositional style with time on the shelf. Rather, all facies coexisted across the shelf, with tidal processes prevailing on the shallow inner shelf and storm processes on the outer shelf. The German Bight in the North Sea provides a modern analogue for the depositional framework envisaged for the Ortega Group.

Introduction

Quartz arenite sequences ranging in thickness from hundreds to thousands of meters owe their existence to a unique tectonic framework in which relative sea level rise is balanced by prolonged influx of terrigeneous sediment (Hobday and Tankard, 1978). Thick, texturally and compositionally mature Phanerozoic terrigeneous sequences are confined to the Lower Paleozoic (Otvos, 1966; Banks, 1973; McCave, 1973; Anderton, 1976; Hobday and Tankard, 1978; Hiscott, 1982). These quartz arenite packages coincide with a first order sea level rise (Vail et al., 1977) resulting in overall transgressive sequences. Thick quartz arenite successions are also characteristic of the latest Archean

and Proterozoic where they developed following cratonization (see for example Button, 1973; Hoffman et al., 1974; von Brunn and Hobday, 1976; Button and Vos, 1977; Trevena, 1979; Eriksson et al., 1981; Tankard et al., 1982; Dott, 1983).

Despite the abundance of thick quartz arenites in the geologic record, their depositional framework is poorly understood because no modern analogue exists. The sequences generally commence with an alluvial to shallow-marine transition which is evident when alluvial deposits are mineralogically and texturally immature. However, where intense source area weathering produces quartz rich sands, as in the Precambrian Baraboo Quartzite of Wisconsin (Dott, 1983), alluvial and shallow-marine arenites are petrologically indistinguishable and the transition is less obvious (Cotter, 1983). Additional criteria for distinguishing shelf sediments from those deposited in adjacent environments therefore must be developed. A further problem surrounding shelf sedimentation is the mechanism for transport of coarse grained material onto the outer shelf (Allen, 1982a). Creager and Sternberg (1972) discuss the distribution of sand and mud on modern shelves and conclude that no satisfactory mechanism is recognized for transferring sand from the nearshore regime to distal reaches of the shelf. Depositional processes active on the outer shelf are poorly understood since water depth has prevented studies in the modern and the progressive increase in bioturbation through the Phanerozoic (Bambach and Sepkoski, 1979; Thayer, 1983; Miller and Byers, 1984) has destroyed depositional textures, thereby complicating studies of distal shelf sediments in the Phanerozoic rock record.

This paper outlines a detailed sedimentological analysis of the 1,700 m.y. Ortega Group in northern New Mexico which comprises over 1000 m quartz arenites and subordinate mudstones. Evidence is presented for the Ortega Group being a shallow-marine deposit. The study is based on a detailed facies analysis in which individual facies are interpreted in terms of specific shelf processes. A three-end-member process-response model is adopted and includes tide, storm and wave processes. In addition, a mechanism is proposed for transporting coarse sediment from the nearshore regime onto the outer shelf. The absence of bioturbation in the Ortega succession, due to the antiquity of the sediments, provides an excellent opportunity for documentation of muddy outer-shelf facies.

Regional Geology

Precambrian rocks of northern New Mexico are exposed in a series of basement windows separated by younger Phanerozoic cover rocks (Fig. 15). The oldest rocks are ca. 1,720 m.y. volcanics and volcaniclastics of arc affinity (Bowring and Condie, 1982; Klich and Robertson, 1983). This early terrane has no recognizable basement and represents a period of tectonic instability. At 1,700 m.y. granodiorites intruded the volcanogenic terrane resulting in cratonization of the crust (Soegaard and Eriksson, 1983). The mature terrigeneous sediments of the Ortega Group accumulated unconformably on this stabilized older crust (Fig. 16). Following deposition of the Ortega Group the entire Precambrian section was deformed by two coaxial fold events and

Figure 15: Distribution of Precambrian rocks in northern New Mexico. Inset illustrates Precambrian rocks in southwestern United States (Compiled from Bingler, 1968; Robertson and Moench, 1979; Condie, 1982).

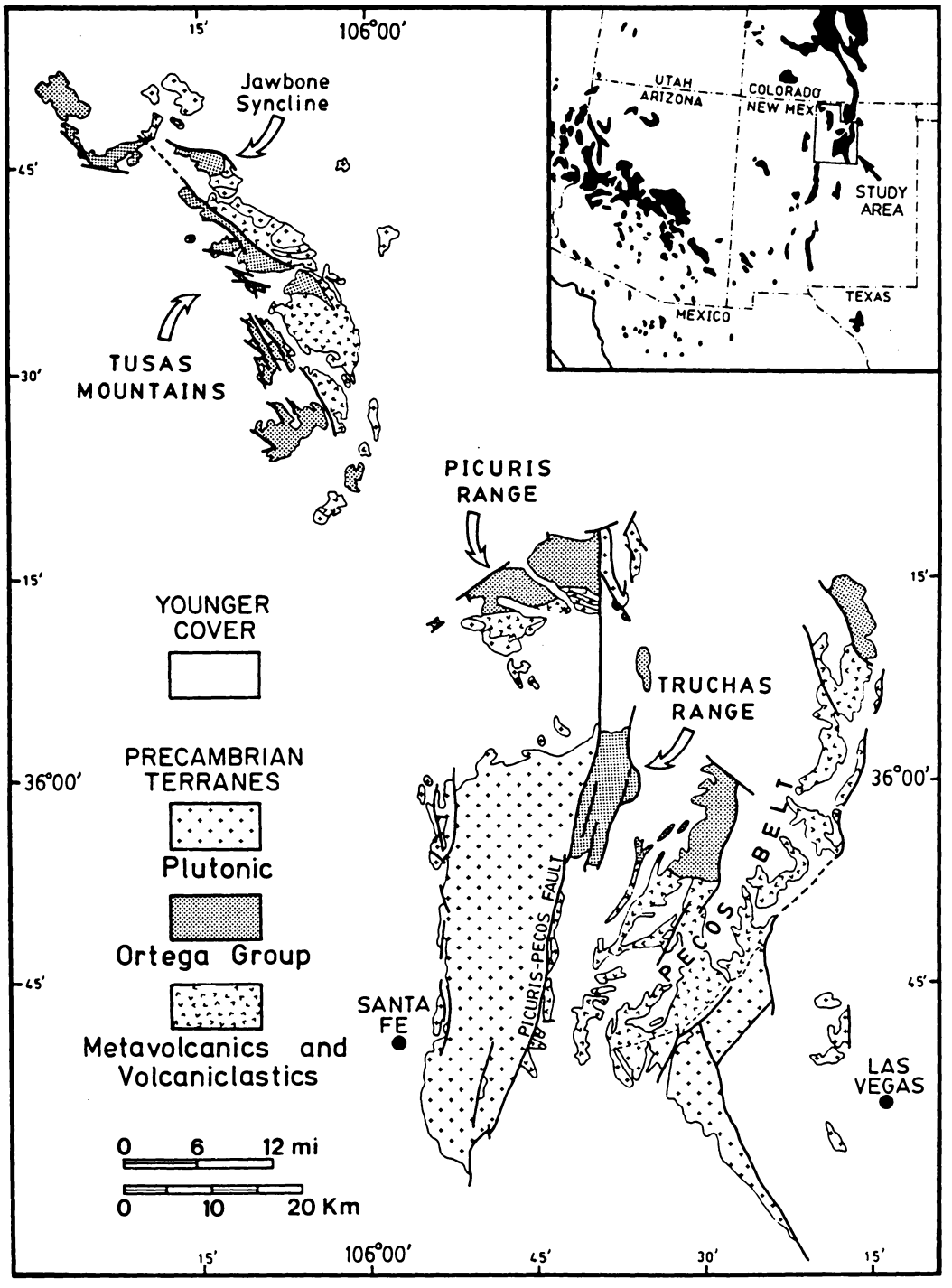
15'
106°00'
Jawbone
Syncline
45'
30'
TUSAS
MOUNTAINS
PICURIS
RANGE
15'
YOUNGER
COVER
TRUCHAS
RANGE
36°00'
PRECAMBRIAN
TERRANES
Plutonic
Ortega Group
Metavolcanics and
Volcaniclastics
SANTA
FE
PICURIS-PECOS FAULT
PECOS BELT
LAS
VEGAS
0 6 12 mi
0 10 20 Km
106°00'
45'
30'
15'
UTAH
ARIZONA
COLORADO
NEW MEX
STUDY
AREA
TEXAS
MEXICO

Figure 16: Genetic stratigraphic cross section of Ortega Group. Position of Truchas range and Pecos belt relative to Picuris range corrected for right-lateral strike-slip displacement along Picuris-Pecos Fault. Location of columns illustrated in paper are; (a) Figure 3; (b) Figure 4; (c) Figure 8; (d) Figure 10. Also shown is unconformable relationship between Ortega Group and underlying rocks. Horizontal and vertical scales are approximate.

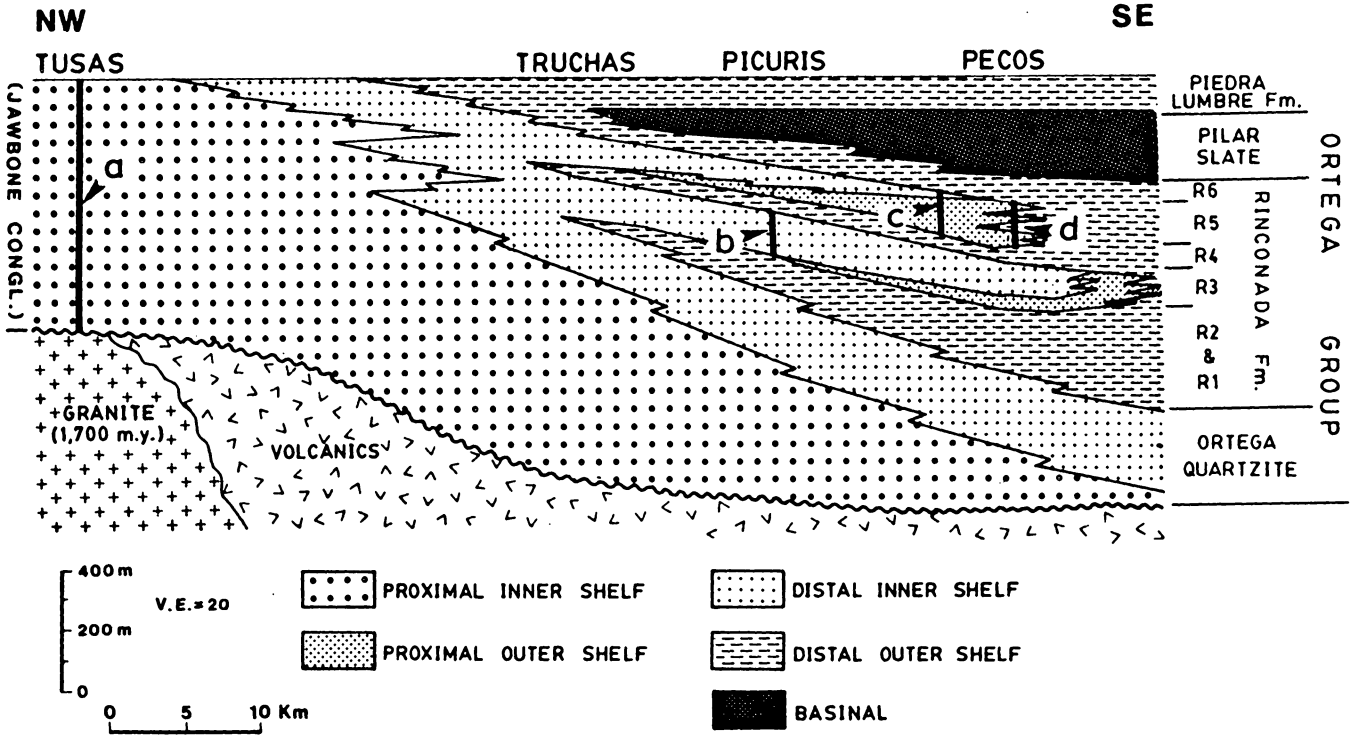
NW
SE
TUSAS
TRUCHAS
PICURIS
PECOS
(JAWBONE CONGL.)
a
b
c
d
GRANITE
(1,700 m.y.)
VOLCANICS
PIEDRA LUMBRE Fm.
PILAR SLATE
R6
R5
R4
R3
R2
&
R1
RINCONADA Fm.
ORTEGA QUARTZITE
ORTEGA GROUP
400 m
200 m
0
V.E.=20
0
5
10 Km
PROXIMAL INNER SHELF
PROXIMAL OUTER SHELF
DISTAL INNER SHELF
DISTAL OUTER SHELF
BASINAL

subsequently metamorphosed to lower amphibolite grade around 1,470 m.y. (Nielsen and Scott, 1979). At a later stage the Picuris range was displaced 36 Km north relative to the Truchas and Pecos belts along the right-lateral, Picuris-Pecos strike-slip fault (Montgomery, 1963 and Grambling, 1979; Fig. 15).

The Ortega Group exhibits a decrease in grain size to the southeast as well as upwards through the section suggesting an overall transgression to the northwest (Fig. 16). In the Picuris, Truchas and Pecos belts, the Ortega Group is subdivided into the Ortega Quartzite, Rinconada Formation, Pilar Slate and Piedra Lumbre Formation (nomenclature modified after Nielsen and Scott, 1979 and Grambling and Codding, 1982). The Rinconada Formation is further subdivided into six members termed the R1 through R6 (Nielsen, 1972; Fig. 16). In the Tusas Mountains, the Jawbone Conglomerate of Barker (1958) is considered to be lateral equivalents to the Ortega Group and is referred to as the Ortega Quartzite in this paper (Fig. 16).

Facies Analysis

Sediments within the Ortega Group can be separated into tide-dominated and storm-dominated facies associations. The tidal facies comprise quartz-pebble conglomerates and coarse- to fine-grained quartz arenites with subordinate mudstones, and are dominated by a diverse suite of cross beds. In contrast, the storm-generated facies association is essentially devoid of traction-produced structures and consists of mudstones and thinly-bedded, fine-grained sandstones. Evidence is

presented to show that these two facies associations accumulated, respectively in inner- and outer-shelf environments.

Tide-Dominated Facies Association

Three tidal facies are recognized; these are best represented in the Jawbone Syncline where the Ortega Quartzite is over 850 m thick and in the R3 Member of the Rinconada Formation in the Picuris, Truchas and Pecos belts (Fig. 16).

Large-Scale Trough Cross-Bedded Facies

Large-scale, trough cross beds up to 40 cm thick are restricted to the basal Ortega Quartzite in the Jawbone Syncline (Fig. 17a). Angular, intraformational mudstone rip-up clasts and well-rounded vein quartz pebbles less than 3 cm in diameter define the erosive base of trough cross beds. Pebbles occur as a single layer conglomerate lag. Cross bed foresets are normally graded and up to 2 cm in thickness. Thin mudstone veneers may drape the toe of foresets (Figs. 18 and 19). Upper boundaries of trough cross-bed sets are commonly defined by a winnowed pebble lag consisting of well-rounded and well-sorted vein quartz pebbles less than 1 cm in diameter. This upper pebble lag varies laterally in thickness, attaining a maximum of 12 cm. Paleocurrents for this facies are unimodal with a narrow spread to the south (Fig. 19).

Figure 17: Measured stratigraphic column through proximal, inner-shelf facies in the Jawbone Syncline, Tusas mountains. The sequence is overall transgressive (see Fig. 16 for location of section).

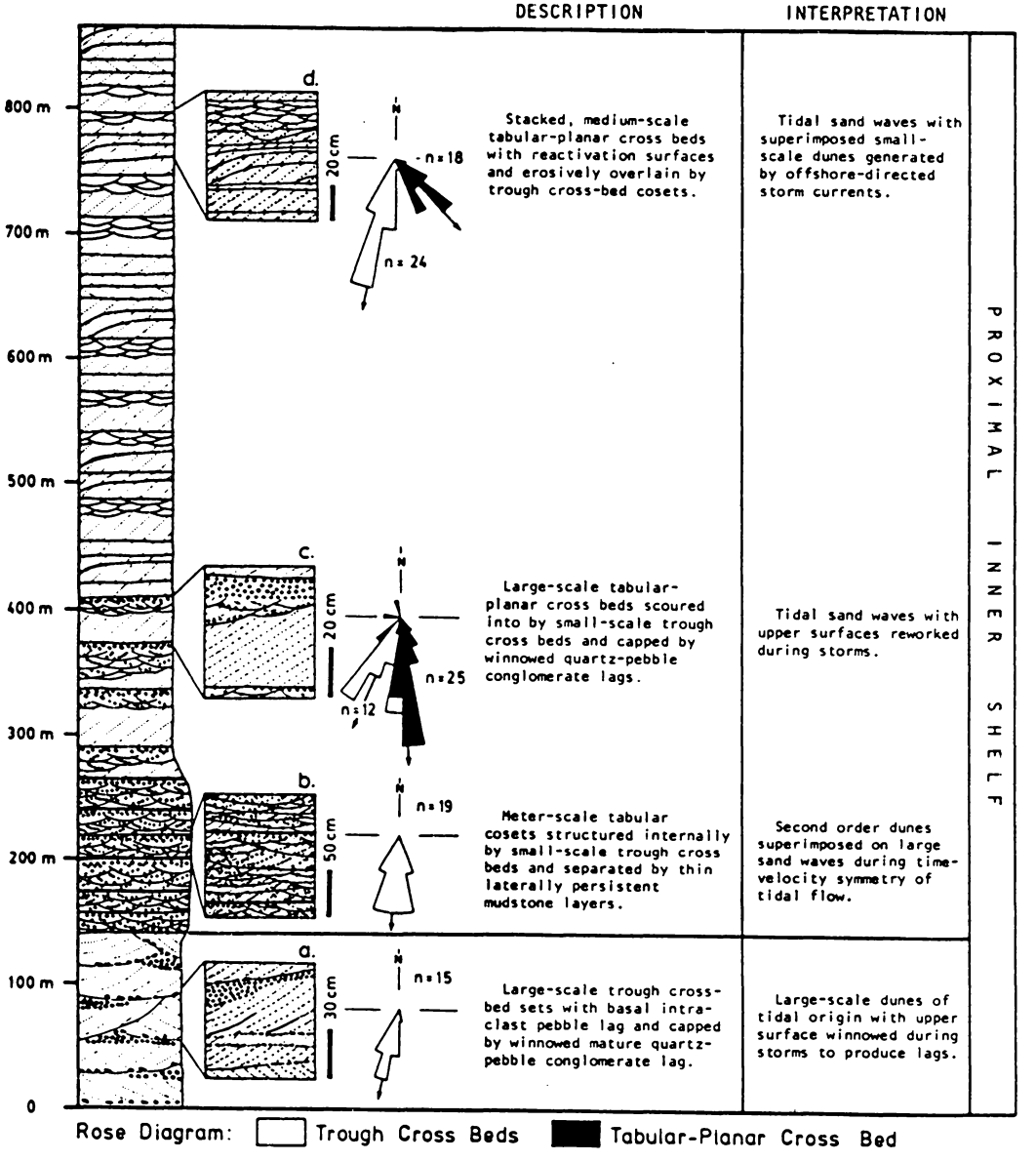
DESCRIPTION
INTERPRETATION
800 m
700 m
600 m
500 m
400 m
300 m
200 m
100 m
0
d.
20 cm
n=18
n=24
Stacked, medium-scale tabular-planar cross beds with reactivation surfaces and erosively overlain by trough cross-bed cosets.
Tidal sand waves with superimposed small-scale dunes generated by offshore-directed storm currents.
c.
20 cm
n=25
n=12
Large-scale tabular-planar cross beds scoured into by small-scale trough cross beds and capped by winnowed quartz-pebble conglomerate lags.
Tidal sand waves with upper surfaces reworked during storms.
b.
50 cm
n=19
Meter-scale tabular cosets structured internally by small-scale trough cross beds and separated by thin laterally persistent mudstone layers.
Second order dunes superimposed on large sand waves during time-velocity symmetry of tidal flow.
a.
30 cm
n=15
Large-scale trough cross-bed sets with basal intra-clast pebble lag and capped by winnowed mature quartz-pebble conglomerate lag.
Large-scale dunes of tidal origin with upper surface winnowed during storms to produce lags.
PROXIMAL INNER SHELF
Rose Diagram:
Trough Cross Beds
Tabular-Planar Cross Bed

Figure 18: Large-scale trough cross bedded facies in the lower Ortega Quartzite, Jawbone Syncline (see Fig. 17a). Note mudstone intraclast pebble lag along the base of the trough cross-bed set.

Figure 19: Field sketch of large-scale trough cross bedded facies in lower Ortega Quartzite, Jawbone Syncline (see Fig. 17a). Note mudstone drape along trough cross bed foreset.

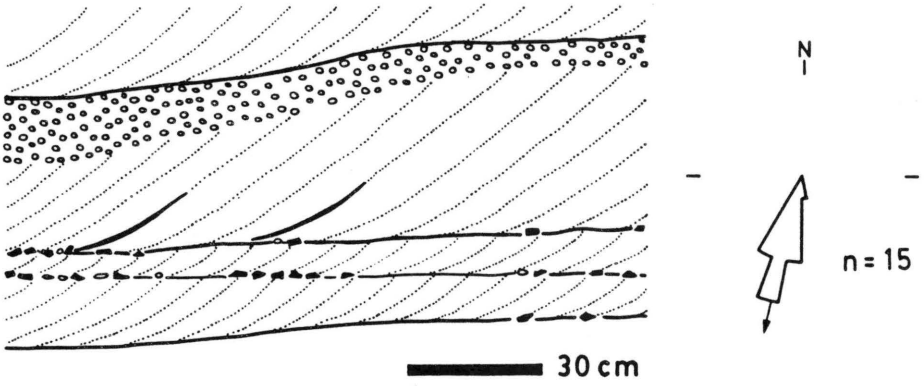
N
n = 15
30 cm

Meter-Scale Tabular Coset Facies

In the lower Ortega Quartzite in the Tusas mountains and northern Picuris range (Fig. 16), meter-scale tabular cosets are structured internally by small- and medium-scale trough cross beds (Figs. 17b and 20). The sediments are medium-grained to conglomeratic with well-rounded quartz pebbles and rare mudstone intraclasts, none of which exceed 1.4 cm in diameter. Tabular cosets persist laterally for several tens of meters, across the extent of outcrops, and are capped by discontinous quartz-pebble layers less than 8 cm thick. The tabular cosets are generally separated by thin, continous mudstone drapes.

In both the Tusas mountains and Picuris range, rare tabular-planar cross beds up to 1.1 m in thickness with non-erosive lower set-boundaries are interbedded with the trough cross beds. These tabular-planar cross beds persist more than 10 m laterally and exhibit reactivation surfaces draped by mudstone veneers. Foresets are 0.5 to 3.5 cm thick and display normal grading with grain sizes varying from medium to very-coarse sand. Rare quartz pebbles are randomly scattered along foresets. Cosets of small-scale trough cross beds scour into the larger tabular-planar cross beds (Figs. 17c and 21). Some trough cross beds resulted from reworking of tabular-planar cross-bed sets. Almost all large tabular-planar and overlying smaller trough cross beds are capped by a mature quartz-pebble conglomerate lag (Fig. 22).

Figure 20: Field sketch of meter-scale tabular cosets structured internally by small-scale trough cross beds in lower Ortega Quartzite, Jawbone Syncline (see Fig. 17b). Tabular cosets are separated by thin, laterally-persistent mudstones. Black rose diagram indicates paleocurrent mode of tabular-planar cross beds and white rose diagram represents trough cross bedded paleocurrent trend.

Figure 21: Field sketch of large-scale, tabular-planar cross beds scoured into by small-scale trough cross beds in lower Ortega Quartzite (see Fig. 17c). Note multiple reactivation surfaces within tabular-planar cross beds.

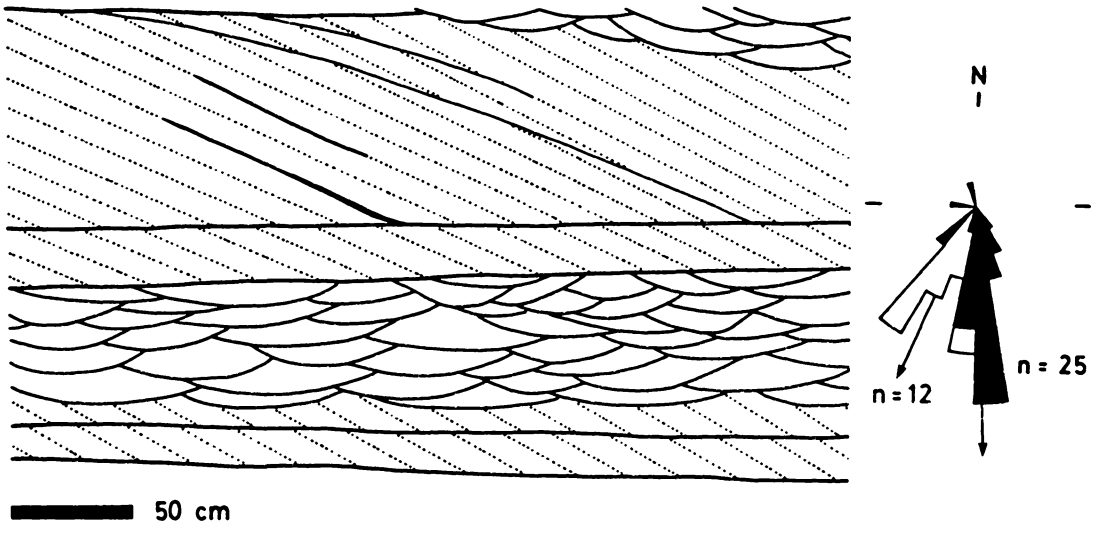
N
n = 12
n = 25
50 cm

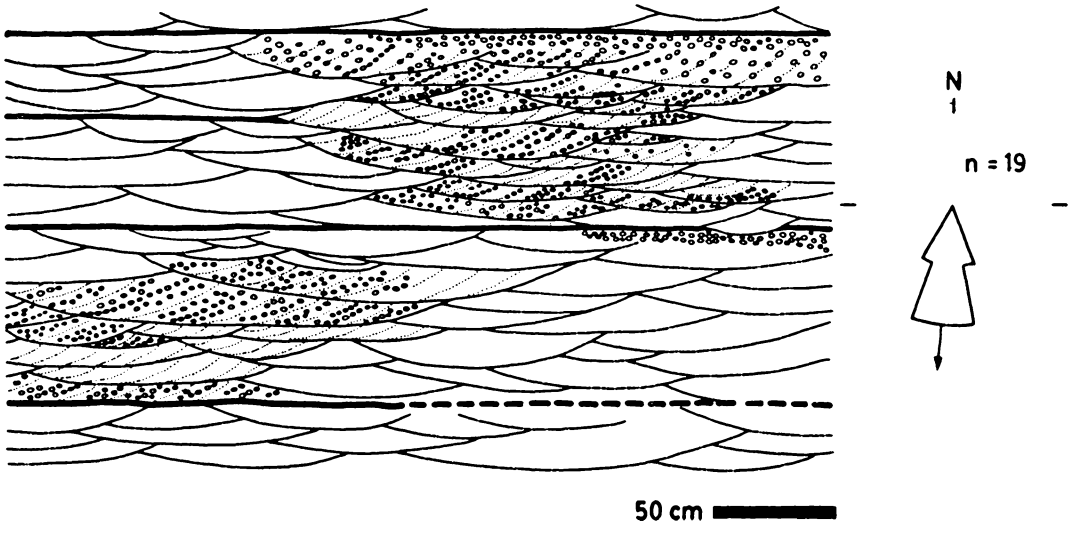
N
n = 19
50 cm

Figure 22: Winnowed pebble lag capping large-scale, tabular-planar cross-bed set in lower Ortega Quartzite, Jawbone Syncline (see Fig. 17c).

Trough and tabular-planar cross beds each have unimodal paleocurrent trends. The two modes may be superimposed but more commonly are separated by 8 to 28 degrees with the trough cross-bedded mode lying west of the tabular cross-bedded mode (Fig. 21). Rare tabular-planar cross beds have bimodal-bipolar paleocurrent trends with a dominant mode to the south and a subordinate northerly mode.

Medium-Scale Tabular-Planar Cross-Bed Facies

The best exposures of this facies are in the upper half of the Ortega Quartzite in the Jawbone Syncline (Fig. 17) and in the R3 Member of the Rinconada Formation (Fig. 23). Small- to medium-scale, tabular-planar cross beds also predominate in the upper two thirds of the Ortega Quartzite in the Picuris and Truchas ranges and Pecos belt (Fig. 16).

Cross beds are tabular or wedge shaped and are 2 to 30 cm thick. Foresets are planar, and commonly have multiple reactivation surfaces (Figs. 17d and 24) draped by mudstone partings (Fig. 23a). Bimodal-bipolar paleocurrent trends are dominated by a southerly mode with a subordinate mode to the north (Fig. 25). Examples of westerly and northwesterly modes exist in the Picuris and Pecos belts (Fig. 25). In rare instances, herringbone cross beds are developed (Fig. 26).

In the R3 Member, tabular-planar cross-bedded cosets are capped by symmetrical ripples. The ripples have irregular lower set-boundaries and are commonly structured internally by complex, bundled cross laminations. Ripple crests are sharp and straight with paleocurrent

Figure 23: Generalized stratigraphic column through prograding distal inner shelf facies, R3 Member, Rinconada Formation (see Fig. 16 for location of section).

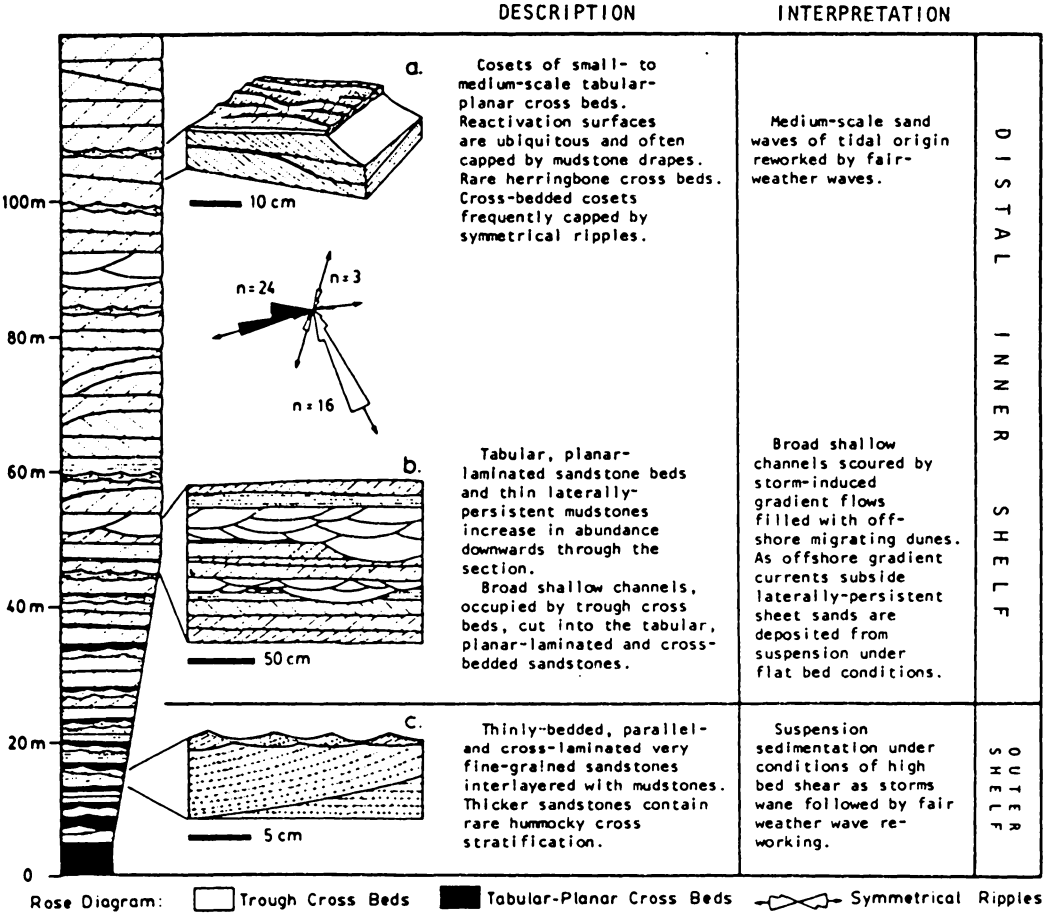
DESCRIPTION
INTERPRETATION
a.
Cosets of small- to medium-scale tabular-planar cross beds. Reactivation surfaces are ubiquitous and often capped by mudstone drapes. Rare herringbone cross beds. Cross-bedded cosets frequently capped by symmetrical ripples.
Medium-scale sand waves of tidal origin reworked by fair-weather waves.
10 cm
n=24
n=3
n=16
b.
Tabular, planar-laminated sandstone beds and thin laterally-persistent mudstones increase in abundance downwards through the section.
Broad shallow channels, occupied by trough cross beds, cut into the tabular, planar-laminated and cross-bedded sandstones.
Broad shallow channels scoured by storm-induced gradient flows filled with off-shore migrating dunes. As offshore gradient currents subside laterally-persistent sheet sands are deposited from suspension under flat bed conditions.
50 cm
c.
Thinly-bedded, parallel- and cross-laminated very fine-grained sandstones interlayered with mudstones. Thicker sandstones contain rare hummocky cross stratification.
Suspension sedimentation under conditions of high bed shear as storms wane followed by fair weather wave re-working.
5 cm
100m
80m
60m
40m
20m
0
DISTAL INNER SHELF
OUTER SHELF
Rose Diagram:
Trough Cross Beds
Tabular-Planar Cross Beds
Symmetrical Ripples

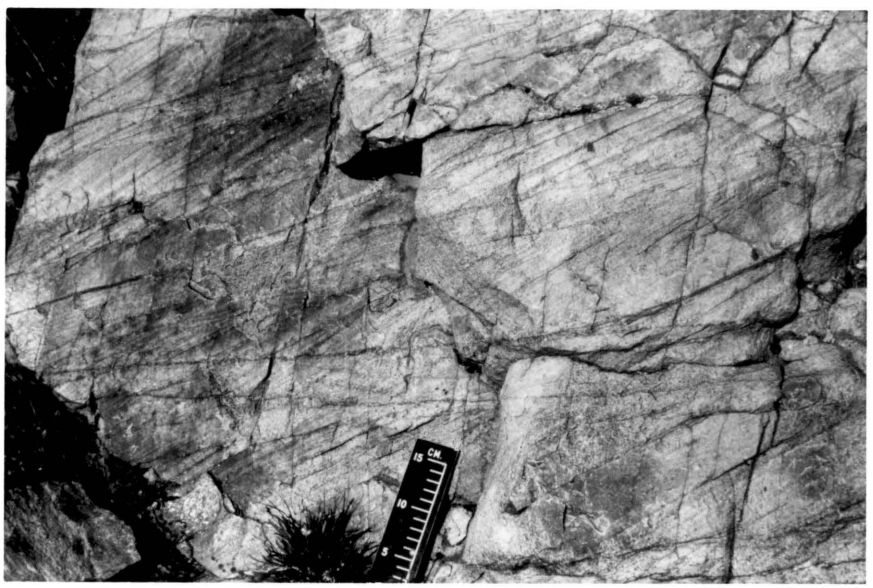

Figure 24: Multiple reactivation surfaces in medium-scale, tabular-planar cross beds, upper Ortega Quartzite, northern limb of Jawbone Syncline, Tusas mountains.

Figure 25: Paleocurrent data for the R3 Member, Rinconada Formation, in the Picuris and Truchas ranges and the Pecos belt. Paleocurrent data for the Jawbone Syncline (Fig. 1) is from upper Ortega Quartzite. 36 Km of right-lateral, strike-slip movement along Picuris-Pecos Fault has been restored according to Montgomery (1963) and Grambling (1979).

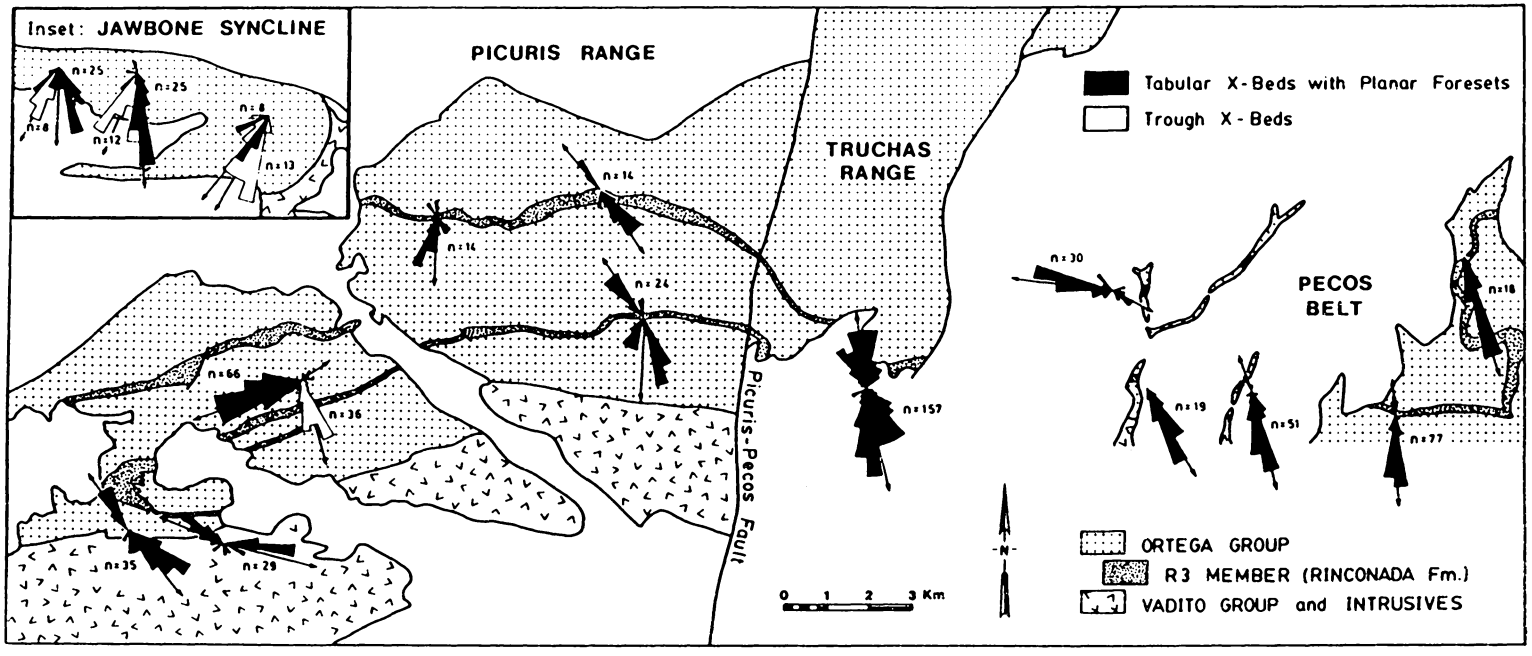
Inset: JAWBONE SYNCLINE
n=25
n=25
n=8
n=8
n=12
n=13
PICURIS RANGE
TRUCHAS RANGE
n=14
n=14
n=24
n=66
n=36
n=35
n=29
n=157
Picuris-Pecos Fault
Tabular X-Beds with Planar Foresets
Trough X-Beds
n=30
PECOS BELT
n=18
n=19
n=51
n=77
0 1 2 3 Km
N
ORTEGA GROUP
R3 MEMBER (RINCONADA Fm.)
VADITO GROUP and INTRUSIVES

Figure 26: Exumed foresets in herringbone crosss beds, R3 Member, Rinconada Formation, southwestern Picuris range.


CM.
15
10
5

modes oblique to the underlying tabular-planar cross beds (Fig. 23). Thin, laterally-persistent mudstones often drape symmetrical ripples. In absence of ripples, mudstones separate cross-bed cosets. Mudstones decrease progressively in thickness and abundance upwards through the R3 Member.

Interpretation of the Tide-Dominated Facies Association

The frequent occurrence of reactivation surfaces draped by mudstone veneers, coupled with the presence of herringbone cross bedding and bimodal-bipolar paleocurrent trends suggests a tidal origin for the suite of cross beds described in the above facies association (Klein, 1970a). The large-scale trough cross-bedded facies resulted from southerly migration of large dunes in response to unidirectional tidal currents. Minimum dune height of 40 cm can be inferred indicating minimum water depths of 3 to 4 m during deposition (cf. Allen, 1968, Fig. 6-4; 1982a, Fig. 8.20).

Large-scale tabular-planar cross beds within the meter-scale tabular coset facies (Fig. 21) result from migration of large tidal sand waves, and are similar to shallow-subtidal, sand-wave facies described by Homewood and Allen (1981). The internal structure of tidal sand waves is a function of time-velocity asymmetry of tidal flow (Allen, 1980). Under conditions of extreme time-velocity asymmetry, flow separation develops on the lee side of sand waves in response to unidirectional currents producing steep avalanche foresets (Fig. 21). During less pronounced time-velocity asymmetry, migration of sand

waves becomes episodic , resulting in the development of reactivation surfaces (Figs. 21 and 24). Flow separation downcurrent of sand waves still prevails and consequently lee face avalanching governs propagation of large first order bedforms (Allen, 1980). Under conditions approaching time-velocity symmetry, flow separation behind the lee face of sand waves no longer exists. As a result, transport of sand is confined to migration of small dunes on first-order sand waves (Fig. 21; Allen, 1980). Since large sand waves tend to migrate oblique to water flow, and smaller dunes propagate in the direction of tidal currents (High and Picard, 1974), a limited departure between average paleocurrent modes for first order sand waves and second order dunes is recognized (Fig. 21). Eventually the internal structure of large sand waves is erased and only thinner, trough cross-bed sets are preserved. Vertical dimensions of first order bedforms are, however, still retained. The meter-scale, tabular cosets structured internally by small trough cross beds (Fig. 20), therefore result from pronounced time-velocity symmetry of tidal currents.

Mudstone drapes along toes of foresets of large trough cross beds (Fig. 19) and along reactivation surfaces of tabular planar cross beds (Figs. 23a and 24) result from intermittent dune and sand wave migration. Episodic migration of bed forms implies time-velocity asymmetry of tidal flow in which mud is deposited from suspension during slack water periods in the tidal rhythm (Reineck and Wunderlich, 1968). McCave (1970), however, argues that mud layers up to 1 cm thick, as seen in the tidal facies association in the Ortega

Group, cannot accumulate from passive suspension sedimentation alone. This author postulates that high concentrations of mud within the water column immediately above the sediment water interface is not only conducive to more rapid sedimentation rates, but that mud may be deposited at relatively high flow velocities. The time span in the tidal rhythm during which fine grained material can accumulate is thus increased, enabling thicker mud layers to develop. Mud drapes deposited during the quiet periods in the tidal rhythm are reworked and preserved as mudstone intraclasts along foresets of small trough cross beds (Fig. 18).

Oscillation ripples capping medium-scale, tabular-planar cross beds in the R3 Member (Fig. 23a) reflect fair-weather wave reworking of the upper surface of tidal sand waves during quiet periods within the tidal cycle. Wave fetch was oblique to tidal currents rather than strictly orthogonal and consequently the wave ripples should not be confused with intertidal, late-stage emergence outflow ripples capping the BC sequences of Klein (1970b). The absence of bundled sets of wave ripples similar to those described by de Raaf et al. (1977), suggests that wave action was subordinate to tidal processes during deposition of the R3 Member.

Storm-Dominated Facies Association

The storm-dominated facies association is characterized by a greater mudstone to sandstone ratio than the tide-dominated facies association, and traction-produced structures are rare. Four separate facies are identified and occur in the mudstone rich R1-2, R4 and R6 Members of the Rinconada Formation, and in the overlying Piedra Lumbre Formation (Fig. 16). The facies are also present in the sandstone-dominated R5 Member and basal portion of the R3 Member of the Rinconada Formation in the Picuris and Pecos belts (Fig. 16).

Tabular, Planar-Laminated Sandstone Facies

Tabular, planar-laminated sandstone beds between 2 and 55 cm thick are interbedded with tabular-planar cross beds in the lower R3 Member (Fig. 23b) and occur as cosets in the R5 Member in which tabular-planar cross bedding is absent (Figs. 27, 28 and 29). Planar-laminated sandstone beds can be traced laterally for tens of meters. Individual laminations persist for several meters and parallel upper and lower set-boundaries of tabular sandstone beds. Lower contacts of tabular sandstones are sharp but non-erosive. Sole marks are absent and instead parallel-laminated sandstones are form-concordant and drape underlying irregularities. Current lineations are absent on upper surfaces of planar-laminated sandstone beds.

Symmetrical ripples cap tabular planar-laminated cosets in the R3 and R5 Members in the Picuris and western Pecos belt and are in turn

Figure 27: Measured section through proximal outer-shelf facies in R5 Member, Rinconada Formation, western Pecos belt (see Fig. 16 for location of section).

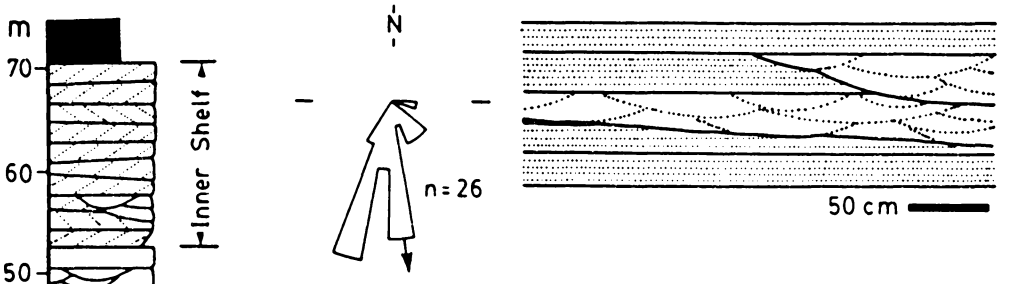

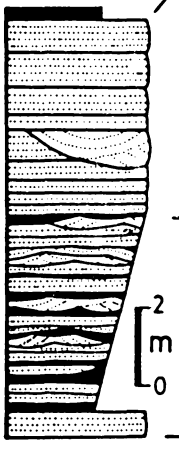

DESCRIPTION	INTERPRETATION	
Upward thickening co-sets of tabular, planar-laminated sandstones. Individual cosets are capped by symmetrical ripples. Broad shallow channels scour into tabular cosets and are occupied by small-scale cross beds.	Storm-induced gradient flows scoured broad shallow channels subsequently filled by offshore-migrating dunes. Suspension sedimentation of sheet sands under flat bed conditions in response to waning gradient currents. Upper surfaces of storm sands reworked by wave processes.	PROXIMAL OUTER SHELF
Interlayered mudstones and thinly-bedded cross- and parallel-laminated sandstoned	Suspension sedimentation from storm currents under conditions of high bed shear followed by wave reworking, and fair weather suspension fallout.	

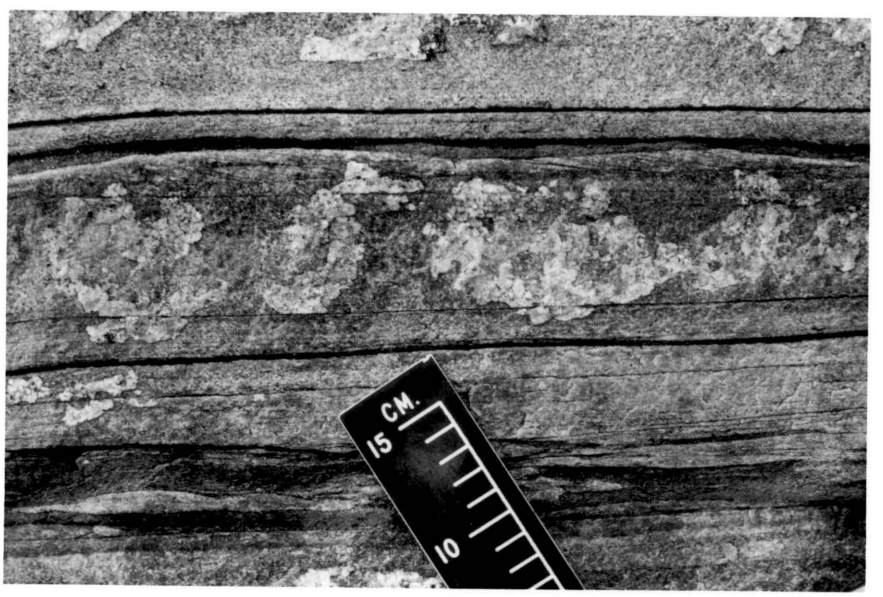

Figure 28: Tabular, planar-laminated sandstone cosets capped by wave current ripples, R5 Member, Rinconada Formation, northwestern Picuris range. The wave current ripples display high vertical form index and low ripple symmetry index whereas cross laminations indicate unidirectional transport from left to right.

Figure 29: Measured section through distal outer-shelf facies in R5 Member, Rinconada Formation, eastern Pecos belt (see Fig. 16 for location of section).

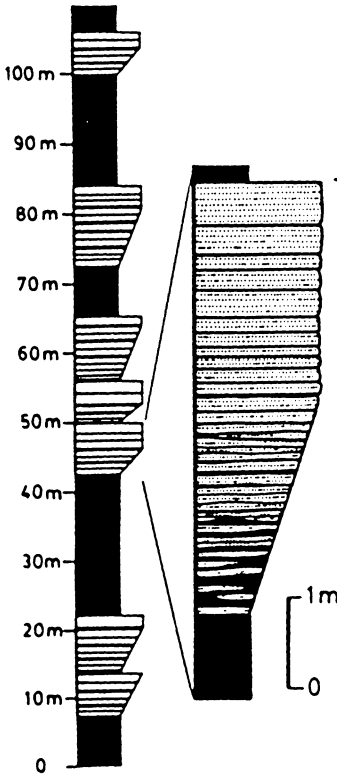

DESCRIPTION	INTERPRETATION	
Tabular, planar-laminated sandstones showing upward-increase in set thickness.	Suspension sedimentation of storm sheet sands under flat bed conditions from waning gradient currents.	DISTAL OUTER SHELF
Planar-laminated sandstones less than 1 cm thick interlayered with laterally-persistent mudstones.	Distal storm sheet sands deposited from suspension by waning gradient currents.	
Mudstone	Pelagic muds.	

draped by thin mudstone veneers (Figs. 27 and 28). In contrast, symmetrical ripples are absent in the R5 Member in the eastern Pecos belt (Fig. 29).

Small-Scale Trough Cross-Bedded Sandstone Facies

In the upper Ortega Quartzite and R3 and upper R5 Members of the Rinconada Formation, small-scale trough cross beds, less than 18 cm thick, are arranged in cosets that overlie basal scours into underlying tabular cross bedded and planar-laminated sandstone facies (Figs. 17d, 23b, 27 and 30). Generally the lower contact of trough cross-bedded cosets defines an irregular erosive surface (Fig. 23b), similar to the type 1 scour surface described by Anderton (1976). The small-scale trough cross beds in figure 27 clearly occupy broad shallow channels and are equivalent to type 2 scour surfaces defined by Anderton (1976). Trough cross beds are unidirectional to the south; these deviate from modes of tabular-planar cross beds of tidal origin in the upper Ortega Quartzite (Fig. 17d) and R3 Member (Fig. 23).

Interlayered Mudstone and Planar-Laminated Sandstone Facies

Planar-laminated siltstones and very fine-grained sandstones, from less than 1 mm and rarely up to 2 cm thick (Fig. 31) are interlayered with mudstones throughout the mudstone dominated R1-2, R4 and R6 Members of the Rinconada Formation, and in the Piedra Lumbre Formation. Furthermore, the facies exists in the lowermost R3 Member

Figure 30: Trough cross beds scouring into tabular sandstone units in R3 Member, southern Picuris range (see Fig. 23b).

Figure 31: Interlayered mudstone and planar-laminated very fine-grained sandstone, R6 Member, Rinconada Formation, southwestern Picuris range.

and the R5 Member in the Pecos belt (Fig. 16). Sandstone to mudstone ratios vary from less than 1:10 to 5:1 in instances where thinly-bedded sandstones and siltstones dominate with thin intervening mudstone veneers. Sandstone layers thicker than 3 mm persist laterally for several tens of meters. Thinner units extend for only a few meters, appearing as sandstone streaks within mudstones. Lower set-boundaries are sharp but exhibit no evidence of scouring. Individual laminations appear massive internally but show no evidence of grading.

Interlayered Mudstone and Cross- and Parallel-Laminated Sandstone Facies

Associated with the planar-laminated sandstones and siltstones in the lowermost R3 Member and in the R5 Member in the Picuris and Pecos belts are a suite of small ripples and cross laminated, very fine-grained sandstones and siltstones (Fig. 32). Planar-laminated siltstones with scoured upper sets display external symmetrical ripple geometry and are in turn draped by form-concordant, parallel-laminated siltstones (Fig. 32a). This structure is analogous to small-scale hummocky cross stratification (HCS) described by Dott and Bourgeois (1982). Similar form-concordant, parallel-laminated siltstones drape ripples with simple internal structure (Fig. 32b) and are likewise produced by oscillatory flow (Allen, 1981). Examples of large hummocky cross stratification are very rare in the Ortega Group. Planar-laminated sandstones with a scoured upper surface, draped by parallel-laminated sandstones which are capped by small-scale wave ripples are confined to the lower R3 Member (Fig. 23c).

Figure 32: Cross-laminated, very fine-grained sandstones and siltstones of wave origin from Rinconada Formation. (a) Planar-laminated siltstones scoured to produce ripple geometry and in turn draped by form-concordant, parallel-laminated siltstone; (b) Cross-laminated siltstone, with simple internal structure, later draped by parallel-laminated form-concordant siltstone. Both (a) and (b) from transition between R2 and R3 Members in southwestern Pecos belt); (c) Bidirectional, bundled lenses with irregular lower set boundaries, R6 Member, southwestern Picuris range; (d) Small-scale three-dimensional ripples in siltstone, R6 Member southwestern Picuris range; (e) Cross-laminated sandstone draped by foresets of overlying cross-laminated set, R4 Member, northern Picuris range.

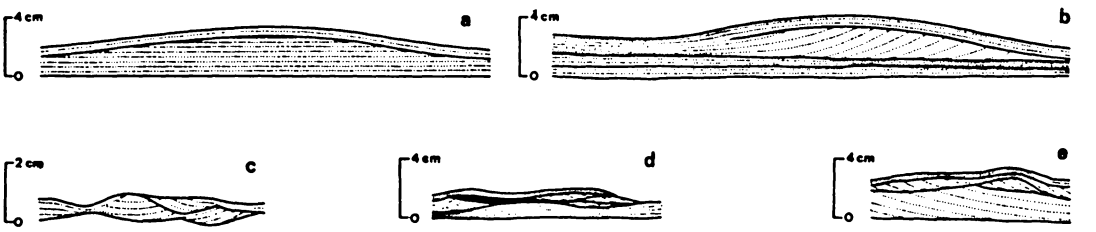
4 cm
a
4 cm
b
2 cm
c
4 cm
d
4 cm
e

Other wave-generated structures in this facies include cross laminated sandstones with bidirectional bundled lenses and irregular lower setboundaries (Fig. 32c) akin to wave ripples described by de Raaf et al. (1977). Sandstone lenses with external ripple geometries but devoid of cross laminations, exhibit internal laminations which pinch and swell laterally (Fig. 32d). These are analogous to larger scale sedimentary structures produced by orbital flow (Dott and Bougeois, 1982). Finally, cross laminations draped by foresets of the following cross laminated set (Fig. 32e) are similar to wave-generated structures described by Allen (1981). In plan view ripple crests are straight, sharp and may bifurcate (Fig. 33). Ripple symmetry indices (cf. Allen, 1982a, p. 449) reach 1.7 but are commonly closer to 1.0. Vertical form index of ripples (cf. Allen, 1982a, p. 446) lie between 6 and 9. Both symmetry index and vertical form index are characteristic of ripples of wave origin.

Associated with the interlayered mudstones and planar- and cross-laminated sandstones in the R6 Member in the western Picuris mountains are small sandstone dikelets which protrude from the base and also from the upper surface of thin sandstone layers into enclosing mudstone (Fig. 34). The dikelets are ptygmatically folded in cross section and display linear subparallel to random cross-cutting relationships with other dikelets on bedding surfaces. Similar features have been described by Donovan and Foster (1972), Anderton (1976), and Grotzinger (1981) and interpreted as subaqueous synaeresis cracks. Although mechanisms for producing synaeresis cracks are not fully

Figure 33: Oblique view of wave-generated symmetrical ripples with straight bifurcating crests, R4 Member, Rinconada Formation, western Picuris range. Note mudstone drapes, preserved as garnet schists, within troughs between ripple crests.

Figure 34: Synaeresis cracks and sandstone filled gutter casts (bottom center) associated with interlayered mudstone and planar- and cross-laminated facies association, R6 Member, Rinconada Formation, western Picuris range.

understood, the above criteria distinguish those in the Ortega Group from desiccation cracks.

Small-scale, narrow and deep, sand-filled channels scouring into mudstones are associated with synaeresis cracks (Fig. 34). The sandstones are laminated and show asymmetrical infilling of channels. Whitaker (1973) has described similar structures and termed them gutter casts. Although Baldwin and Johnson (1977) and Clifton (1983) used deep, narrow channels as positive indicators of emergence, Whitaker (1973) related the gutter casts to subaqueous scours caused by helicoidal currents into a cohesive muddy substrate. Goldring and Aigner (1982) also favor a subaqueous origin for gutter casts and attribute the helicoidal currents to episodic storm events.

Interpretation of the Storm-Dominated Facies Association

The origin of planar lamination in sandstones is difficult to assess because its mode of formation is variable and poorly understood (Turner, 1981). Association of tabular planar-laminated sandstones and thin interlayered mudstones in the Rinconada Formation and absence of structures indicative of subaerial exposure or current reworking in much of the R5 Member suggests that the tabular, planar-laminated sandstones were deposited below the depth of tidal reworking. The simple flow regime concept presented by Harms et al. (1982) for sand particles transported by saltation cannot be applied in this instance. Planar-laminated sandstones in the Ortega Group are too fine grained to be the product of "Lower Plane Bed" conditions whereas water depths

were too great to achieve upper flow regime conditions necessary for "Upper Plane Beds." Hamblin and Walker (1979) and Hobday and Morton (1984) describe ancient shallow-water turbidites of storm affinity deposited below storm wave base in which planar-laminated sandstones form part of a Bouma bc sequence (cf. Bouma, 1962). In the Rinconada Formation, planar-laminated sandstones are capped only by wave-generated symmetrical ripples and therefore genetic units of parallel-laminated and cross-laminated sandstones draped by mudstones cannot be equated with bce turbidite beds.

Reineck and Singh (1972) have documented planar-laminated sands in the North Sea in water depths exceeding 22 m. They argue that during storms sand is taken into suspension by turbulence and deposited as planar-laminated layers as storms abate. Aigner and Reineck (1982) attribute the origin of planar-laminated sands to suspension sedimentation from offshore-directed gradient currents. Gradient flows are driven by the hydraulic gradient developed across continental shelves in response to the water body amassed along coastlines during storms (Allen, 1982b, p. 472-481). Whereas surface currents are driven shoreward in response to high wind shear, bottom currents up to 150 cm/sec transport fine-grained sand offshore in suspension (Aigner and Reineck, 1982 after Gienapp, 1973). Reineck and Singh (1972) have reproduced planar-laminated sands in flumes where sand is deposited from suspension at current velocities of 16-20 cm/sec. Deposition from suspension under conditions of moderate bed shear is invoked for the tabular planar laminated sandstone facies.

Thin, planar-laminated sandstones and siltstones in the interlayered mudstone and planar-laminated sandstone facies are interpreted as distal equivalents of the tabular planar-laminated sandstone facies. The thin planar-laminated sandstones were deposited during episodic storm events whereas mudstones represent background suspension sedimentation during fair-weather conditions.

Mature, quartz-pebble conglomerates capping the large-scale trough cross bedded and meter-scale tabular cosets in the tide-dominated facies association (Figs. 19 and 22) are also considered to be the products of storms and represent winnowed lags remaining on the upper surface of tidal sand bodies after finer sand was entrained into the water column by storm waves and removed by offshore directed gradient currents. Large-scale cross beds capped by mature, winnowed conglomerate lags are considered to be an important criterion for differentiating shallow-marine from fluvial sediments in the absence of fossils (Reading, personal communication, 1980). Similar winnowed pebble lags of storm origin are reported from the Jura Quartzite shelf succession (Anderton, 1976).

The departure between paleocurrent trends of small trough cross beds and tabular-planar cross bedding of tidal origin (Fig. 25) implies that a tidal origin for the trough cross beds is unlikely. The close association between trough cross beds and tabular parallel-laminated sandstones deposited by storm-induced gradient flows suggests a similar origin for the two facies. In the German Bight, Aigner and Reineck (1982) identified broad shallow channels scoured by gradient currents

which were subsequently infilled by offshore-migrating dunes. In addition, small ripples and sheet sands were found in and adjacent to the channels.

Wave ripples capping planar-laminated sandstones in the Picuris, Truchas and Pecos belts indicate that waves modified the upper surface of sheet sands as storms abated (Fig. 23c and 27). The presence of wave ripples imply that sedimentation took place above storm wave base.

Depositional Model for the Ortega Group

The preceding facies analysis has shown that tidal, wave and storm processes were active during deposition of the Ortega Group. No evidence of subaerial exposure exists in the Ortega Group and consequently the sediments are interpreted as subtidal shelf deposits. Harms et al. (1982) have subdivided the continental shelf environment into three separate zones based on the dominant depositional process operative in each zone. Along tide-influenced coasts the nearshore and inner shelf zones are dominated by tidal processes. The outer shelf zone, below depths of 50 to 200 m, is affected by intruding oceanic currents and major storms. Adopting this scenario for the Ortega Group, the tide-dominated facies association is considered to have accumulated on the inner shelf and storm dominated facies association mainly on the outer shelf. The absence of unconformities or major breaks in the Ortega Group stratigraphy implies that laterally coexisting sedimentary facies may be inferred from the vertical stacking of facies in Figures 17, 23, 27 and 29.

The Jawbone Syncline and the R3 and R5 Members in the Picuris mountains contain complete sections of tide-dominated facies. Upward-fining of sediments and upward thinning of bedding in the Jawbone Syncline indicates that the Ortega Quartzite is overall transgressive (Fig. 17). In contrast, the R3 Member (Fig. 23) as well as the R5 Member are upward coarsening and upward thickening and clearly represents progradational intervals within the overall transgressive sequence. The most proximal facies in the tide-dominated facies association are large-scale dunes (Fig. 19) which pass seaward into large-scale sand wave cosets (Fig. 20 and 21) and medium- and small-scale sand waves (Figs. 17d and 23a). Transition from tide- generated large dunes to sand waves which decrease progressively in size basinward, reflects a decrease in tidal energy across the inner shelf (Fig. 35a). During slack water periods within the tidal rhythm fair-weather waves rework the upper surface of tidal sands.

The sandy, tide-dominated inner shelf can be subdivided into proximal and distal zones based on subordinate storm processes affecting the inner shelf. On the proximal inner shelf, storm processes are erosional. Here storm waves entrain sand into the water column leaving behind winnowed conglomerate lags (Fig. 22). In addition, offshore directed gradient currents scour broad shallow channels on the inner shelf while transporting finer sand in suspension onto more distal reaches of the shelf (Fig. 35b). On the distal inner shelf, storm processes deposit hummocky cross-stratified and tabular, planar-laminated sheet sandstones (Figs. 23b and 23c). Scarcity of HCS on the

Figure 35: Depositional model for the Ortega Group. (a) Spatial relationship between recognized subenvironments during fair-weather, tide-dominated conditions. (b) Spatial relationship between storm-produced facies within the proximal and distal inner- and outer-shelf zones. SWB = Storm Wave Base.

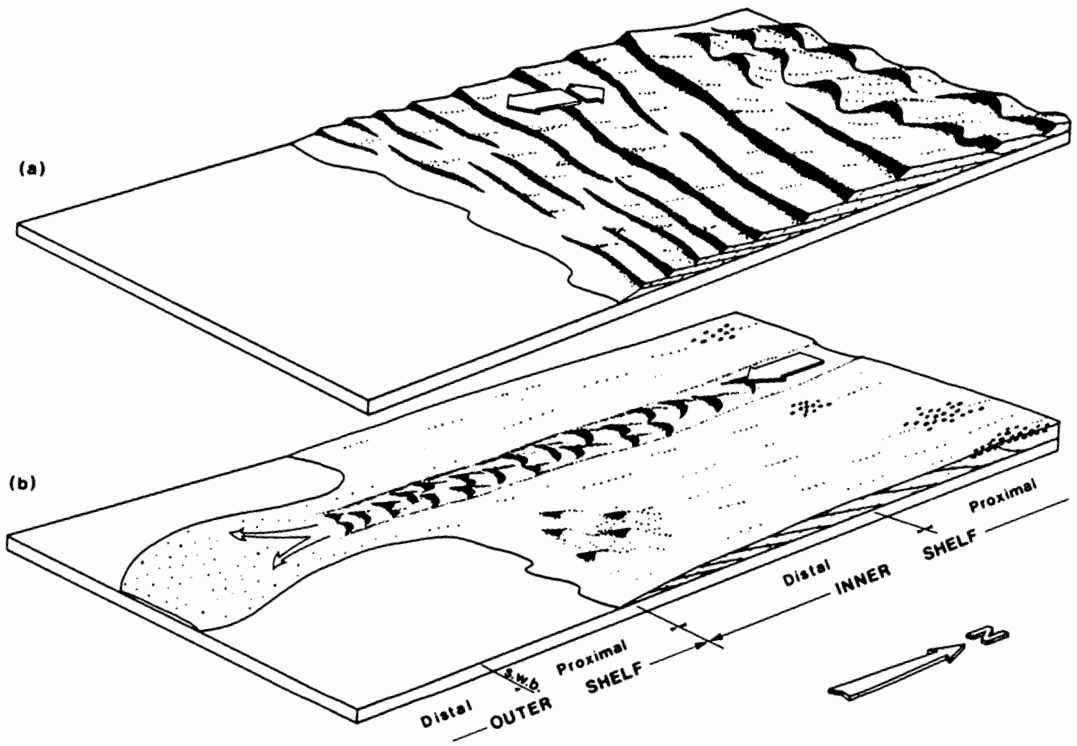
(a)
(b)
Proximal
SHELF
Distal
INNER
Proximal
SHELF
Distal
OUTER

storm-influenced inner shelf is attributed to day-by-day reworking by the dominating tidal currents. Storm-deposited sands are modified by tidal processes within a few days and therefore have a low preservation potential on tide-dominated shelves (Butman et al., 1979).

The storm dominated facies association shows no evidence of tidal processes and therefore is interpreted as an outer-shelf sequence which accumulated basinwards of the effects of tides. In the R1-R2, R4 and R6 Members, Rinconada Formation, and Piedra Lumbre Formation no systematic relationship exists between the fine grained facies. Consequently, depositional sequences are not recognized within these mudstone-dominated units. In the R5 Member in the Picuris and Pecos Belts and basal R3 Member in the Pecos Belt, in contrast, the storm-dominated facies are developed in upward-coarsening and upward-thickening packages between .1 and 11 m thick (Fig. 27 and 29). In the Picuris range and western Pecos belt, complete upward-thickening cycles commence with mudstone which pass upwards into planar-laminated sandstone, interlayered mudstones and planar- and cross-laminated sandstones. Cycles are capped by cosets of tabular, planar-laminated sandstones with wave reworked upper setboundaries and rare mudstone partings (Fig. 28). Broad shallow channels, filled by trough cross-bedded sandstones, scour into the amalgamated tabular cosets at the top of upward-coarsening cycles (Fig. 27). In the eastern Pecos belt, in contrast, upward-thickening cycles in the R5 Member are devoid of traction produced structures. Here cycles pass from mudstones into interlayered mudstones and thin planar-laminated

sandstones and are capped by cosets of thicker, tabular, planar-laminated sandstones (Fig. 29).

Individual upward-thickening cycles cannot be correlated between sections, and consequently, cycles are considered laterally discontinous rather than sheet-like. The upward-increase in bed thickness within cycles is a result of progradation of individual sand lobes on the outer shelf (Fig. 35b). From the facies analysis it has been shown that facies which comprise upward-thickening cycles were deposited by storm-induced gradient currents. On the proximal outer shelf, sand lobes are characterized by broad, shallow channels scoured by gradient flows and filled by offshore-directed dunes. Adjacent to channels, sheet sands were deposited from suspension by gradient currents. The upper surface of sheet sands were reworked by storm waves producing oscillation ripples. Proximity to the sand source on the proximal outer shelf caused sand lobes to become amalgamated (Fig. 36a). On distal portions of sand lobes gradient currents were less intense. Broad scour channels were thus absent and sheet sands became progressively thinner and less amalgamated outwards on the shelf. Secondary wave reworking of storm sands was absent on distal outer shelf sand lobes and consequently deposition must have occured below storm wave base (Figs. 35b and 36b).

Brenchley and Newall (1982) have recognized shallow-marine sand lobes in the middle Ordovician of Wales and attribute their formation to offshore-directed storm rip currents. They found that sandstones within depositional lobes are hummocky cross-stratified in contrast to

Figure 36: Schematic representation of outer shelf sand lobes. (a) Proximal outer shelf has sand lobes dissected by storm-induced gradient currents (arrow). Proximity to sand source results in amalgamation of sand lobes. (b). Discrete sand lobes on distal reaches of outer shelf encased within pelagic mudsones.

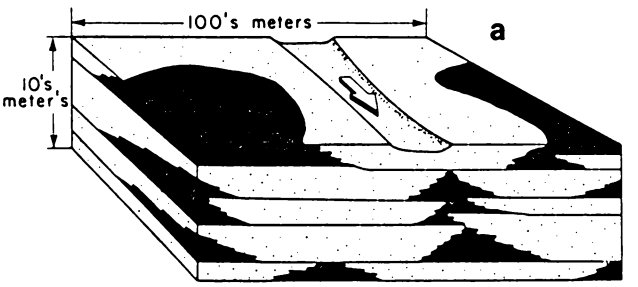
100's meters
a
10's
meter's

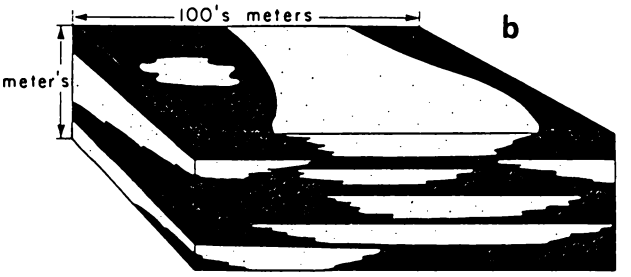
100's meters
b
meter's

dominantly tabular planar-laminated beds in the R5 Member. Aigner and Reineck (1982) identified sand lobes of storm affinity in the Helgoland Bight and developed a depositional model which included cycles similar to those illustrated in figures 27 and 29. Repeated supply of sand to a single lobe by gradient currents is thought to be governed by coastline configuration. Storm surges in the Helgoland Bight are exaggerated by funneling of water into the estuary south of Busum and into the Elbe River estuary. The storm-induced gradient currents are likely to be most intense on the shelf adjacent to estuaries. In the case of the North Sea, gradient currents transport sand from the estuary to more than 50 Km offshore (Aigner and Reineck, 1982). Storm surges adjacent to the Norton Sound, in Alaska, carry sand more than 100 miles out onto the Bering shelf (Nelson, 1982). Offshore-directed, storm-induced currents therefore provide a viable process for transporting sand from the near shore regime to distal reaches of the shelf.

The lack of shallow-marine turbidites, such as those described by Hamblin and Walker (1979) and Hobday and Morton (1984), in the outer-shelf facies association, and in particular in those facies which accumulated below storm wave base (Fig. 29), is attributed to very low shelf gradients during deposition of the Ortega Group. Turbidity currents are driven by gravitational forces and therefore require relatively steep gradients in order to develop (Fig. 37a). As shelf gradients decrease, turbidity currents become weaker and more diffuse. Less complete Bouma sequences are deposited with no evidence of intense scouring prior to deposition (Hayes, 1967; Fig. 37b). Gradient

Figure 37: Depositional sequences resulting from storm-induced currents as a function of shelf gradient. These sequences are preserved below storm wave base in shallow-water shelf environments.

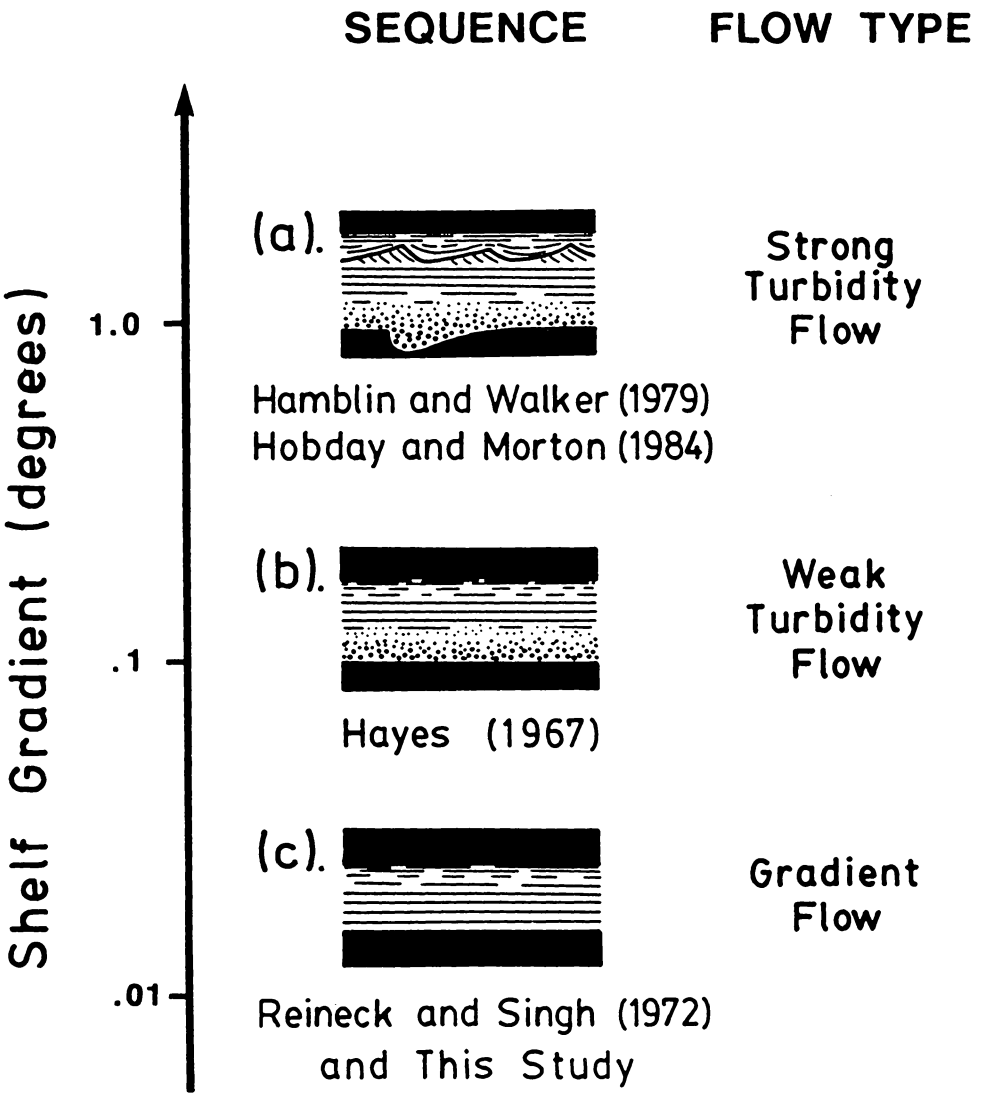
SEQUENCE
FLOW TYPE
Shelf Gradient (degrees)
1.0
.1
.01
(a).
Strong Turbidity Flow
Hamblin and Walker (1979)
Hobday and Morton (1984)
(b).
Weak Turbidity Flow
Hayes (1967)
(c).
Gradient Flow
Reineck and Singh (1972)
and This Study

currents, in contrast, are largely independent of shelf gradient and result in the development of thin, planar-laminated sands which may be equated with a bd turbidite unit (Fig. 37c).

Conclusion

A detailed facies analysis has shown that the Ortega Group accumulated on a shallow-marine shelf affected by tidal, storm and wave processes. Facies distributions and paleocurrent data indicate that the shelf sloped gently to the south and southeast. The basin experienced prolonged subsidence matched by continous supply of sediment and the sequence represents an overall transgression which culminated in drowning of the outer shelf and subsequent onlap of black basinal muds from the southeast (Fig. 16).

Absence of unconformities and major breaks in the stratigraphy between the tide- and storm-dominated facies associations suggests that all facies coexisted across the shelf. Vertical transition from tide- to storm-dominated sedimentation therefore does not represent a change in depositional style with time (cf. Klein, 1982). Rather, tidal processes prevailed on the shallow inner shelf whereas storm processes dominated on the deeper-water outer shelf.

The inner shelf was mainly a sandy environment subjected to tidal and subordinate storm and wave processes. Sand was eroded by storm waves on the proximal inner shelf and transported basinward by storm-induced gradient currents. On the distal inner shelf storm processes were depositional rather than erosive. These storm deposits were,

however, reworked by day-to-day tidal currents and to a lesser extent by fair-weather waves. Beyond the effect of tides, on the muddier outer shelf, deposition of sand was strictly by storm processes. Sand was transported onto the outer shelf by gradient currents and deposited as discrete lobes. On the proximal outer shelf the upper surface of storm sands were reworked by wave processes whereas storm deposits on the distal outer shelf remained unmodified. The absence of shallow water turbidites in the outer shelf succession reflects very low shelf gradients during accumulation of the Ortega Group. The lack of any evidence in the sequence for steep slope gradients suggests that the shelf break lay somewhere to the southeast of the study area.

REFERENCES

Aigner, T. and Reineck, H.E., 1982, Proximality trends in modern storm sands from the Helgoland Bight (North Sea) and their implications for basin analysis: Senckenbergiana Maritima, v. 14, p. 183-215.

Allen, J.R.L., 1968, Current Ripples: North Holland, Amsterdam, 433 p.

Allen, J.R.L., 1980, Sand waves: A model of origin and internal structure: Sedimentary Geology, v. 26, p. 281-328.

Allen, J.R.L., 1982a, Sedimentary Structures: Their Character and Physical Basis, Volume 1: Elsevier, Amsterdam, 593 p.

Allen, J.R.L., 1982b, Sedimentary Structures: Their Character and Physical Basis, Volume 2: Elsevier, Amsterdam, 663 p.

Allen, P.A. 1981, Wave-generated structures in the Devonian lacustrine sediments of south-east Shetland and ancient wave conditions: Sedimentology, v. 28, p. 369-379.

Anderson, C.A., Blacet, P.M., Silver, L.T. and Stern, T.W., 1971, Revision of the Precambrian stratigraphy in the Prescott-Jerome area, Yavapai County, Arizona: U.S. Geological Survey Bull. 1324c, p. 1-16.

Anderton, R., 1976. Tidal-shelf sedimentation: an example from the scottish Dalradian: Sedimentology, v. 23, p. 429-458.

Baldwin, C.T. and Johnson, H.D., 1977, Sandstone mounds and associated facies sequences in some Late Precambrian and Cambro-Ordovician inshore tidal flat lagoonal deposits: Sedimentology, v. 24, p. 801-818.

Bally, A.W., 1981, Atlantic-type margins. In Geology of Passive Continental Margins: Am. Assoc. Petroleum Geologists Education Course Note Series 19, p. 1-48.

Bambach, R.K. and Sepkoski, J.J., 1979, The increase influence of biologic activity on sedimentary stratification through time (abs.): Geol. Soc. America Abstracts with Programs, v. 11, p. 383.

Banks, N.L. 1973, Tide-dominated offshore sedimentation, Lower Cambrian, north Norway: Sedimentology, v. 20, p. 213-228.

Barker, F., 1958, Precambrian and Tertiary geology of Las Tablas quadrangle, New Mexico: New Mexico Bureau Mines Mineral Resources, Bull. 45, 104 p.

Beaumont, c., Keen, C.E. and Boutilier, R., 1982, A comparison of foreland and rift margin sedimentary basins: Phil. Trans. R. Soc. Lond., v. 305, p.295-317.

Bickford, M.E. and Boardman, S.J., in review, A Proterozoic volcano-plutonic terrane, Gunnison and Salida areas, Colorado:

Bicle, M.J., 1978, Heat loss from the earth: A constraint on Archean tectonics from the relation between geothermal gradients and the rate of plate production: Earth and Planetary Sci. Letters, v. 40, p. 301-315.

Bingler, E.C., 1968, Geology and mineral resources of Rio Arriba county, New Mexico: New Mex. Bureau Mines Mineral Resources, Bull. 91, 158 p.

Bond, G.C. and Kominz, M.A., 1984, Construction of tectonic subsidence curves for the Early Paleozoic miogeocline, southern Canadian Rocky Mountains: Implications for subsidence mechanisms, age of breakup, and crustal thinning: Geol. Soc. America Bull., v. 95, p. 155-173.

Bott, M.H.P., 1979, Subsidence mechanisms at passive continental margins, in , Watkins, J.S., Montadert, L., and Dickerson, P.W. (eds.), Geological and Geophysical Investigations of Continental Margins: Am. Assoc. Petroleum Geologists Memoir 29, p. 3-9.

Bouma, A.H., 1962, Sedimentology of Some Flysch Deposits: Elsevier, Amsterdam, 168 p.

Bowring, S.A. and Condie, K.C., 1982, U-Pb zircon ages from northern and central New Mexico (abs.): Geol. Soc. America Abstracts with Programs, Rocky Mountain Section, v. 14, p. 304.

Brenchley, P.J. and Newall, G., 1982, Storm-influenced inner-shelf sand lobes in the Caradoc (Ordovician) of Shropshire, England: Jour. Sed. Petrology, v. 52, p. 1257-1269.

Burchfiel, B.C. and Davis, G.A., 1975, Nature and controls of Cordilleran orogenesis, western United States: Extensions of an earlier synthesis: Am. Jour. Sci., v. 275-A, p. 363-396.

Burns, L.K. and Wobus, R.A., 1983, Correlations and revisions of precambrian stratigraphy, Needle Mountains, southwest Colorado,

and Tusas Mountains, north-central New Mexico (abs.): Geol. Soc. America Abstracts with Programs, v. 15, p. 424.

Butman, B., Noble, M. and Folger, D.W., 1979, Long term observations of bottom sediment movement on the Mid Atlantic continental Shelf: Jour. Geophysical Res., v. 84, p. 1182-1205.

Button, A., 1973, A regional study of the stratigraphy and development of the Transvaal basin in the eastern and northern Transvaal: Unpubl. PhD Thesis, Univ. of the Witwatersrand, Johannesburg, South africa.

Button, A. and Vos, R.G., 1977, Subtidal and intertidal clastic and carbonate sedimentation in a macrotidal environment: An example from the Lower Proterozoic of South Africa: Sedimentary Geology, v. 18, p. 175-200.

Cant, D.J., 1978, Development of a facies model for sandy braided river sedimentation: Comparison of the South Saskatchewan River and the Battery Point Formation, in Miall, A.D. (ed.), Fluvial Sedimentology: Canadian Soc. Petroleum Geologists Memoir 5, p. 627-639.

Clifton, H.E., 1983, Discrimination between subtidal and intertidal facies in Pleistocene deposits, Willapa Bay, Washington: Jour. Sed. Petrology, v. 53, p. 353-369.

Condie, K.C., 1982, Plate-tectonics model for Proterozoic continental accretion in the southwestern United States: Geology, v. 10, p. 37-42.

Condie, K.C. and McCrink, T.P., 1982, Geochemistry of Proterozoic volcanic rocks from the Gold Hill-Weeler Peak area, northern New Mexico: Precambrian Research, v. 19, p. 141-166.

Condie, K.C. and Nuter, J.A., 1981, Geochemistry of the Dubois greenstone succession: An Early Proterozoic bimodal volcanic association in west-central Colorado: Precambrian Research, v. 15, p. 131-155.

Cotter, E., 1983, Shelf, paralic, and fluvial environments and eustatic sea-level fluctuations in the origin of the Tuscarora Formation (Lower Silurian) of central Pennsylvania: Jour. Sed. Petrology, v. 53, p. 25-49.

Creager, J.S. and Sternberg, R.W., 1972, Some specific problems in understanding bottom sediment distribution and dispersal on the continental shelf, in Swift, D.J.P., Duane, D.B. and Pilkey, O.H. (eds.), Shelf Sediment Transport: Process and Pattern: Dowden, Hutchinson and Ross inc., Stroudsburg, p. 347-362.

DePaolo, D.J., 1981, Neodymium isotopes in the Colorado Front Range and crust-mantle evolution in the Proterozoic: Nature, v. 291, p. 193-196.

de Raaf, J.M.F., Boersma, J.R. and van Gelder, A., 1977, Wave-generated structures and sequences from a shallow marine succession, Lower Carboniferous, County Cork, Ireland: Sedimentology, v. 24, p. 451-483.

Donovan, R.N. and Foster, R.J., 1972, Subaqueous shrinkage cracks from the Caithness Flagstone Series (Middle Devonian) of north Scotland: Jour. Sed. Petrology, v. 42, p. 309-317.

Dott, R.H., 1983, The Proterozoic red quartzite enigma in the north-central United States: Solved by plate collision? Geol. Soc. America Memoir 160, p. 129-141.

Dott, R.H. and Bourgeois, J., 1982, Hummocky stratification: Significance of its variable bedding sequences: Geol. Soc. America Bull., v. 93, p. 663-680.

Engel, A.E.J., 1963, Geologic evolution of North America: Science, v. 140, p. 143-152.

Eriksson, K.A., Turner, B.R. and Vos, R.G., 1981, Evidence of tidal processes from the lower of the Witwatersrand Supergroup, South Africa: Sedimentary Geology, v. 29, p. 309-325.

Fullager, P.D. and Shiver, W.S., 1973, Geochronology and petrochemistry of the Embudo Granite, New Mexico: Geol. Soc. America Bull., v. 84, p. 2705-2712.

Gienapp, H., 1973, Stromungen wahrend der sturmflut vom 2. November 1965 in der Deutchen Bucht und ihre bedeutung fur den sedimenttransport: Senckenbergiana Maritima, v. 5, p. 135-151.

Goldring, R. and Aigner, T., 1982, Scour and fill: The significance of event separation, in Einsele, G. and Seilacher, A. (eds.), Cyclic and event stratification: Springer Verlag, Berlin, p. 355-362.

Gole, C.V. and Chitale, C.V., 1966, Inland delta building activity of the Kosi River: Am. Soc. Civil Engng. Proc., Jour. Hydr. Div. 92, p. 111-126.

Grambling, J.A., 1979a, Precambrian geology of the Truchas peaks region, north-central New Mexico, and some regional implications: New Mex. Geol. Soc. Guidebook, 30th Field Conf., Santa Fe Country, p. 135-143.

Grambling, J.A., 1979b, Geology of Precambrian metamorphic rocks of the Truchas Peaks area, north-central New Mexico: Unpubl. PhD Thesis, Princeton Univ., 199 p.

Grambling, J.A., 1981, Pressures and temperatures in Precambrian metamorphic rocks: Earth Planet. Sci. Letters, v. 53, p. 63-68.

Grambling, J.A., 1984, Proterozoic isobaric surfaces and tectonism in northern and central New Mexico (abs.): Geol. Soc. America Abstracts with Programs, Rocky Mountain Sectn., v. 16, p. 222.

Grambling, J.A. and Codding, J.B., 1982, Stratigraphic and structural relationships of multiply deformed Precambrian metamorphic rocks in the Rio Mora area, New Mexico: Geol. Soc. America Bull., v. 93, p. 127-137.

Gresens, R.L. and Stensrud, H.L., 1974, Recognition of more metarhyolite occurrences in northern New Mexico and a possible Precambrian stratigraphy: Mountain Geologist, v. 11, p. 109-124.

Grotzinger, J.P., 1981, The stratigraphy and sedimentation of the Wallace Formation, northwest Montana and Idaho: Unpubl. M.S. Thesis, Univ. Montana, Missoula, 153 p.

Hamblin, A.P. and Walker, R.G., 1979, Storm-dominated shallow marine deposits: The Fernie-Kootenay (Jurassic) transition, southern Rocky Mountains: Canadian Jour. Earth Sci., v. 16, p. 1673-1690.

Harms, J.C., Southard, J.B. and Walker, R.G., 1982, Structures and sequences in clastic rocks: Soc. Econ. Paleontologists Mineralogists Short Course 9, Calgary, 251 p.

Hayes, M.O., 1967, Hurricanes as geologic agents, south Texas coast: Am. Assoc. Petroleum Geologists Bull., v. 51, p. 937-942.

Heward, A.P., 1978, Alluvial fan sequences and megasequence models: with examples from Westphalian D - Stephanian B coalfields, northern Spain, in Miall, A.D. (ed.), Fluvial Sedimentology: Canadian Soc. Petroleum Geologists Memoir 5, p. 669-702.

High, L.R. and Picard, M.D., 1974, Reliability of cross-stratification types as paleocurrent indicators in fluvial rocks: Jour. Sed. Petrology, v. 44, p. 158-168.

Hiscott, R.N., 1982, Tidal deposits of the Lower Cambrian Rnadom Formation, eastern Newfoundland: Facies and paleoenvironments: Canadian Jour. Earth Sci., v. 19, p. 2028-2042.

Hobday, D.K. and Morton, R.A., 1984, Lower Cretaceous shelf storm-deposits, northeast Texas, in Siliciclastic Shelf Sediments: Soc. Econ. Paleontologists Mineralogists Spec. Publ. 34, p. 205-213.

Hobday, D.K. and Tankard, A.J. 1978, Transgressive-barrier and shallow shelf interpretation of the Lower Paleozoic Peninsular Formation, South Africa: Geol. Soc. America Bull., v. 89, p. 1733-1744.

Holcombe, R.J. and Callender, J.F., 1982, Structural analysis and stratigraphic problems of Precambrian rocks of the Picuris range, New Mexico: Geol. Soc. America Bull., v. 93, p. 138-149.

Holdaway, M.J., 1978, Significance of chloritoid-bearing and staurolite-bearing rocks in the Picuris range, New Mexico: Geol. Soc. America Bull., v. 89, p. 1404-1414.

Hoffman, P.F. and Bowring, S.A., 1984, Short-lived 1.9 Ga. continental margin and its destruction, Wopmay Orogen, northwest Canada: Geology, v. 12, p. 68-72.

Hoffman, P.F., Dewey, J.F. and Burke, K., 1974, Aulacogens and their genetic relation to geosynclines, with a Proterozoic example from Great Slave Lake, Canada, in Modern and Ancient Geosynclinal Sedimentation: Soc. Econ. Paleontologists Mineralogists Spec. Publ. 19, p. 38-55.

Homewood, P. and Allen, P., 1981, Wave-, tide-, and current-controlled sandbodies of Miocene Molasse, western Switzerland: Am. Assoc. Petroleum Geologists Bull., v. 65, p. 2534-2545.

Hubert, J.F., 1962, A zircon-tourmaline-rutile maturity index and interdependence of composition of heavy mineral assemblages with the gross composition and texture of sandstones: Jour. Sed. Petrology, v. 32, p. 440-450.

Klein, G. de V., 1970a, Tidal origin of a Precambrian quartzite - the lower fine-grained quartzite (Middle Daldadian) of Islay, Scotland: Jour. Sed. Petrology, v 40, p. 973-985.

Klein, G. de V., 1970b, Depositional and dispersal dynamics of intertidal sand bars: Jour. Sed. Petrol., v. 40, p. 1095-1127.

Klein, G. de V., 1982, Probable sequential arrangement of depositional systems on cratons: Geology, v. 10, p. 17-22.

Klich, I. and Robertson, J.M., 1983, Proterozoic pillow basalts and pillow breccias from the Pecos Greenstone Belt, Sangre de Cristo Mountains, north-central New Mexico (abs.): Geol. Soc. America Abstracts with Programs, Rocky Mountain and Cordilleran Sects., v. 15, p.423.

Lanphere, M.A., Irwin, W.P. and Hotz, P.E., 1968, Isotopic age of the Nevadan orogeny and older plutonic and metamorphic events in the Klamath Mountains, California: Geol. Soc. America Bull., v. 79, p. 1027-1052.

Long, P.E. 1974, Contrasting types of Precambrian granitic rocks in the Dixon-Penasco area, northern New Mexico. New Mexico Geol. Soc. Guidebook, 25th Field Conf., Ghost Ranch, p. 101-108.

Long, P.E., 1976, Precambrian granitic rocks of the Dixon-Penasco area, northern New Mexico: A study in contrasts: Unpubl. PhD thesis, Stanford University, 533 p.

McCave, I.N., 1970, Deposition of fine grained suspended sediment from tidal currents: Jour. Geophysical Research, v. 75, p. 4151-4159.

McCave, I.N., 1973, The sedimentology of a transgression: Portland Point and Cooksburg Members (Middle Devonian), New York State: Jour. Sed. Petrology, v. 43, p. 484-504.

McKee, E.D., Crosby, E.J. and Berryhill, H.L., 1967, Flood deposits, Bijou Creek, Colorado, June 1965: Jour. Sed. Petrology, v. 37, p. 829-851.

Miall, A.D., 1977, A review of the braided-river depositional environment: Earth Sci. Rev., v. 13, p. 1-62.

Miller, M.F. and Byers, C.W., 1984, Abundant and diverse Early Paleozoic infauna indicated by the stratigraphic record: Geology, v. 12, p. 40-43.

Montgomery, A., 1953, Precambrian geology of the Picuris Range, north-central New Mexico: New Mex. Bureau Mines Mineral Res., Bull. 30, 89 p.

Montgomery, A., 1963, Precambrian rocks. In Miller, J.P., Montgomery, A. and Sutherland, P.K. (eds.), Geology of Part of the Southern Sangre De Cristo Mountains, New Mexico: New Mex. Inst. Mining and Techn. Campus Station, Socorro, New Mex., Memoir 11, p. 7-20.

Nelson, C.H., 1982, Modern shallow-water graded sand layers from storm surges, Bering Shelf: A mimic of Bouma sequences and turbidite systems: Jour. Sed. Petrology., v. 52, p. 537-545.

Nielsen, K.C., 1972, Structural evolution of the Picuris Mountains, New Mexico: Unpubl. M.S. Thesis, Univ. North Carolina, Chapel Hill, 47 p.

Nielsen, K.C. and Scott, T.E., 1979, Precambrian deformational history of the Picuris Mountains, New Mexico: New Mexico Geol. Soc. Guidebook, 30th Field Conf., Santa Fe Country, p. 113-120.

Nielsen, K.C. and Scott, T.E., in prep., Precambrian deformational history and associated strain patterns in the Picuris Mountains, New Mexico.

Otvos, E.G., 1966, Sedimentary structures and depositional environments, Potsdam Formation, Upper Cambrian: Am. Assoc. Petroleum Geologists, v. 50, p. 159-165.

Pitman, W.C., 1978, The relationship between eustacy and stratigraphic sequences of passive margins: Geol. Soc. America Bull., v. 89, p. 1389-1402.

Reineck, H.E. and Singh, I.B., 1972, Genesis of laminated sands and graded rhythmites in storm-sand layers of shelf mud: Sedimentology, v. 18, p. 123-128.

Reineck, H.E. and Wunderlich, F., 1968, Classification and origin of flaser and lenticular bedding: Sedimentology, v. 11, p. 99-104.

Robertson, J.M., 1984, Geology and geochemistry of the Early Protorozoic Pecos Greenstone Belt, southern Sangre de Cristo Mountains, New Mexico (abs.): Geol. Soc. America Abstracts with Programs, Rocky Mountain Section, v. 16, p. 252.

Robertson, J.M. and Moench, R.H., 1979, The Pecos Greenstone Belt: A Proterozoic volcano-sedimentary sequence in the southern Sangre de Cristo Mountains, New Mexico: New Mex. Geol. Soc. Guidebook, 30th Field Conf., Santa Fe Country, p. 165-173.

Scott, T.E., 1980, A strain analysis of the Marquenas Quartzite and contact relationships of the Ortega-Vadito Groups: Unpubl. M.S. Thesis, Univ. of Texas at Dallas, 175 p.

Shore, P.J. and Duncan, I.J., 1983, New evidence for Precambrian plate tectonics: An 1.7 Ga melange unit in the Vadito Group of the Picuris Mountains, New Mexico: EOS, v. 64, p. 844.

Silver, L.T., 1965, Mazatzal orgeny and tectonic episodicity (abs.): Geol. Soc. America Special Paper 82, p. 185-186.

Silver, L.T., 1968, Precambrian batholiths of Arizona (abs.): Geol. Soc. America Special Paper 121, p. 558-559.

Silver, L.T., 1984, Observations on Precambrian evolution of northern New Mexico and adjacent regions (abs.): Geol. Soc. America Abstracts with Programs, Rocky Mountain Sect., v. 16, p. 256.

Silver, L.T., Anderson, C.A., Crittenden, M. and Robertson, J.M., 1977, Chronostratigraphic elements of Precambrian rocks of the southwestern and far western United States (abs.): Geol. Soc. America Abstracts with Programs, v. 9, p. 1176.

Sleep, N.H., 1976, Platform subsidence mechanism and "eustatic" sea-level changes: Tectonophysics, v. 36, p. 45-56.

Sneh, A., 1983, Desert stream sequences in the Sinai Peninsular: Jour. Sed. Petrology, v. 53, p. 1271-1279.

Soegaard, K. and Eriksson, K.A., 1983. Transition from arc volcanism to stable shelf and subsequent convergent margin sedimentation in northern New Mexico between 1.8 and 1.5 Ga. (abs.): Geol. Soc. America Abstracts with Programs, v. 15, p. 691.

Soegaard, K. and Eriksson, K.A., submitted, Evidence of tide, storm and wave interaction on a Precambrian siliciclastic shelf: The 1,700 m.y. Ortega Group, northern New Mexico: Jour. Sed. Petrology.

Stacey, J.S. and Hedlund, D.C., 1983, Lead-isotopic compositions of diverse igneous rocks and ore deposits from southwestern New Mexico and their implications for Early Proterozoic crustal evolution in the western United States: Geol. Soc. America Bull., v. 94, p. 43-57.

Tankard, A.J., Jackson, M.P.A., Eriksson, K.A., Hobday, D.K., Hunter, D.R., and Minter, W.E.L., 1982, Cructal Evolution of Southern Africa: 3.8 Billion Years of Earth History: Springer Verlag, New York, 523 p.

Thayer, C.W., 1983, Sediment-mediated biological disturbance and the evolution of marine benthos, in Trevesz, M.J.S. and McCall, P.L. (eds.), Biotic Interactions in Recent and Fossil Benthic Communities: Plenum Press, New York, p. 480-625.

Trevena, A.S., 1979, Studies in sandstone petrology: Origin of the Precambrian Mazatzal Quartzite and provenance of detrital feldspar: Unpubl. PhD Thesis, Univ. of Utah, 390 p.

Turnbridge, I.P., 1981, Sandy high-energy flood sedimentation - Some criteria for recognition, with an example from the Devonian of S.W. England: Sedimentary Geology, v. 28, p. 79-95.

Turner, B.R., 1981, Possible origin of low angle cross-strata and horizontal lamination in Beaufort Group sandstones of the southern Karoo Basin: Trans. Geol. Soc. S. Afr., v. 84, p. 193-197.

Vail, P.R., Mitchum, R.M., Jr. and Thompson, S., 1977, Seismic stratigraphy and global changes of sea level, part 4: Global cycles of relative changes in sea level, in Payton, C.E. (ed.), Seismic Stratigraphy-Applications in Hydrocarbon Exploration: Amer. Assoc. Petroleum Geol. Memoir 26, p. 83-97.

van Schmus, W.R., 1980, Chronology of igneous rocks associated with the Penokean Orogeny in Wisconsin: Geol. Soc. America Special Paper 182, p. 159-168.

van Schmuss, W.R. and Bickford, M.E., 1981, Proterozoic chronology and evolution of the midcontinent region, North America, in Kroner, A. (ed.), Precambrian Plate Tectonics: Elsevier, Amsterdam, p. 261-296.

van Schmus, W.R., Thurman, M.E. and Peterman, M.E., 1975, Geology and Rb-Sr chronology of Middle Precambrian rocks in eastern and central Wisconsin: Geol. Soc. America Bull. v. 86, p.1255-1265.

von Brunn, V. and Hobday, D.K., 1976, Early Precambrian tidal sedimentation in the Pongola Supergroup of South Africa: Jour. Sed. Petrology, v. 46, p. 670-679.

Whitaker, J.H. McD., 1973, "Gutter sasts," a new name for scour-and-fill structures: With examples from the Llandoverian of Ringerike and Malmoya, southern Norway: Norsk Geologisk Tidsskrift, v. 53, p. 403-417.

Wilson, E.D. 1939, Precambrian Mazatzal revolution in central Arizona: Geol. Soc. America Bull., v. 50, p. 1113-1164.

Wobus, R.A. and Manley, K., 1982, Reconnaissance geologic map of the Burned Mountain Quadrangle, Rio Arriba Co., New Mexico: U.S. Geol. Surv. Map MF-1409.

Appendix A

LOCATION MAPS

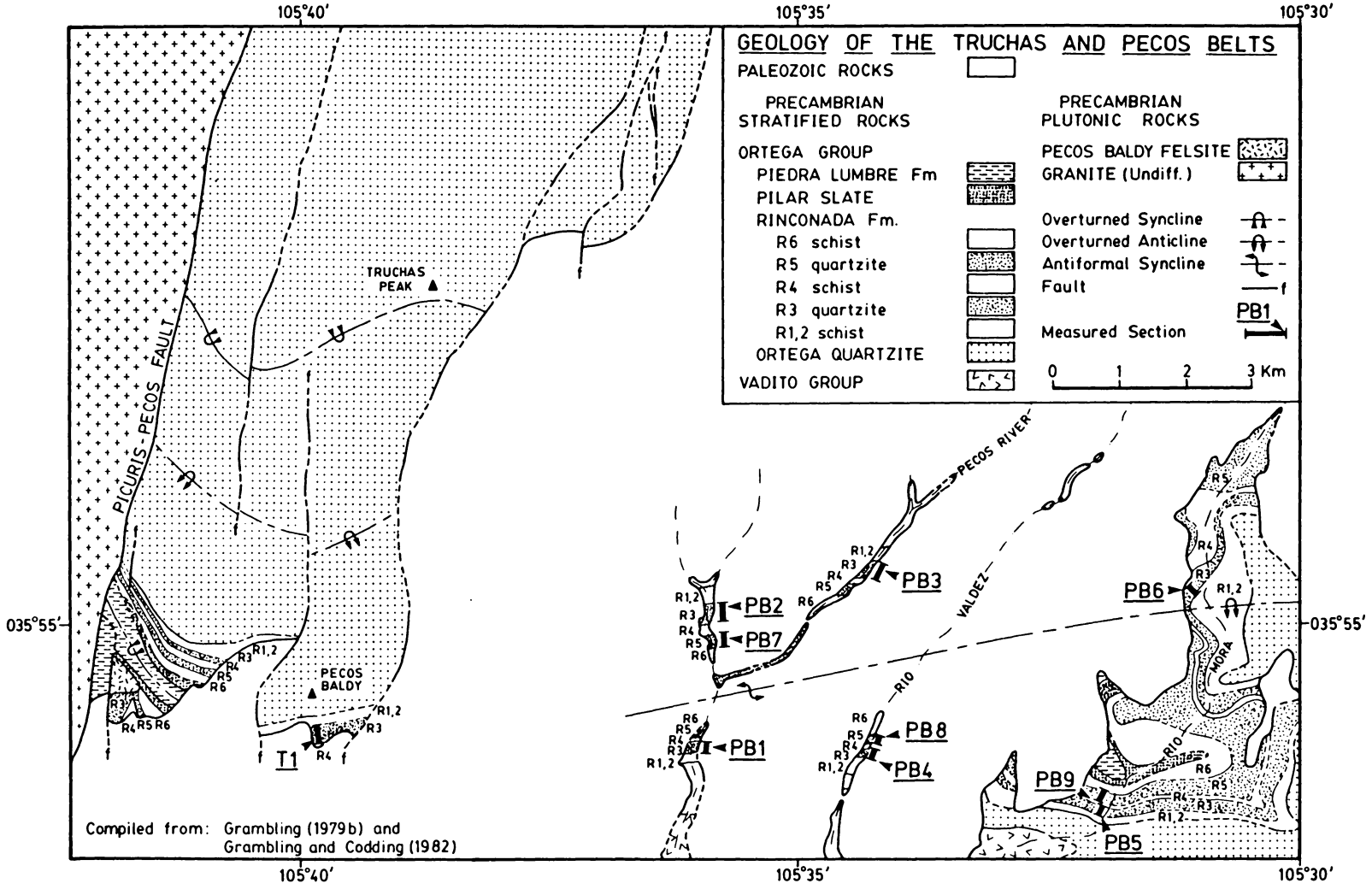
105°40'
105°35'
105°30'
035°55'
GEOLOGY OF THE TRUCHAS AND PECOS BELTS
PALEOZOIC ROCKS
PRECAMBRIAN STRATIFIED ROCKS
ORTEGA GROUP
PIEDRA LUMBRE Fm
PILAR SLATE
RINCONADA Fm.
R6 schist
R5 quartzite
R4 schist
R3 quartzite
R1,2 schist
ORTEGA QUARTZITE
VADITO GROUP
PRECAMBRIAN PLUTONIC ROCKS
PECOS BALDY FELSITE
GRANITE (Undiff.)
Overturned Syncline
Overturned Anticline
Antiformal Syncline
Fault
Measured Section
0 1 2 3 Km
TRUCHAS PEAK
PICURIS-PECOS FAULT
PECOS BALDY
T1
PECOS RIVER
VALDEZ
R10
AMORA
PB1
PB2
PB3
PB4
PB5
PB6
PB7
PB8
PB9
Compiled from: Grambling (1979b) and Grambling and Codding (1982)

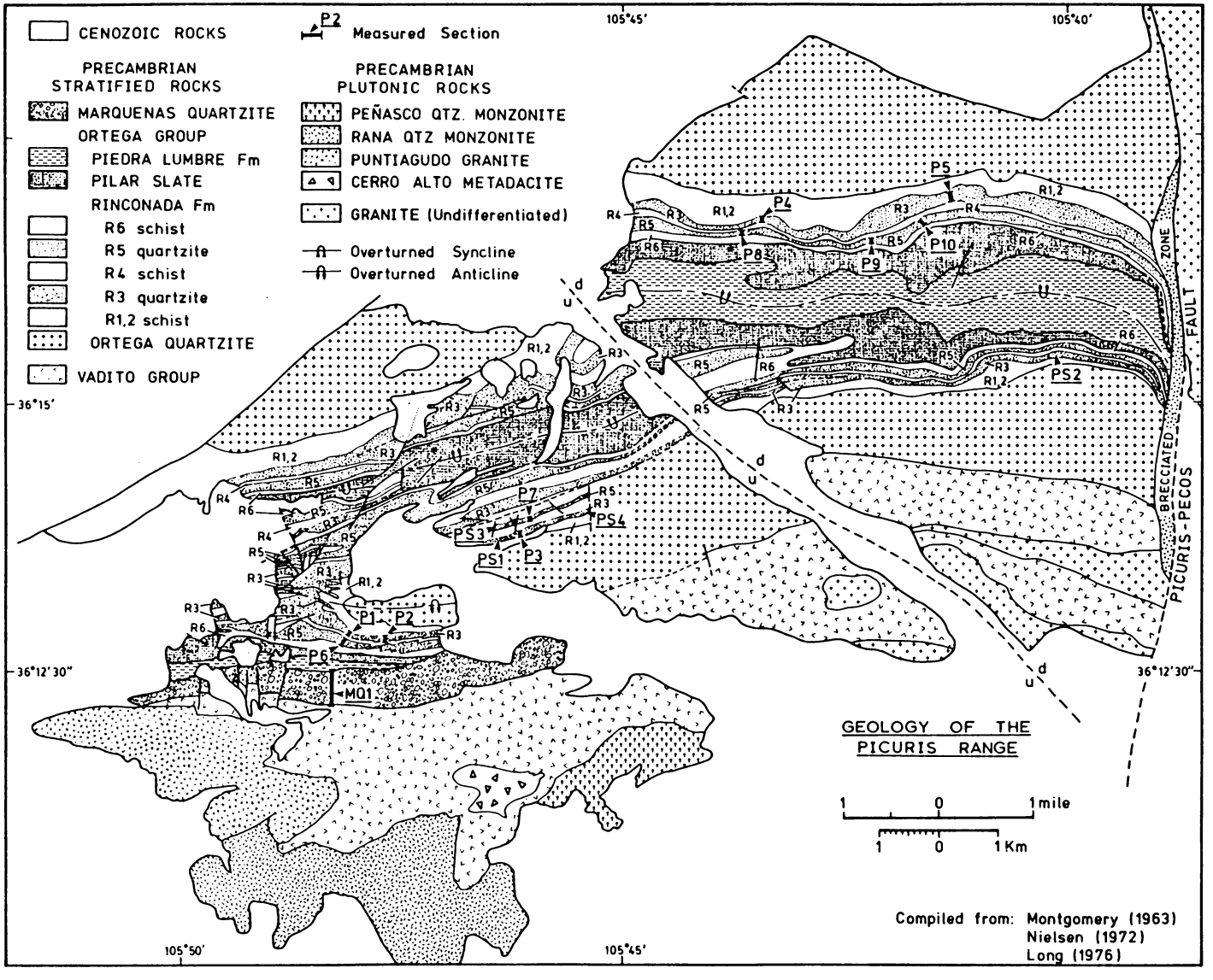
CENOZOIC ROCKS
P2 Measured Section
PRECAMBRIAN STRATIFIED ROCKS
MARQUENAS QUARTZITE
ORTEGA GROUP
PIEDRA LUMBRE Fm
PILAR SLATE
RINCONADA Fm
R6 schist
R5 quartzite
R4 schist
R3 quartzite
R1,2 schist
ORTEGA QUARTZITE
VADITO GROUP
PRECAMBRIAN PLUTONIC ROCKS
PEÑASCO QTZ. MONZONITE
RANA QTZ MONZONITE
PUNTIAGUDO GRANITE
CERRO ALTO METADACITE
GRANITE (Undifferentiated)
Overturned Syncline
Overturned Anticline
105°45'
105°40'
36°15'
36°12'30"
105°50'
BRECCIATED ZONE
PICURIS-PECOS FAULT
P1
P2
P3
P4
P5
P6
P7
P8
P9
P10
PS1
PS2
PS3
PS4
MQ1
GEOLOGY OF THE PICURIS RANGE
1 0 1 mile
1 0 1 Km
Compiled from: Montgomery (1963)
Nielsen (1972)
Long (1976)

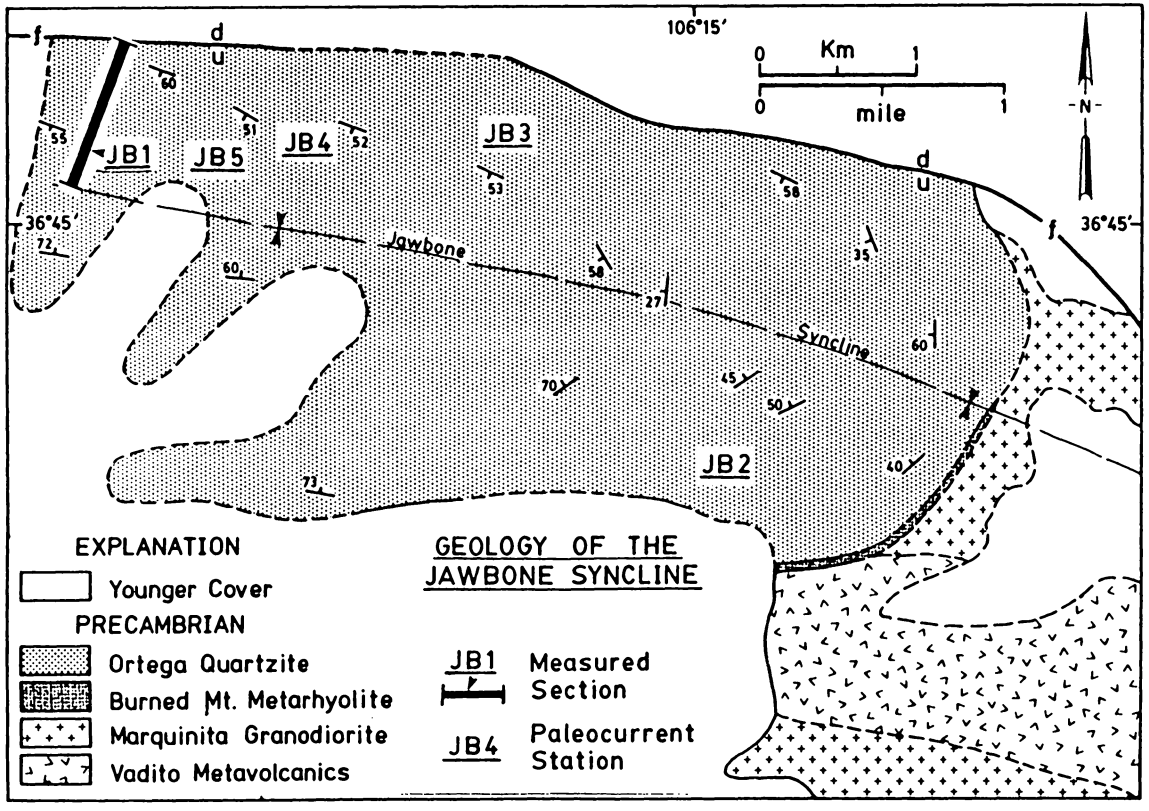
106°15'
0 Km 1
0 mile 1
N
f
d
u
JB1
JB5
JB4
JB3
JB2
36°45'
Jawbone
Syncline
EXPLANATION
Younger Cover
PRECAMBRIAN
Ortega Quartzite
Burned Mt. Metarhyolite
Marquinita Granodiorite
Vadito Metavolcanics
GEOLOGY OF THE JAWBONE SYNCLINE
JB1 Measured Section
JB4 Paleocurrent Station

Appendix B

MEASURED SECTIONS

Location of measured sections in Appendix A.

FACIES

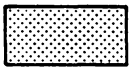
MASSIVE SANDSTONE


BOULDER CONGLOMERATE

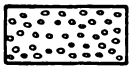
QUARTZ PEBBLE CONGLOMERATE


INTERLAYERED MUDSTONE AND PLANAR-LAMINATED SANDSTONE

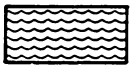
INTERLAYERED MUDSTONE AND CROSS-LAMINATED SANDSTONE


MUDSTONE

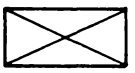
NO EXPOSURE

STRUCTURES

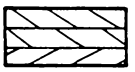
TABULAR-PLANAR CROSS BEDS

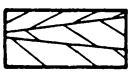
WEDGE-PLANAR CROSS BEDS

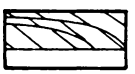
REACTIVATION SURFACE

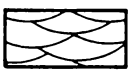
TROUGH CROSS BEDS

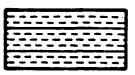
PLANAR LAMINATION

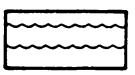
WAVE RIPPLES

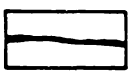
MUDSTONE DRAPE


SHEARED SANDSTONE

ROSE DIAGRAM


TABULAR-PLANAR CROSS BED

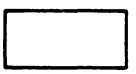
TROUGH CROSS BED

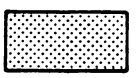
PRIMARY CURRENT LINEATION

SECTION PB1, R3 Member, Pecos

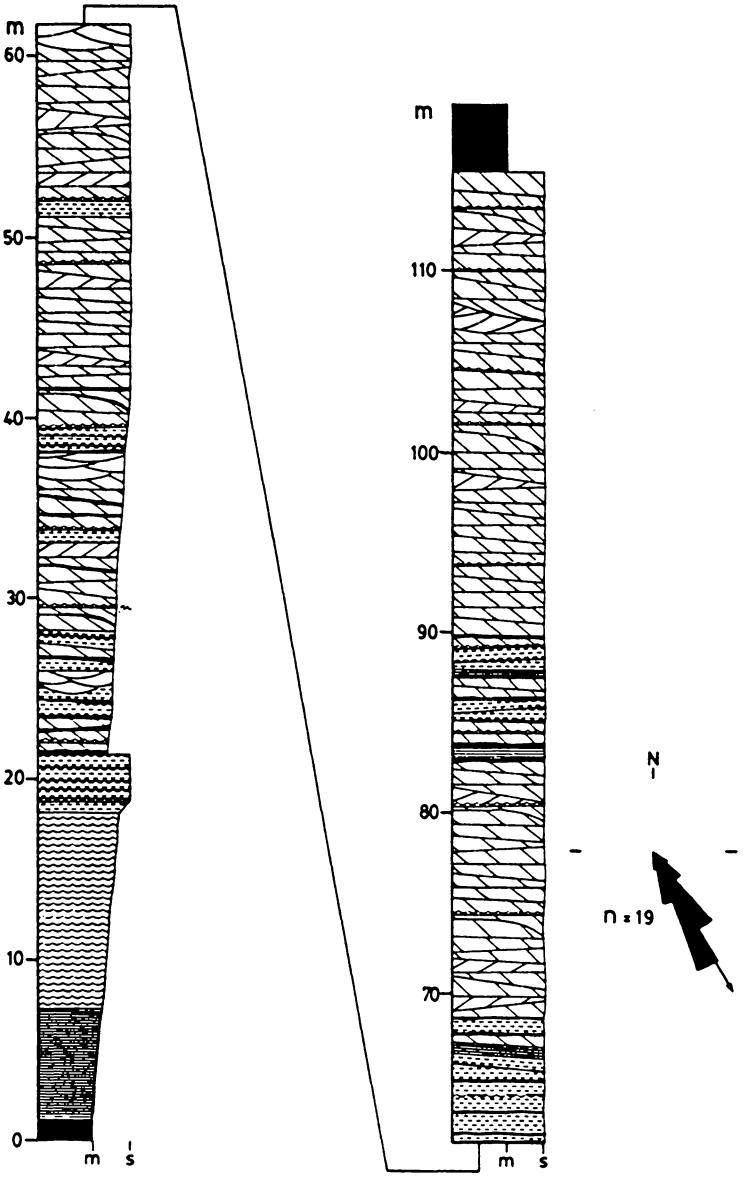

SECTION PB2, R3 Member, Pecos

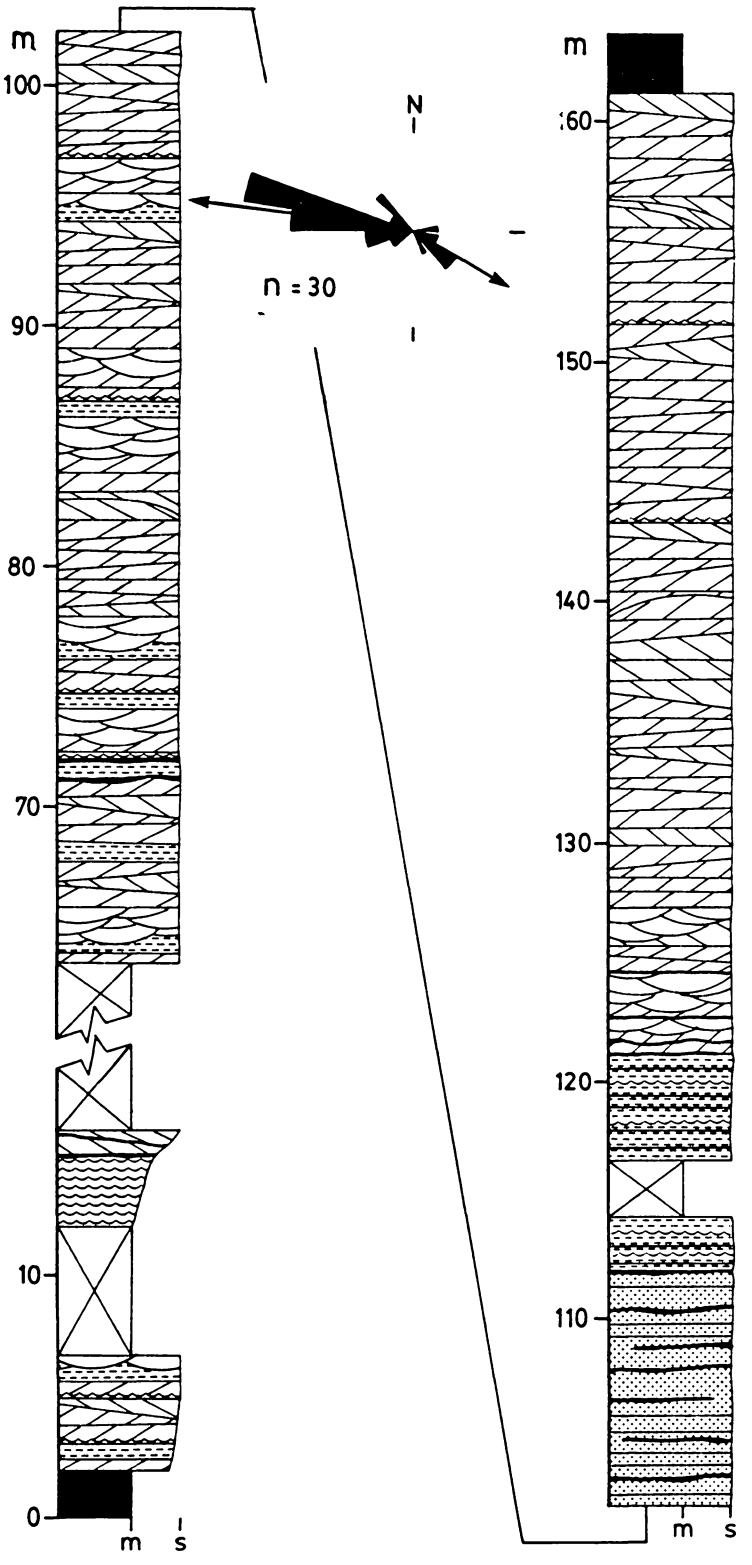

SECTION PB3, R3 Member, Pecos

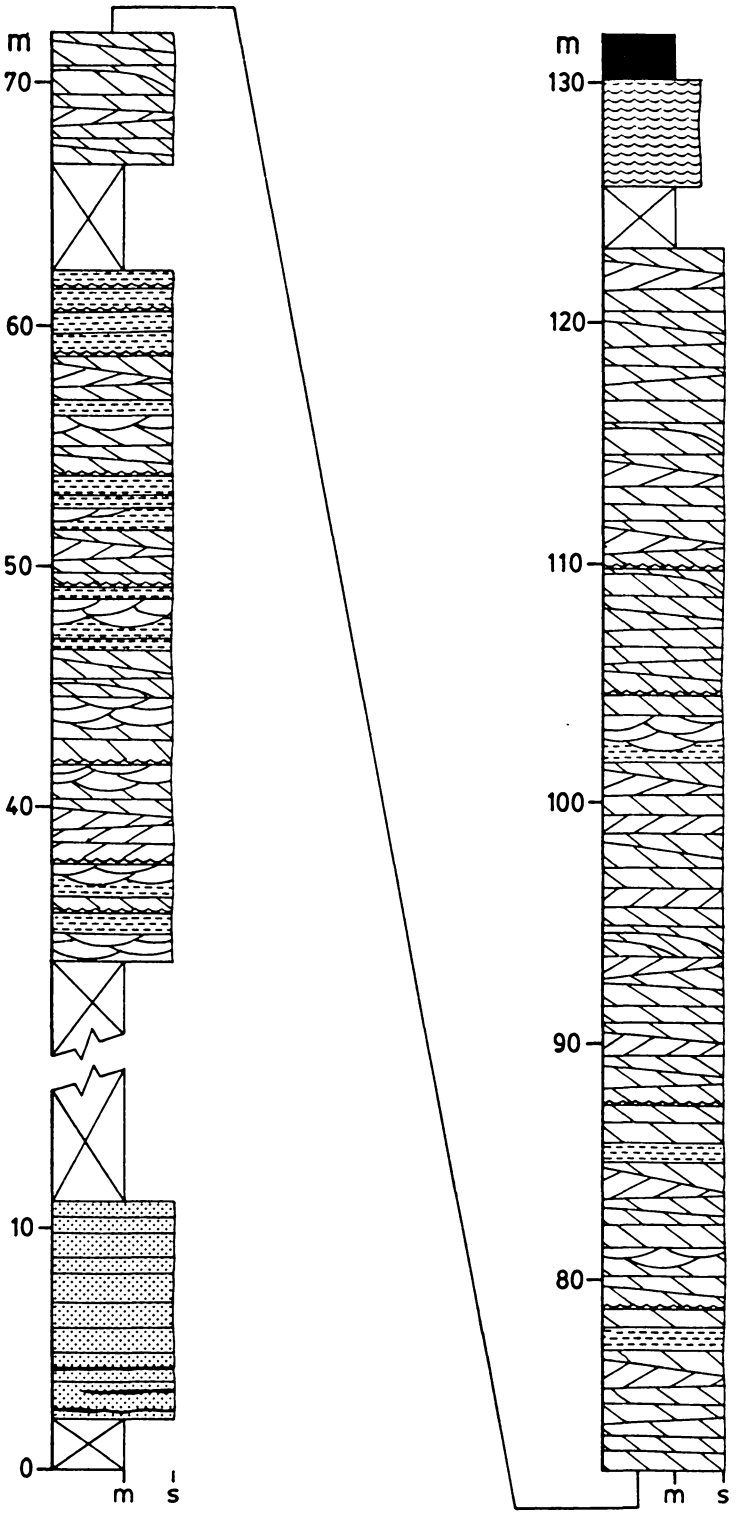

SECTION PB4, R3 Member, Pecos

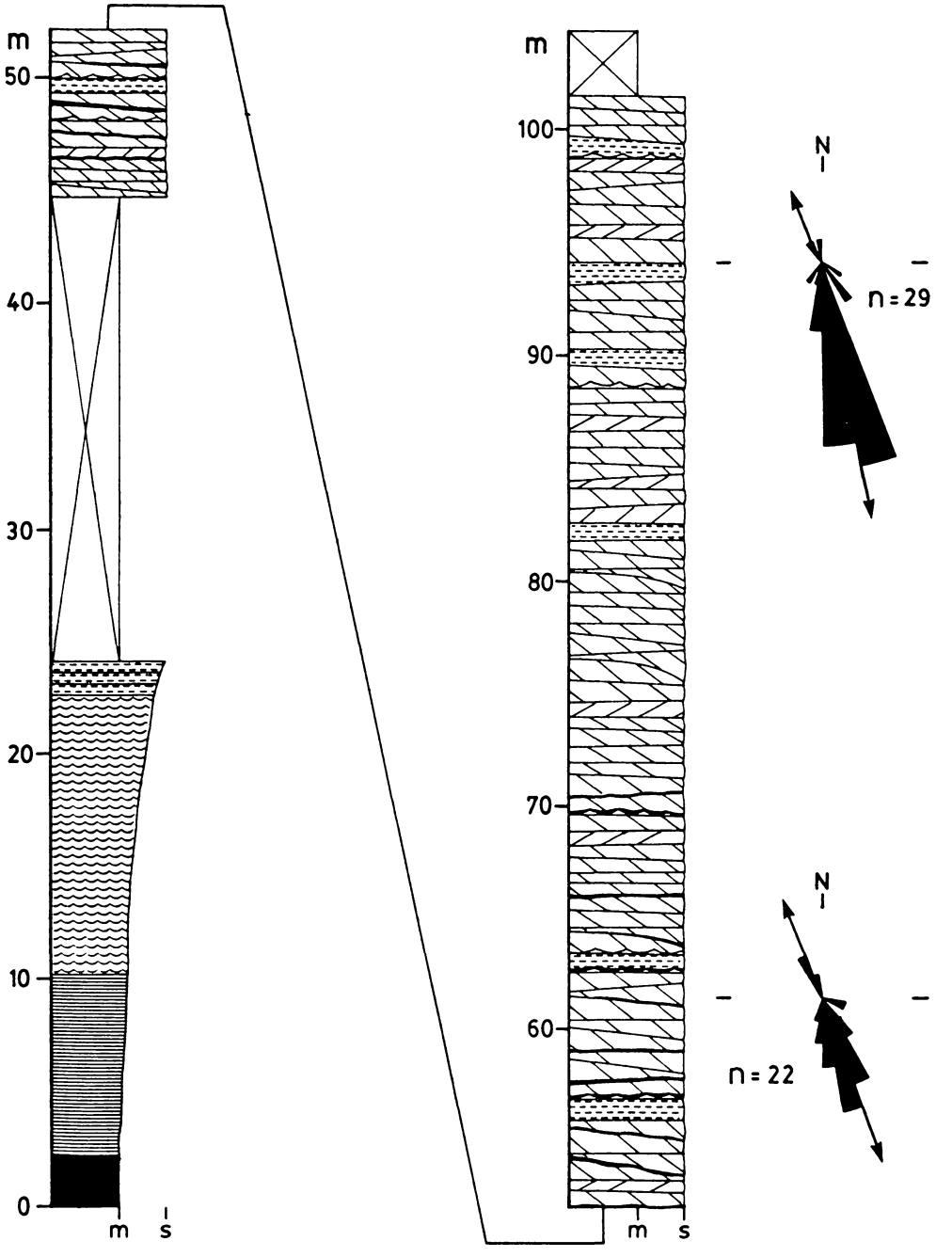

SECTION PB5, R3 Member, Pecos

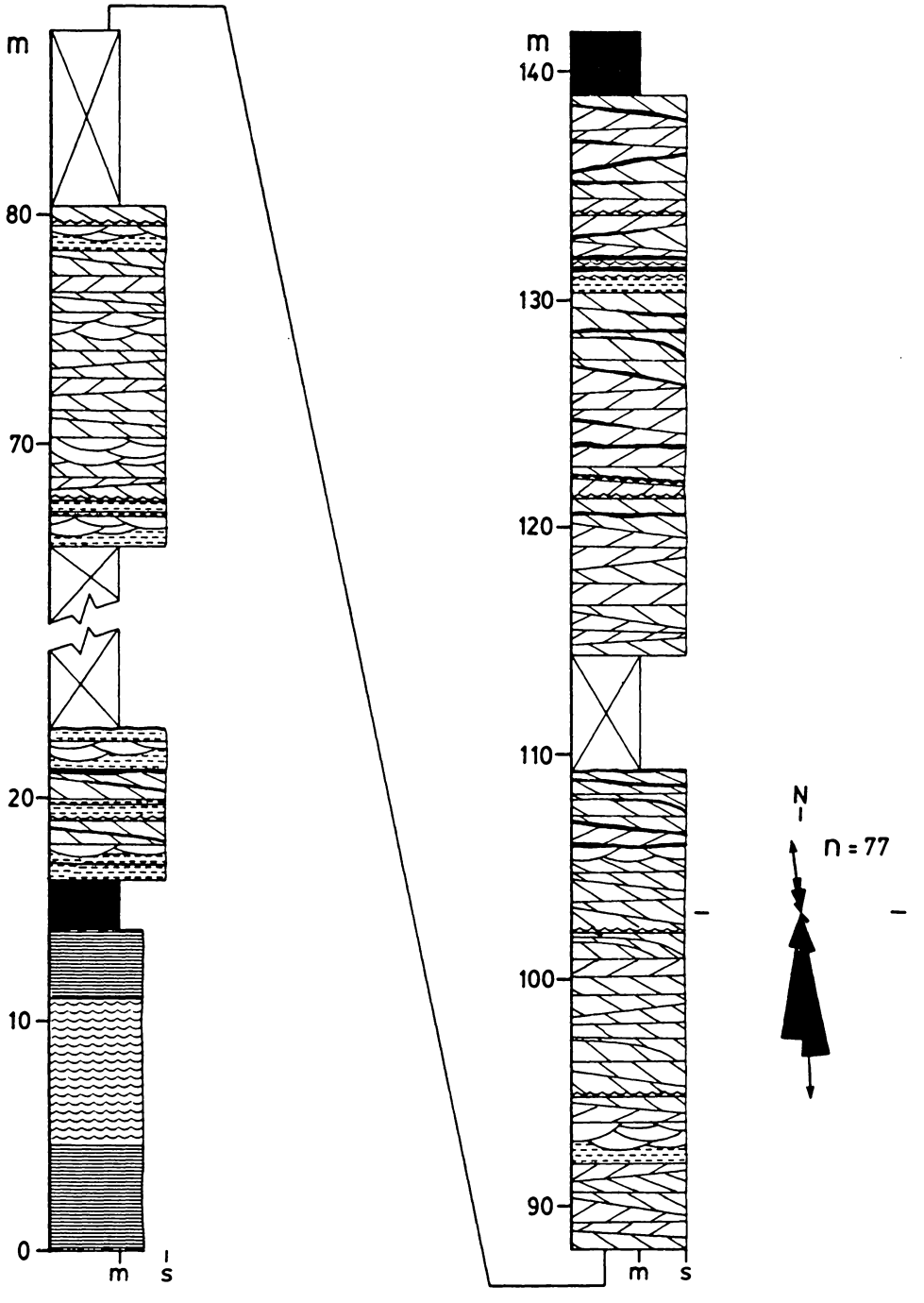

SECTION PB6, R3 Member, Pecos

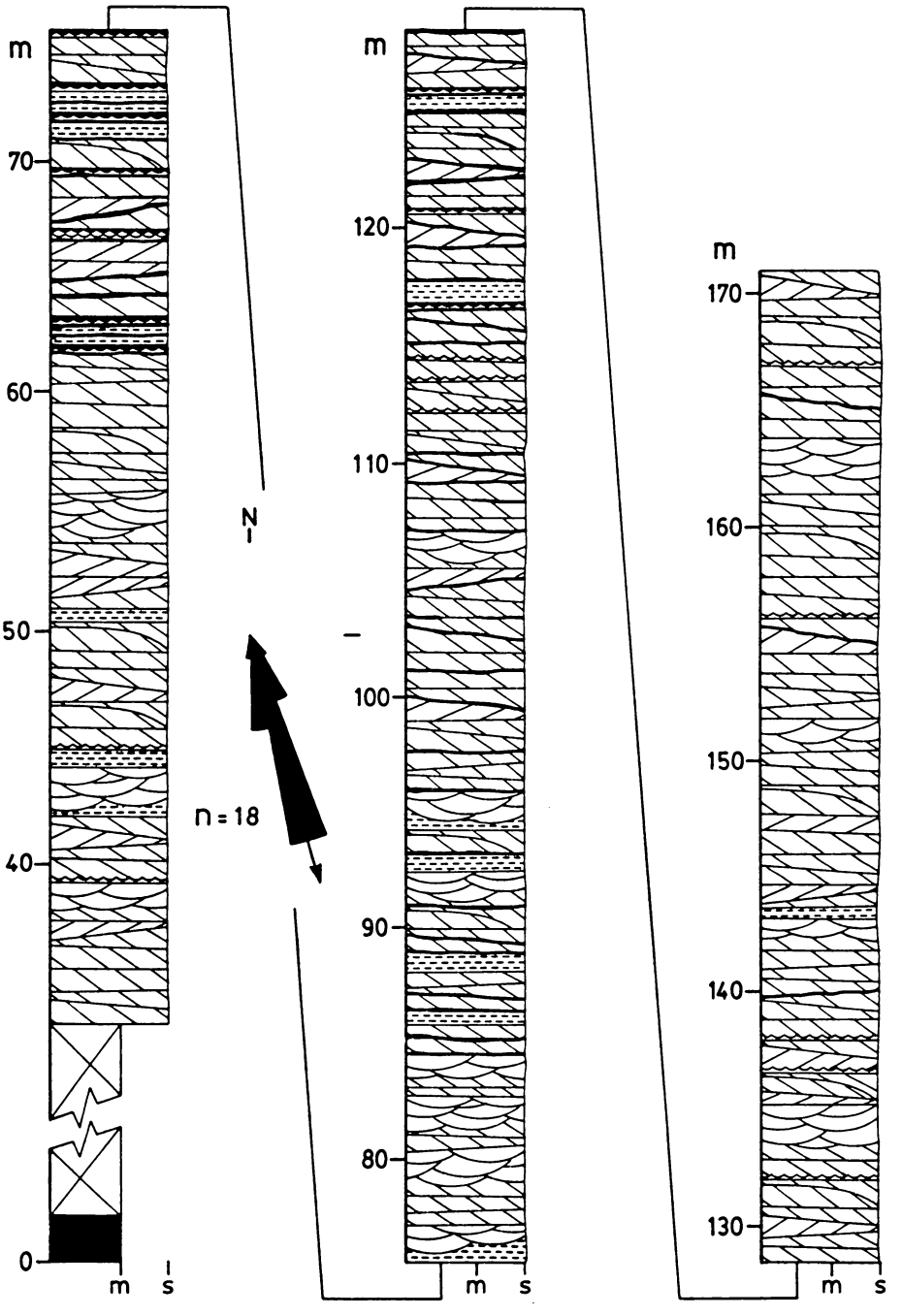

SECTION PB7, R5 Member, Pecos

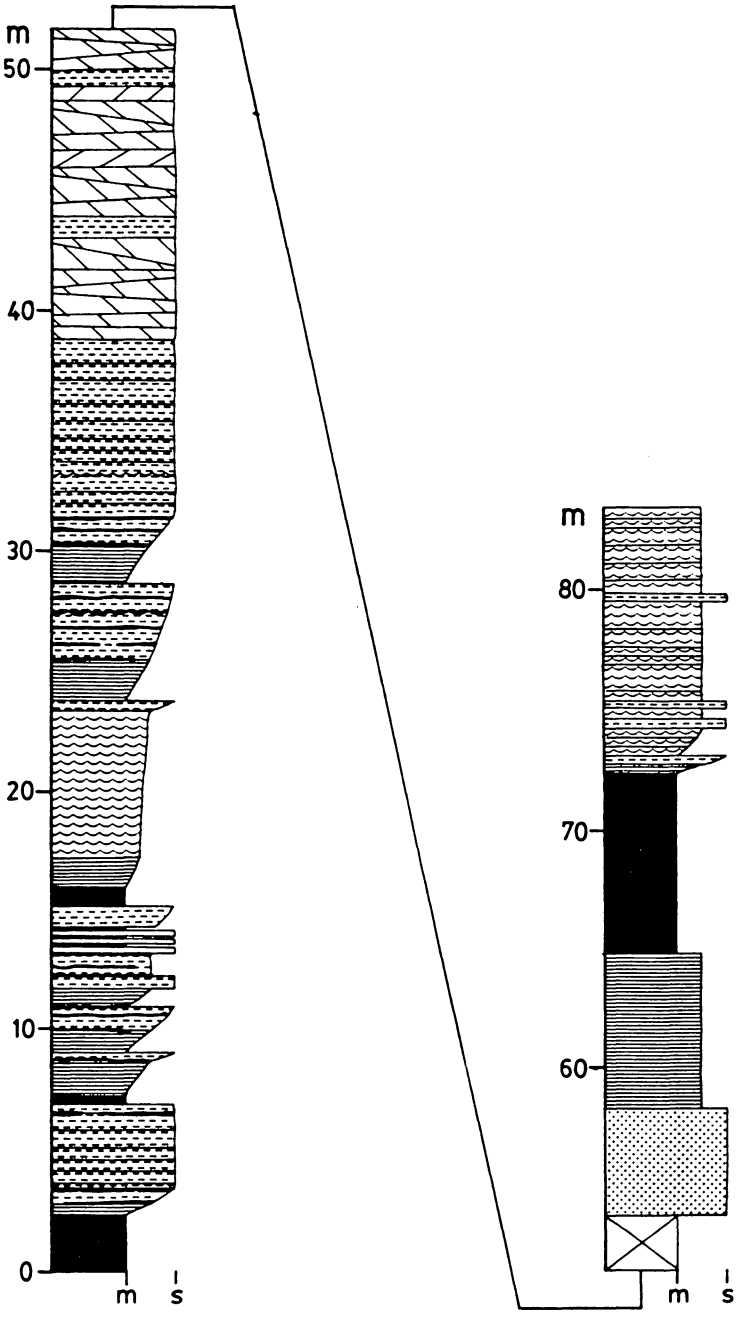

SECTION PB8, R5 Member, Pecos

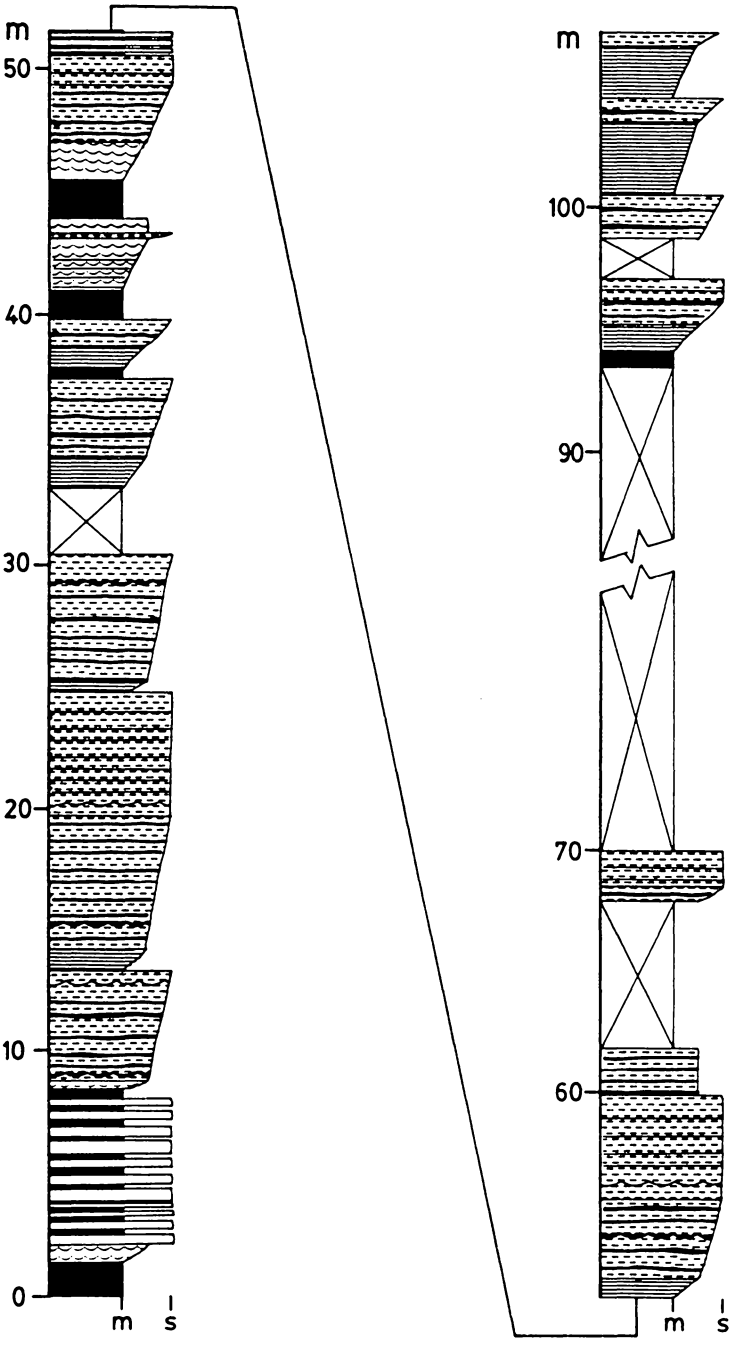

SECTION PB9, R5 Member, Pecos

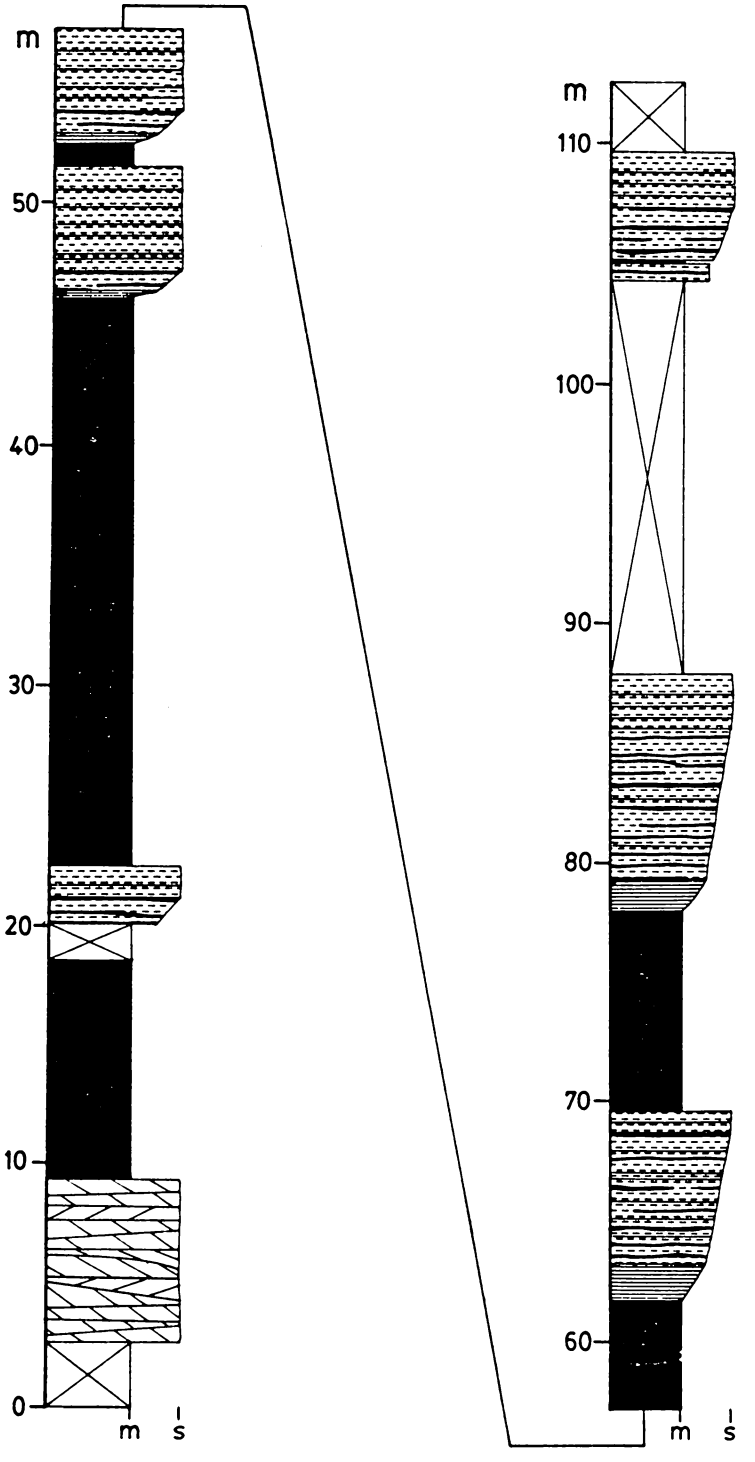

SECTION T1, R3 Member, Truchas

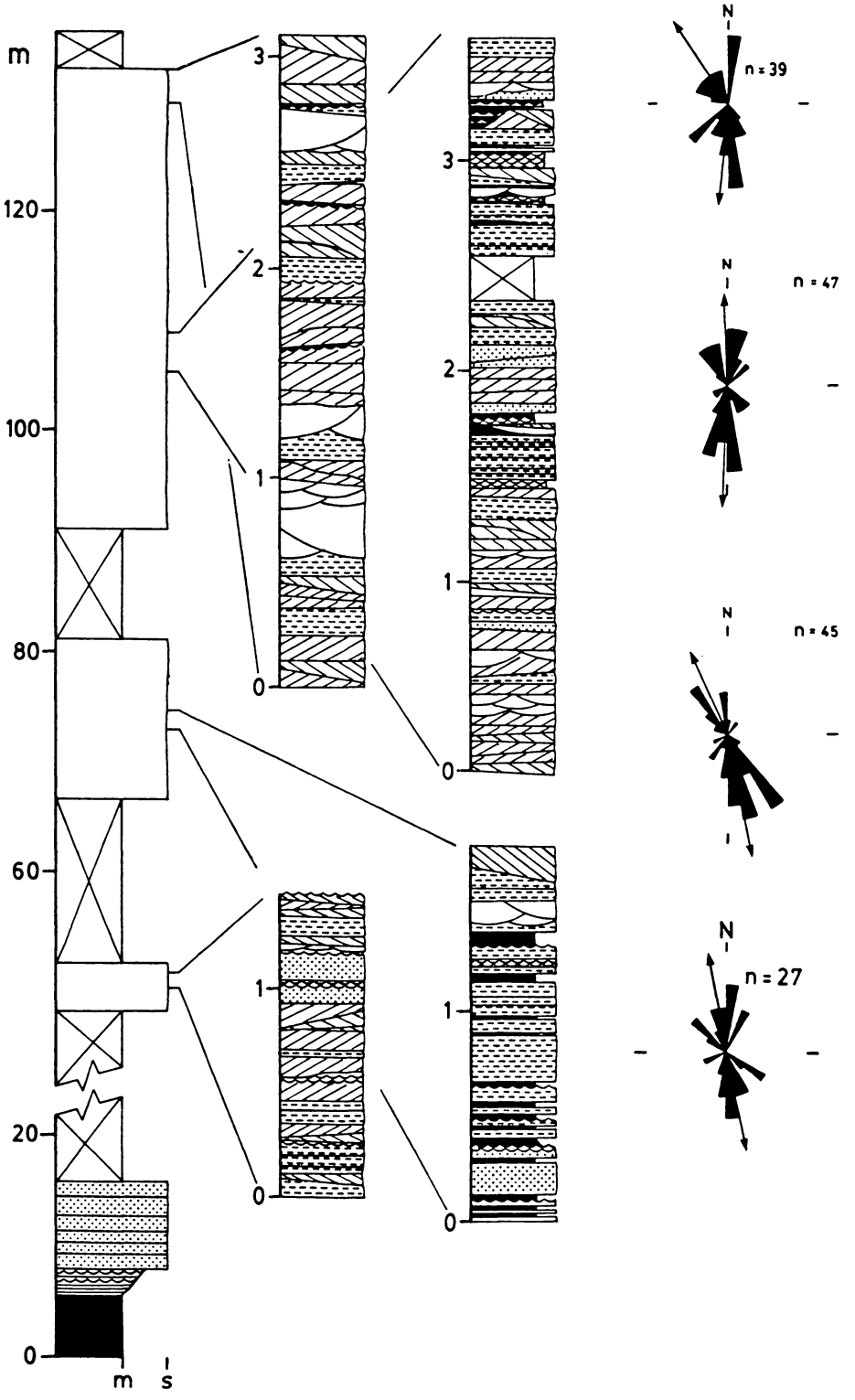

SECTION P1, R3 Member, Picuris

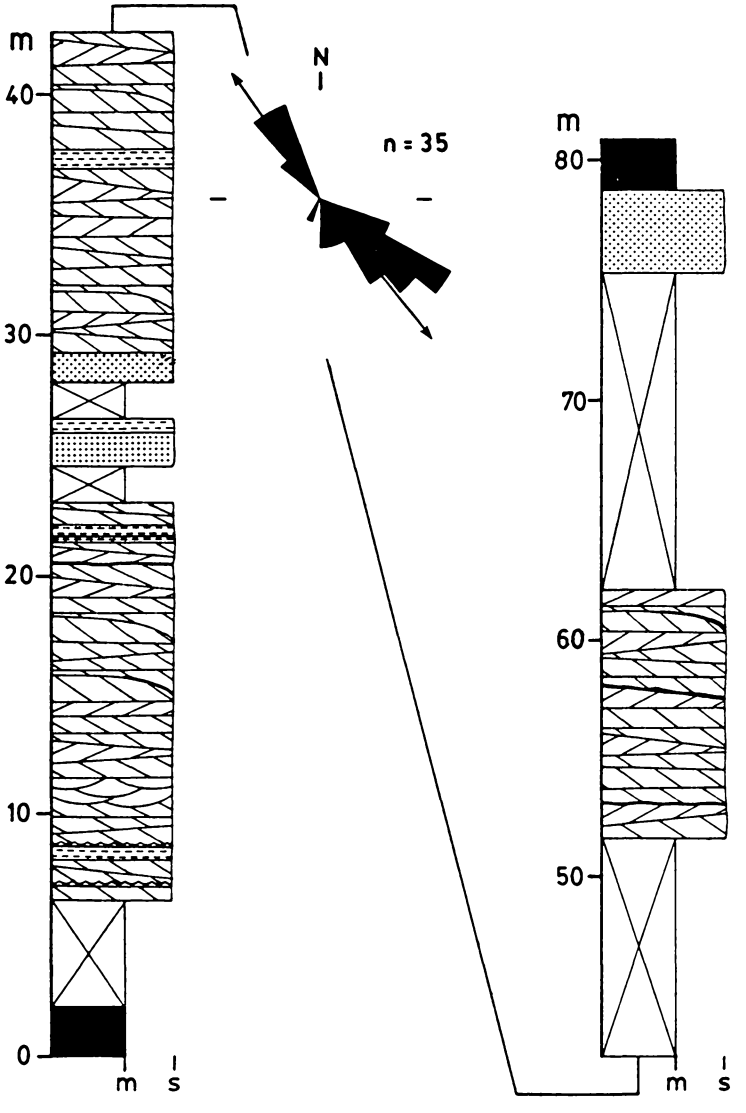

SECTION P2, R3 Member, Picuris

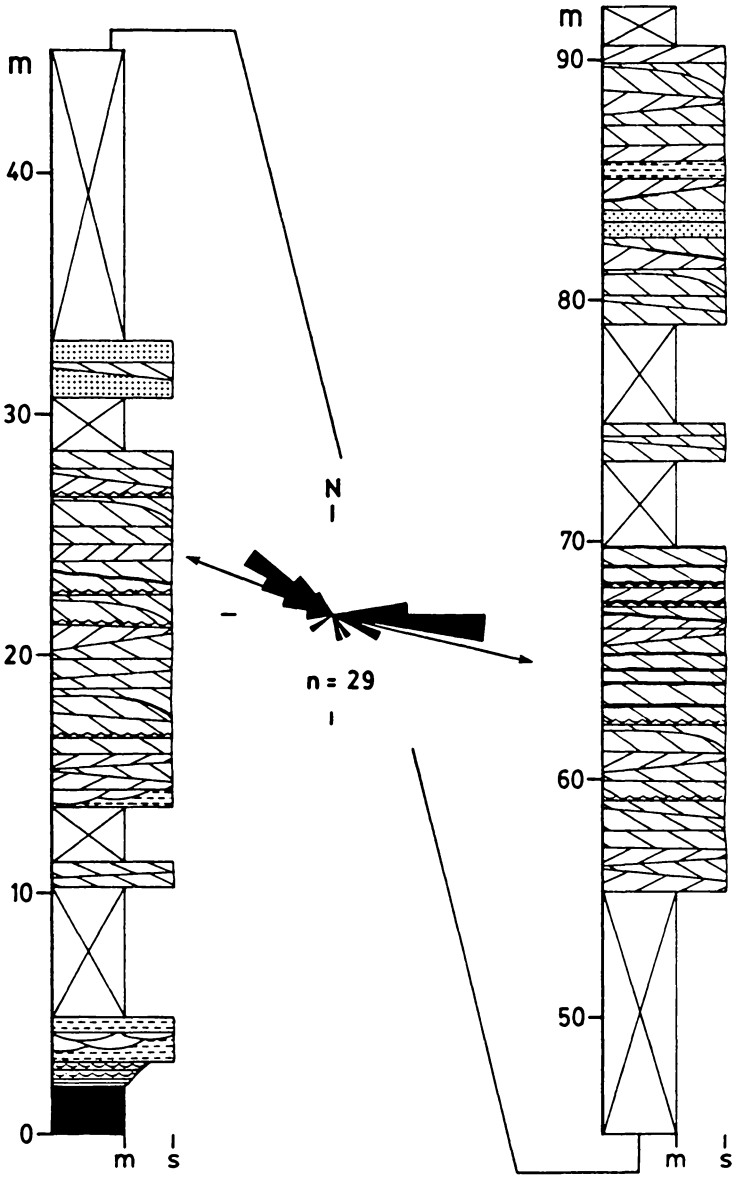

SECTION P3,
R3 Member, Picuris

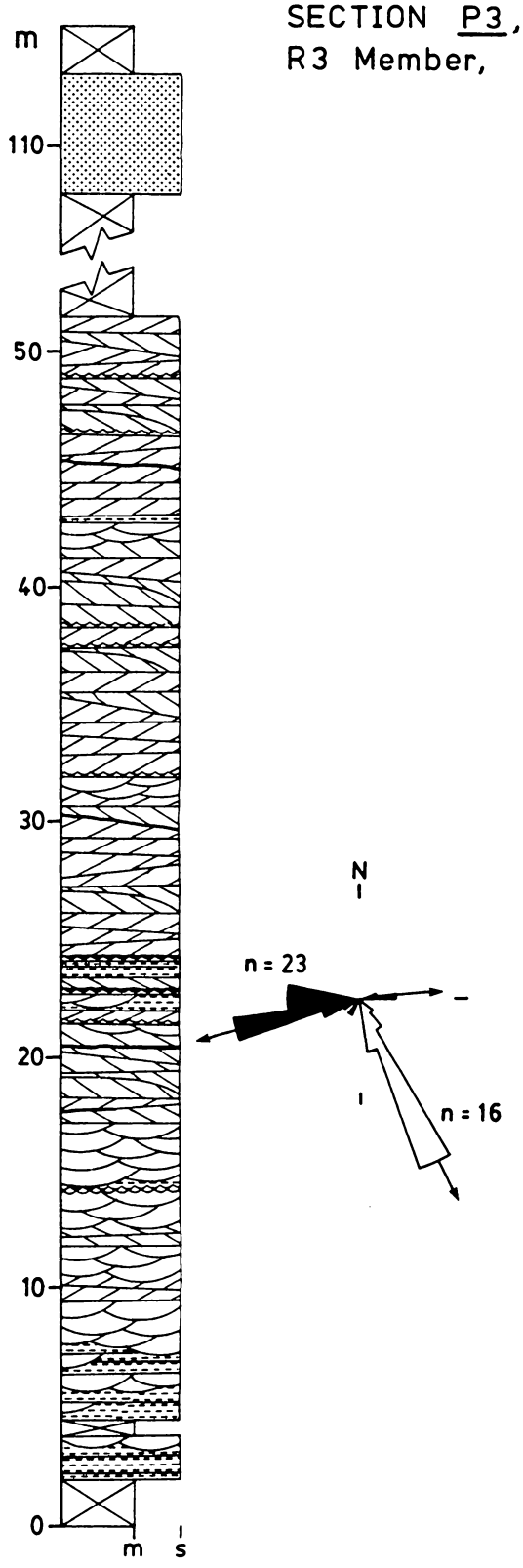

SECTION P4,
R3 Member, Picuris

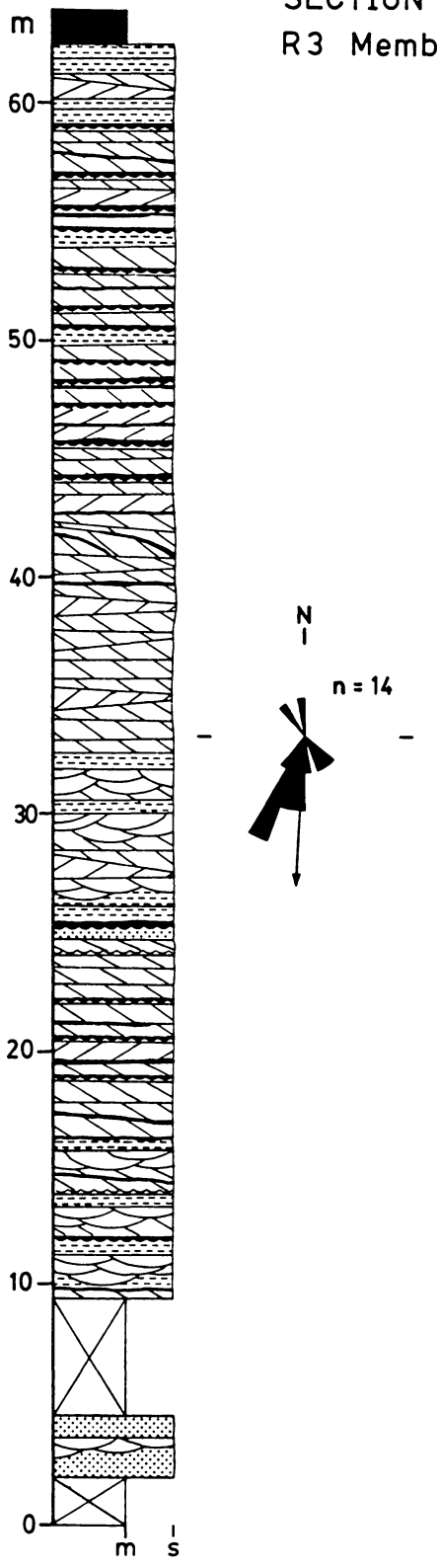

SECTION P5, R3 Member, Picuris

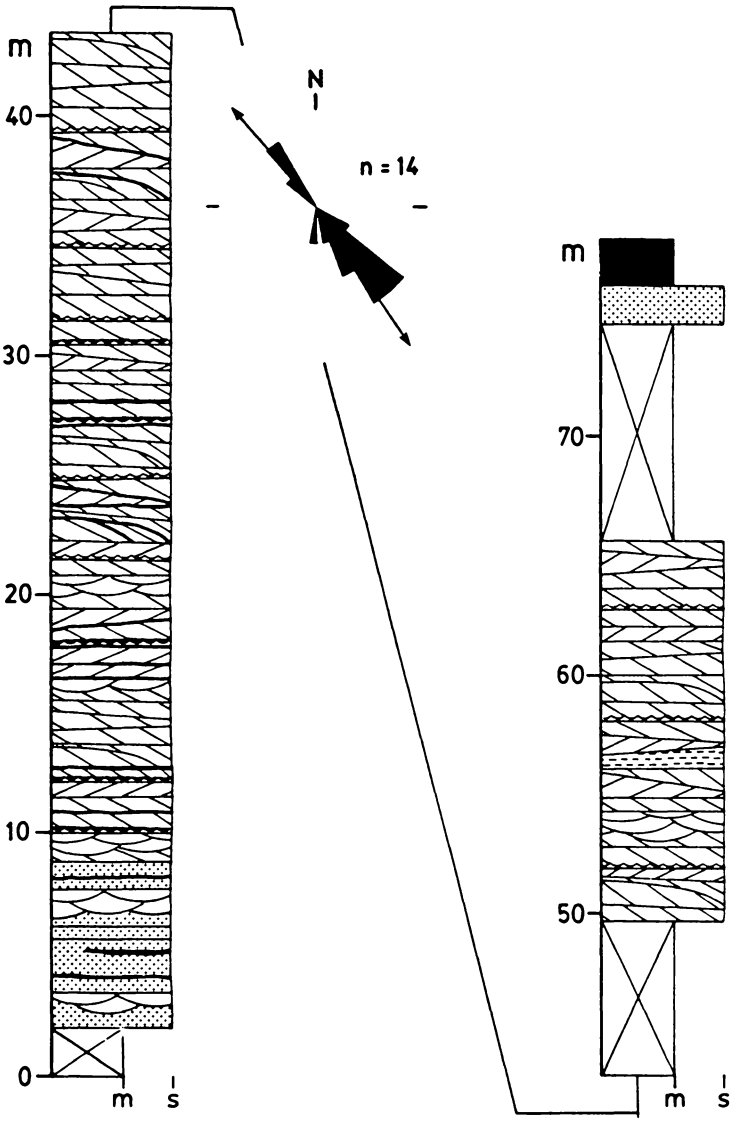

SECTION P6,
R5 Member, Picuris

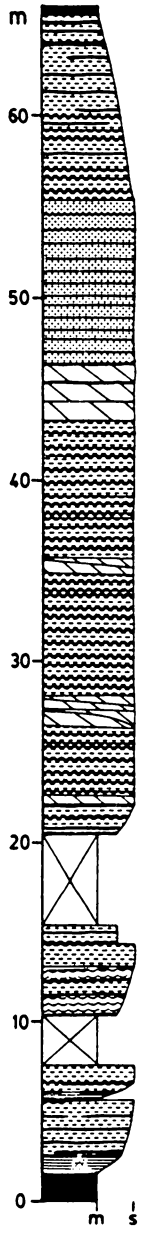

SECTION P7, R5 Member, Picuris

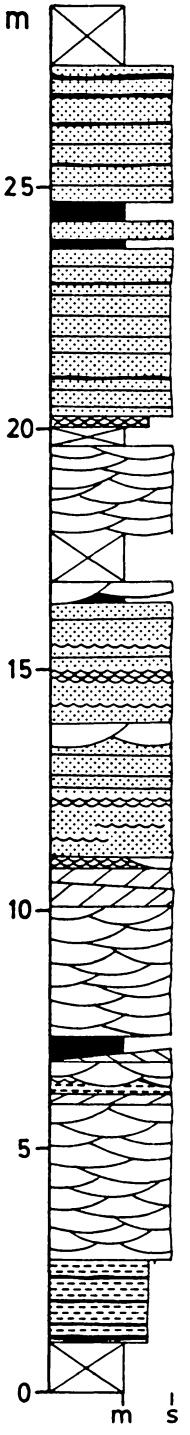

SECTION P8, R5 Member, Picuris

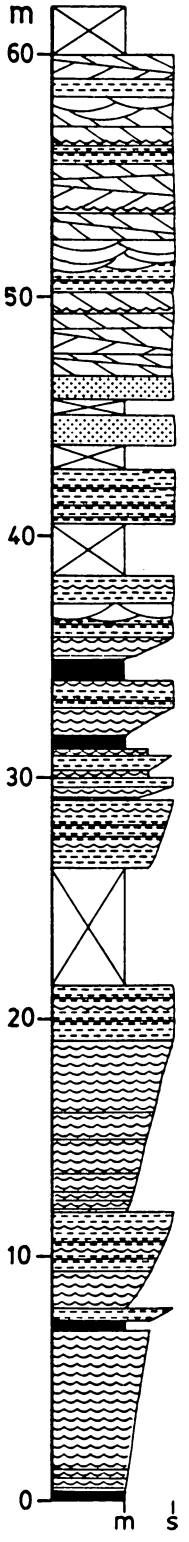

SECTION P9, R5 Member, Picuris

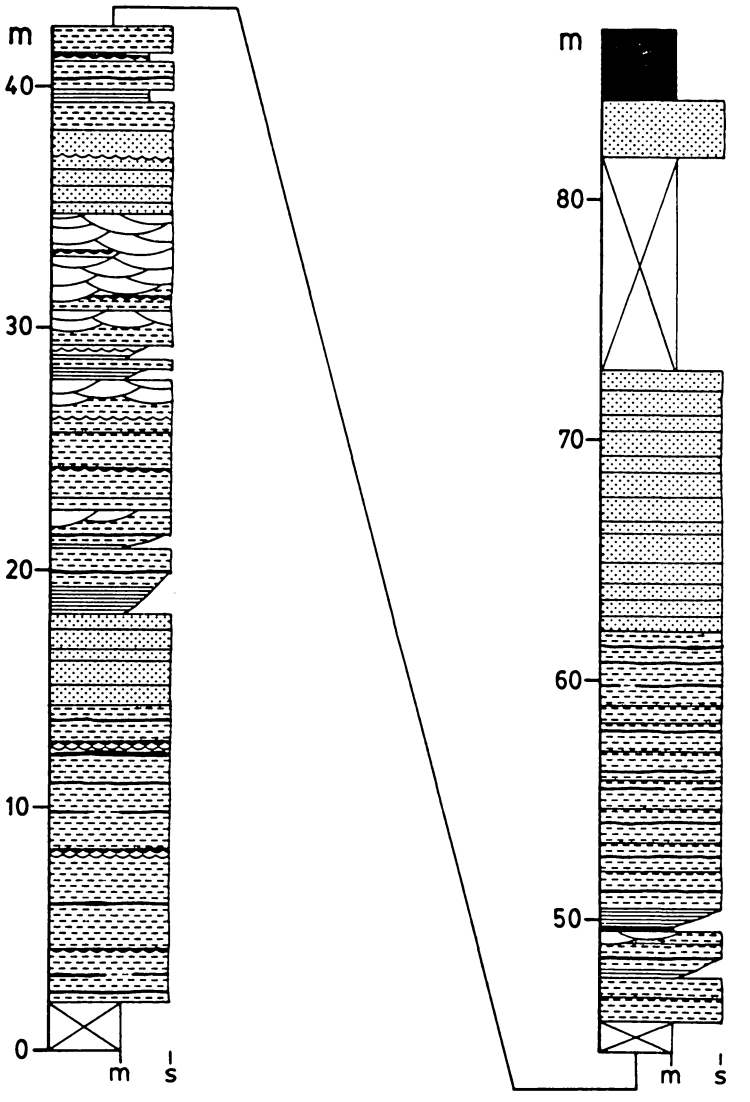

SECTION P10, R5 Member, Picuris

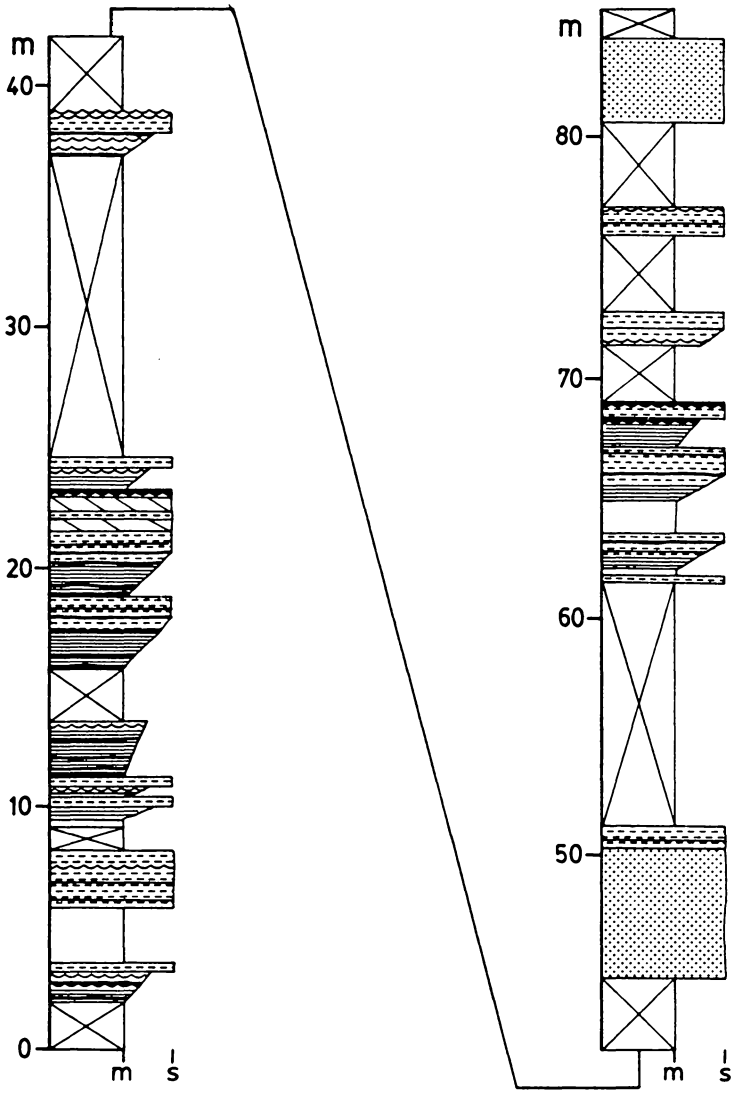

SECTION JB1, ORTEGA QUARTZITE, TUSAS

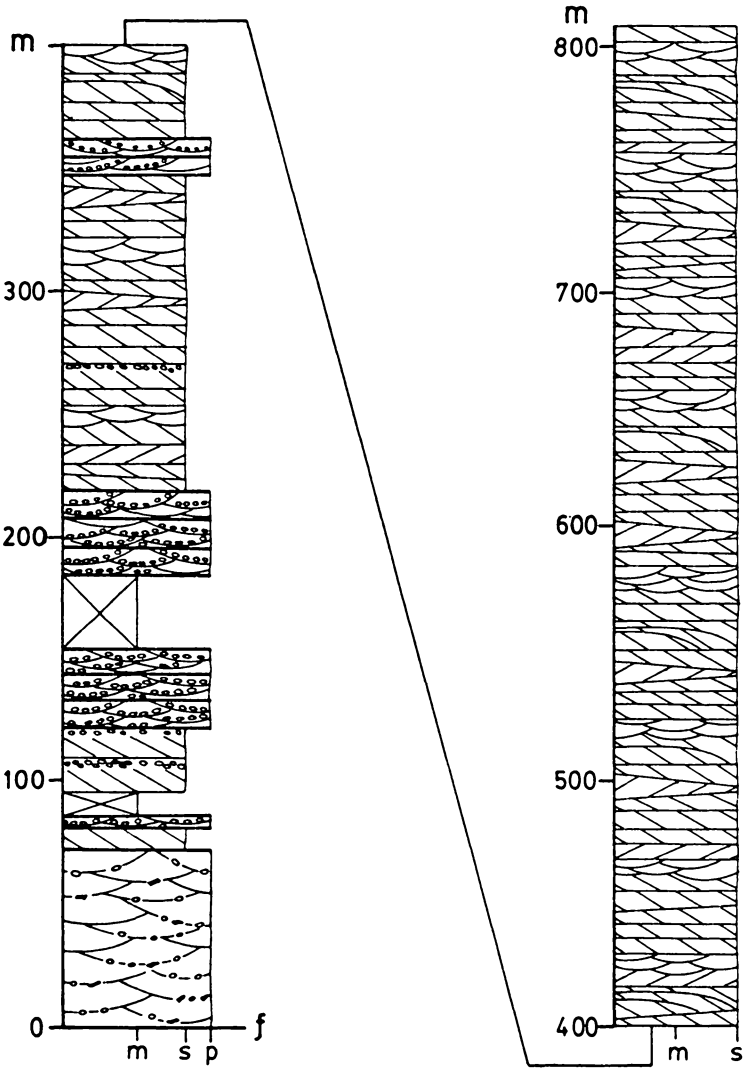

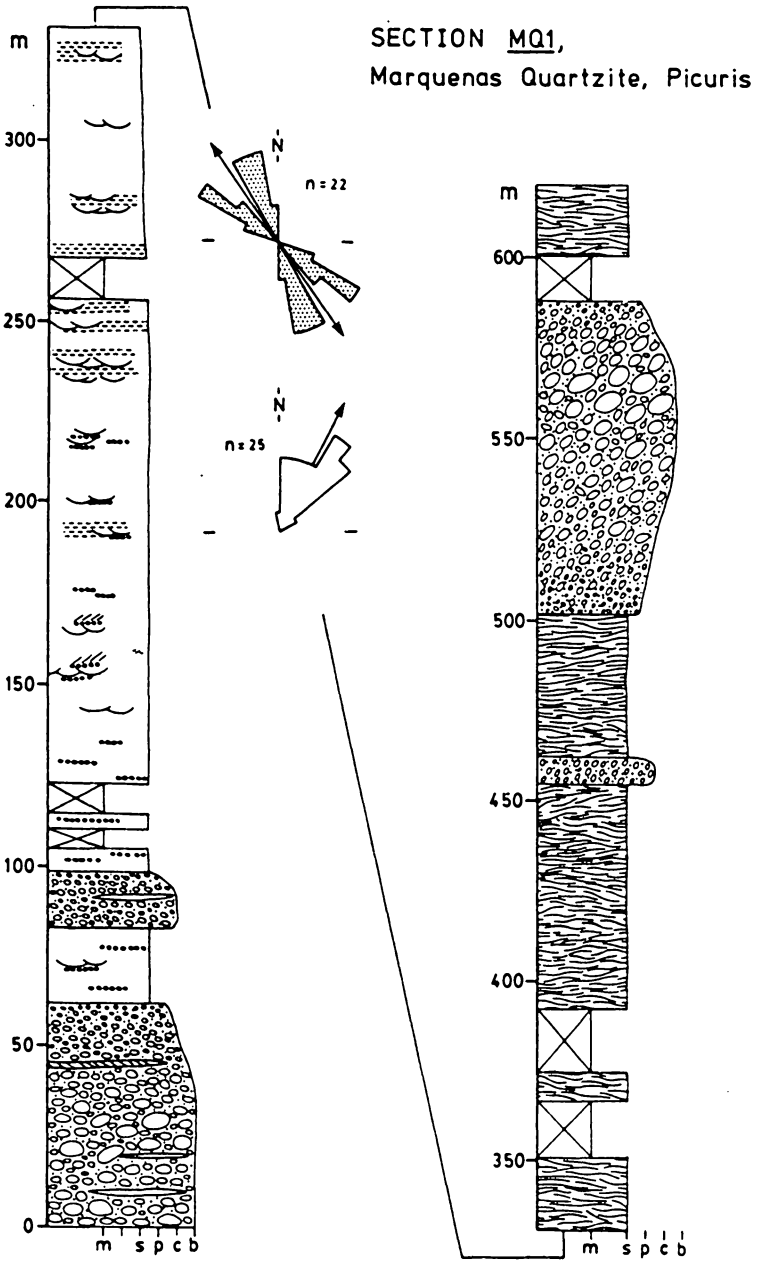
SECTION MQ1,
Marquenas Quartzite, Picuris
m
300
250
200
150
100
50
0
m s p c b
N
n = 22
N
n = 25
m
600
550
500
450
400
350
m s p c b

Appendix C

PALEOCURRENT DATA

Paleocurrent data constituted an integral part of the investigation of Precambrian sediments in northern New Mexico. These paleocurrent data provided insight into processes active during sedimentation and are essential to paleogeographic reconstruction. In undeformed terranes paleocurrent vectors may be inferred directly from primary sedimentary structures. However, in northern New Mexico where the Precambrian succession has been subjected to severe deformation paleocurrent indicators must be restored to their original position by geometric rotation.

Apart from the simple case where sediments have been tilted, and corrections are made by rotating bedding to the horizontal about an axis parallel to its strike, an understanding of fold geometry and fold attitude is imperative in order to restore deformed strata to their original position. Ramsay (1961) has discussed in detail reorientation of primary sedimentary structures in folded rocks and the implications this has on restoring the sedimentary structures to their original position.

Within flexural folds (similar or Ramsay Class-1b folds) shear strain is accomodated by slip along bedding planes so that neither linear nor planar structures are reoriented relative to bedding (Ramsay, 1961). Simple rotation of bedding to a horizontal position will therefore

restore paleocurrent indicators to their original position. In shear folds, in contrast, simple shear occurs within beds and planar and linear structures are reoriented relative to bedding surfaces. If bedding is restored to a horizontal position without compensating for simple shear erroneous paleocurrent vectors will be obtained.

Paleocurrent indicators in the Ortega Group in the Picuris, Truchas and Pecos belts are derived exclusively from the R3 and R5 Members of the Rinconada Formation. Both members are encased within ductile schists. It is believed that shear strain and flattening of folds was accomodated by the schists, thus minimizing internal deformation within the R3 and R5 quartzite members. In the Tusas mountains, paleocurrent data was collected from the Jawbone Syncline. The syncline is an open westward-plunging fold. Internal deformation within the fold is negligble away from the hinge zone, and slickensides along bedding planes suggest flexural folding in the syncline. It is concluded therefore that paleocurrent indicators in the R3 and R5 Members and Jawbone Syncline can be rotated to their original position without compensating for a shear strain component.

The plunges of fold axes have been obtained from the literature and from structural data collected in the field. Plunge of folds in the Ortega Group in the Picuris range are based on bedding measurements, plunges of parasitic folds and bedding-to-cleavage relationships (Nielsen and Scott, in Prep.). Fold attitude in the Marquenas Quartzite, southern Picuris range, has been determined by intersection between bedding and cleavage (Holcombe and Callender, 1982). In the Pecos

belt, the attitude of coaxial F1 and F2 folds is likewise based on bedding to cleavage intersections (Grambling and Codding, 1982) and has been verified by plunges of parasitic folds recorded in the field. Fold plunges in the Truchas range (after J. Grambling, personal communication) are based on bedding-to-cleavage relationships, and have been substantiated by plunges of parasitic folds recorded in the field. Finally, the fold axis of the Jawbone syncline is represented by the pole to the girdle outlined by poles to bedding.

Paleocurrent indicators include tabular-planar cross beds, trough cross beds, symmetrical ripples, and primary current lineations on the upper surface of planar-laminated sandstones. For the purpose of geometric rotation of paleocurrent indicators, primary sedimentary structures are treated either as linear or planar structures. Tabular-planar cross beds are planar structures and are plotted on a stereonet as poles to foresets (Fig. 38a). The paleocurrent vector from tabular-planar cross beds, after bedding has been restored to a horizontal position, is the dip direction of foresets. Paleocurrent indicators represented as linear structures are recorded and plotted as pitches in a bedding plane (Fig. 38a) and fall into two categories; unambiguous indicators, which provide an absolute paleocurrent vector, and ambiguous indicators which only yield a bidirectional paleocurrent azimuth. Unambiguous indicators are trough cross beds in which the paleocurrent vector is oriented in the concave direction outlined by trough cross bed foresets where they intersect bedding planes. Tabular-planar cross beds may be recorded as linear structures in

which case the paleocurrent vector is measured perpendicular to the intersection between linear, planar foresets and bedding with flow in the direction of vergence between foresets and underlying bedding plane. Ambiguous indicators comprise primary current lineations on the surface of planar-laminated sandstones and wave ripples. For current lineations, flow is parallel to the bidirectional azimuth obtained after rotation whereas for wave ripples orbital flow is perpendicular to the bidirectional azimuth defining the crests of symmetrical ripples.

The procedure for restoring paleocurrent indicators to their original position involves two rotations on a Wulf (equal angle) stereonet. The first rotation is to bring the fold axis to a horizontal position. The fold axis is rotated alond the (small) equatorial circle to the edge of the net, and linear structures and poles to planar surfaces (including bedding) are rotated along their respective small circles (Fig. 38b). The second step is to restore bedding to a horizontal position. Pole to bedding is rotated along the equator to a vertical position, whereas linear structures and poles to planar structures are rotated along small circles to their original position (Fig. 38c).

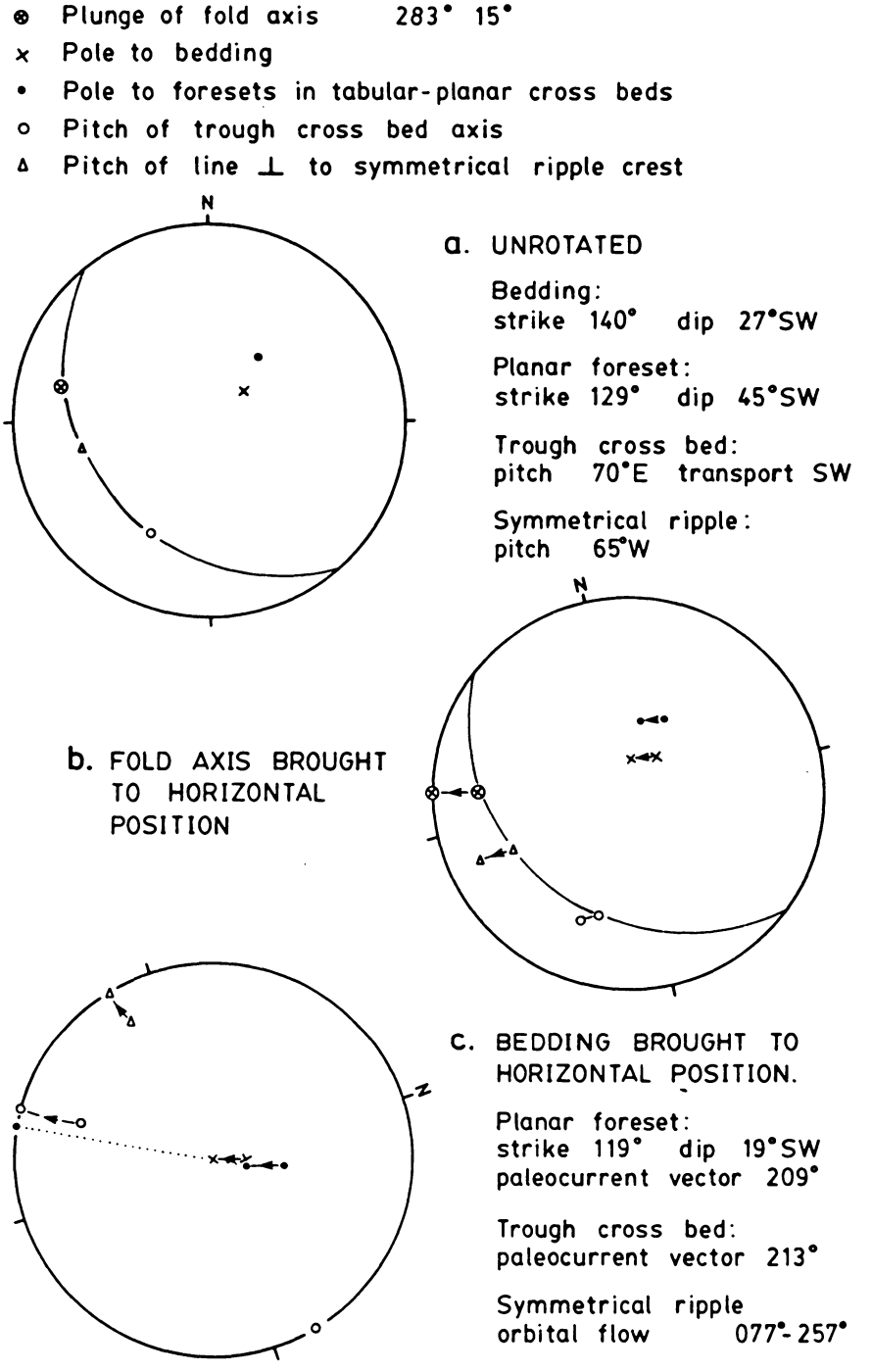

Figure 38: Stereonet rotation procedure for paleocurrent data.

Locality: Section PB1, Pecos
Stratigraphic Position: Upper R3 Member
Plunge of fold axis: 236 38
Paleocurrent indicator: Tabular-planar cross beds
Number of readings: n=19
Vector mean: 151

Bedding		Unrotated		Rotated		Current Direction
Strike	Dip	Strike	Dip	Strike	Dip	Azimuth
073	62 SE (ot.)	073	62 SE	083	6 S	173
		068	70 SE	065	13 SE	155
		071	72 SE	050	14 SE	140
		068	71 SE	052	14 SE	152
		066	71 SE	058	16 SE	158
		069	75 SE	049	16 SE	139
		072	78 SE	045	19 SE	135
		068	80 S	038	21 SE	128
		066	76 SE	056	19 SE	146
		065	75 SE	059	19 SE	149
		064	71 SE	072	17 SE	162
		064	74 SE	067	18 SE	157
		061	71 SE	078	19 SE	168
		062	73 SE	072	19 SE	162
		064	79 SE	055	22 SE	145
		062	81 S	056	25 SE	146
		062	77 SE	061	22 SE	151
		061	78 SE	063	23 SE	153
		057	82 NW	064	41 SE	154

Locality: Section PB2, Pecos
Stratigraphic position: Middle R3 Member
Plunge of fold axis: 245 30
Paleocurrent indicator: Tabular-planar cross beds
Number of readings: n(total)=30 n=25 n=5
Vector mean: Bimodal 278 126

Bedding		Unrotated		Rotated		Current Direction
Strike	Dip	Strike	Dip	Strike	Dip	Azimuth
069	84 S	054	85 SE	192	16 SE	102
		061	89 SE	207	9 SE	117
		062	90	215	10 SE	125
		080	83 S	191	10 NW	281
		080	84 S	181	10 W	271
		081	76 S	221	13 NW	311
		081	88 S	166	12 SW	256
		081	84 S	184	12 W	274
		082	81 S	199	12 NW	289
		082	82 S	192	13 W	282
		082	73 S	229	17 NW	319
		084	75 S	219	17 NW	309
		084	83 S	191	14 NW	281
		083	90	164	15 SW	254
		085	82 S	193	16 NW	283
		085	86 S	181	15 W	271
		085	87 S	176	17 W	266
		087	78 S	202	19 NW	292
		089	82 S	193	19 W	283
		089	84 S	187	20 W	277
		090	82 S	193	21 W	283
		090	88 S	176	21 W	266
		093	85 S	184	23 W	274
		094	68 S	221	27 NW	311
		096	75 S	208	27 NW	298
		086	88 S	173	17 W	263
		060	88 NW	221	13 SE	131
		064	87 NW	245	17 SE	155
		086	89 N	140	21 SW	230
		082	89 N	156	15 SW	246

Locality: Section PB4, Pecos
Stratigraphic position: Lower R3 Member
Plunge of fold axis: 236 38
Paleocurrent indicator: Tabular-planar cross beds
Number of readings: n(total)=22 n=19 n=3
Vector mean: Bimodal 160 339

Bedding		Unrotated		Rotated		Current Direction
Strike	Dip	Strike	Dip	Strike	Dip	Azimuth
105	50 SW (ot.)	085	54 S	273	17 S	183
		086	63 S	245	21 SE	155
		087	55 S	265	16 S	175
		088	56 S	259	17 SE	169
		089	52 S	273	14 S	183
		089	49 S	286	13 SE	196
		090	59 S	248	16 SE	158
		090	59 S	248	16 SE	158
		089	56 S	257	16 SE	167
		091	54 S	254	12 SE	164
		091	60 S	243	16 SE	153
		092	62 S	235	18 SE	145
		094	52 S	269	10 S	179
		094	56 S	261	12 S	171
		095	54 S	254	10 SE	164
		095	58 S	239	12 SE	149
		096	57 S	240	10 SE	150
		097	67 S	209	19 SE	119
		103	64 SW	197	15 SE	107
		126	45 SW	258	17 NW	348
		133	42 SW	249	21 NW	339
		138	39 SW	242	25 NW	332

Locality: Section PB4, Pecos
Stratigraphic position: Upper R3 Member
Plunge of fold axis: 236 38
Paleocurrent indicator: Tabular-planar cross beds
Number of readings: n(total)=30 n=27 n=3
Vector mean: Bimodal 169 339

Bedding		Unrotated		Rotated		Current Direction
Strike	Dip	Strike	dip	Strike	Dip	Azimuth
105	50 S (ot.)	080	61 S	262	23 S	172
		081	58 S	266	22 S	176
		082	57 S	268	20 S	178
		083	58 S	264	20 S	174
		083	59 S	262	20 S	170
		084	46 S	302	16 SW	212
		084	54 S	258	15 SE	168
		084	60 S	258	20 SE	168
		085	56 S	266	17 S	176
		085	57 S	266	17 S	176
		085	60 S	256	19 SE	166
		086	58 S	260	18 S	170
		086	66 S	232	23 SE	152
		087	56 S	257	15 SE	167
		087	57 S	256	15 SE	166
		087	60 S	250	18 SE	160
		088	53 S	277	14 S	187
		089	57 S	255	14 SE	165
		089	60 S	250	17 SE	160
		089	50 S	284	13 SW	194
		090	64 S	225	19 SE	145
		090	56 S	257	14 SE	167
		091	62 S	249	17 SE	149
		093	54 S	264	11 S	174
		096	52 S	270	8 S	180
		099	65 S	202	16 SE	122
		110	46 SW	245	7 NW	335
		111	45 SW	234	8 NW	324
		115	48 SW	266	9 N	356
		088	53 S	273	14 S	183

Locality: Section PB5, Pecos
Stratigraphic position: Middle R3 Member
Plunge of fold axis: 239 32
Paleocurrent indicator: Tabular-planar cross beds
Number of readings: n(total)=52 n=47 n=4
Vector mean: Bimodal 178 352

Bedding		Unrotated		Rotated		Current Direction
Strike	Dip	Strike	Dip	Strike	Dip	Azimuth
101	50 S (ot.)	123	34 SW	065	21 NW	335
		111	43 SW	071	10 NW	341
		124	46 SW	099	17 N	009
		120	44 SW	092	13 N	002
		074	64 SE	271	23 S	181
		092	73 S	232	15 SE	142
		092	69 S	235	21 SE	145
		091	63 S	245	24 SE	155
		086	65 S	253	20 SE	163
		081	71 S	253	28 SE	163
		075	76 SE	253	34 SE	163
		077	74 SE	257	33 SE	167
		078	72 SE	259	31 SE	169
		073	76 SE	261	37 S	171
		071	73 SE	266	35 S	176
		068	73 SE	272	37 S	182
		070	71 SE	270	34 S	180
		071	71 SE	269	33 S	179
		070	69 SE	272	33 S	182
		073	70 SE	269	31 S	178
		074	70 SE	266	31 S	176
		075	71 SE	264	31 S	174
		071	68 SE	273	32 S	183
		072	67 SE	273	31 S	183
		071	66 SE	276	32 S	186
		072	66 SE	275	31 S	185
		079	70 SE	260	28 S	170
		079	69 SE	261	27 S	171
		081	68 S	259	25 SE	169
		067	68 SE	264	28 S	174
		067	67 SE	264	27 S	174
		074	66 SE	272	30 S	182
		074	67 SE	269	30 S	179
		076	67 SE	267	30 S	177
		076	66 SE	267	29 S	177
		075	66 SE	271	29 S	181
		074	65 SE	275	29 S	185
		076	65 SE	273	28 S	183
		076	64 SE	273	27 S	183
		077	64 SE	273	25 S	183
		075	65 SE	267	26 S	177
		079	66 SE	271	25 S	181
		085	63 S	264	20 S	174
		086	62 S	267	18 S	177
		082	60 S	276	19 S	186
		082	61 S	273	20 S	183
		072	63 SE	286	29 SW	196
		071	61 SE	286	28 SW	196
		074	62 SE	282	26 SW	192
		075	61 SE	283	24 SW	193
		078	62 SE	276	23 S	186
		080	62 S	273	22 S	183

Locality: Section PB5, Pecos
Stratigraphic position: Uppermost R3 Member
Plunge of fold axis: 239 32
Paleocurrent indicator: Tabular-planar cross beds
Number of readings: n(total)=26 n=10 n=16
Vector mean: Bimodal 355 178

Bedding		Unrotated		Rotated		Current Direction
Strike	Dip	Strike	Dip	Strike	Dip	Azimuth
100	52 S (ot.)	131	48 SW	279	25 N	009
		130	45 Sw	268	24 N	358
		127	44 SW	266	23 N	356
		127	43 SW	264	23 N	354
		125	43 SW	263	21 N	353
		120	40 SW	255	19 NW	345
		121	40 SW	253	20 NW	343
		131	39 SW	258	26 NW	348
		126	48 SW	268	14 N	358
		121	49 SW	277	10 N	007
		082	69 S	254	24 SE	164
		079	65 SE	266	23 S	176
		080	63 S	268	21 S	178
		082	62 S	267	19 S	177
		072	60 SE	287	25 SW	197
		073	59 SE	290	24 SW	200
		070	68 SE	274	30 S	184
		076	69 SE	264	27 S	174
		075	68 SE	267	27 S	177
		075	71 SE	263	29 S	173
		074	70 SE	266	29 S	176
		070	71 SE	271	33 S	181
		073	69 SE	270	30 S	180
		072	70 SE	269	31 S	179
		071	72 SE	269	33 S	179
		084	77 S	244	38 SE	154

Locality: Section PB6, Pecos
Stratigraphic position: Lower R3 Member
Plunge of fold axis: 242 46
Paleocurrent indicator: Tabular-planar cross beds
Number of readings: n=18
Vector mean: 165

Bedding		Unrotated		Rotated		Current Direction
Strike	Dip	Strike	Dip	Strike	Dip	Azimuth
040	48 NW	009	43 W	266	23 S	176
		007	37 W	251	25 SE	161
		007	36 W	247	26 SE	157
		005	41 W	262	25 S	172
		004	40 W	258	26 SE	168
		002	39 W	255	26 SE	165
		004	41 W	260	27 S	170
		000	36 W	251	29 SE	161
		358	41 W	260	32 S	170
		358	29 W	237	32 SE	143
		355	38 W	254	31 SE	164
		353	33 W	245	34 SE	155
		356	46 W	270	32 S	180
		351	35 W	249	33 SE	159
		350	39 W	257	34 SE	167
		349	36 NW	251	35 SE	161
		343	39 NW	256	39 SE	166
		004	39 W	255	27 SE	165

Locality: Section T1, Truchas
Stratigraphic position: 49 - 51 m within R3 Member
Plunge of fold axes: F1 = 219 52; F2 = 262 9
Paleocurrent indicator: Tabular-planar cross beds
Number of readings: n(total)=27 n=14 n=13
Vector mean: Bimodal 167 350

Bedding		Unrotated		Rotated		Current Direction
Strike	Dip	Strike	Dip	Strike	Dip	Azimuth
082	75 S	075	80 SE	034	12 SE	124
		075	81 SE	038	14 SE	128
		076	82 SE	045	12 SE	135
		080	78 S	061	7 SE	151
		076	88 SE	064	17 SE	154
		080	85 S	072	12 SE	162
		082	85 S	080	11 S	170
		083	84 S	080	10 S	170
		083	83 S	080	8 S	170
		084	85 S	091	11 S	181
		085	84 S	094	10 S	184
		086	83 S	100	8 S	190
		091	81 S	152	12 SW	242
		081	90	080	16 S	170
		096	69 S	031	16 NW	301
		098	63 S	045	19 NW	315
		091	68 S	046	12 NW	316
		092	61 S	063	17 NW	333
		085	62 S	079	13 NW	349
		088	57 S	077	19 NW	347
		084	58 S	087	17 N	357
		081	58 S	094	16 N	004
		081	57 S	097	18 N	007
		086	57 S	087	28 N	357
		083	50 S	093	27 N	003
		071	54 SE	119	23 NE	029
		074	60 SE	119	16 NE	029

Locality: Section T1, Truchas
Stratigraphic position: 73 - 75 m within R3 Member
Plunge of fold axes: F1 = 219 52; F2 = 262 9
Paleocurrent indicator: Tabular-planar cross beds
Number of readings: n(total)=46 n=31 n=15
Vector mean: Bimodal 169 336

Bedding		Unrotated		Rotated		Current Direction
Strike	Dip	Strike	Dip	Strike	Dip	Azimuth
086	73 S	069	90	053	24 SE	143
		068	88 SE	049	23 SE	139
		080	90	080	19 S	170
		081	89 S	082	18 S	172
		080	87 S	080	16 S	170
		086	90	099	18 S	189
		089	90	110	18 SW	200
		092	88 S	122	18 SW	212
		093	85 S	128	15 SW	218
		096	97 S	154	12 SW	244
		070	79 SE	134	16 SW	124
		074	83 SE	051	16 SE	141
		075	84 SE	056	16 SE	146
		076	84 SE	059	15 SE	149
		076	83 SE	054	15 SE	144
		075	81 SE	048	14 SE	138
		078	83 SE	064	14 SE	154
		078	84 SE	066	15 SE	156
		077	85 SE	065	16 SE	155
		078	85 SE	071	15 SE	161
		080	84 S	074	13 SE	164
		081	83 S	078	12 SE	168
		082	82 S	079	11 SE	169
		080	81 S	070	10 SE	160
		082	78 S	071	7 SE	161
		085	80 S	096	9 S	186
		084	82 S	087	10 S	177
		085	82 S	096	10 S	186
		085	84 S	096	12 S	186
		087	82 S	105	11 SW	195
		075	89 NW	065	22 SE	155
		105	68 SW	028	19 NW	298
		112	61 SW	038	27 NW	308
		103	63 SW	043	19 NW	313
		099	65 S	043	15 NW	313
		093	65 S	053	11 NW	321
		093	64 S	054	12 NW	324
		097	60 S	059	17 NW	329
		088	57 S	088	16 N	358
		088	56 S	091	17 N	001
		076	57 SE	068	17 NE	038
		084	50 S	100	22 N	010
		090	51 S	089	21 N	359
		095	54 S	075	20 NW	345
		109	49 SW	069	30 NW	332
		120	45 SW	059	39 NW	329

Locality: Section T1, Truchas
Stratigraphic position: 105 - 109 m within R3 Member
Plunge of fold axes: F1 = 219 52; F2 = 262 9
Paleocurrent indicator: Tabular-planar cross beds
Number of readings: n(total)=49 n=27 n=22
Vector mean: Bimodal 182 358

Bedding		Unrotated		Rotated		Current Direction
Strike	Dip	Strike	Dip	Strike	Dip	Azimuth
084	74 S	093	80 S	154	11 SW	244
		093	80 S	154	11 SW	244
		090	83 S	132	13 SW	222
		085	82 S	106	9 SW	196
		085	84 S	105	11 SW	195
		074	80 SE	040	12 SE	130
		069	84 SE	042	18 SE	132
		071	87 SE	054	18 SE	144
		070	88 SE	053	20 SE	143
		072	90	059	21 SE	149
		077	85 SE	068	14 SE	158
		078	85 SE	072	13 SE	162
		080	87 S	086	14 S	176
		081	87 S	087	13 S	177
		083	88 S	092	14 S	182
		080	89 S	088	16 S	178
		079	89 SE	083	16 S	173
		080	90	085	17 S	175
		083	90	095	17 S	185
		088	90	116	17 SW	206
		090	89 N	118	20 SW	208
		084	88 N	103	19 SW	193
		083	87 N	097	20 S	187
		083	86 N	100	21 S	190
		079	89 NW	087	19 S	177
		080	87 N	088	21 S	178
		085	81 N	103	25 SW	193
		087	40 S	093	30 N	003
		094	51 S	086	24 NW	346
		079	50 SE	104	25 NE	014
		080	54 S	106	30 NE	016
		083	55 S	097	18 N	007
		080	56 S	107	19 NE	017
		070	60 SE	135	18 NE	045
		078	59 SE	111	15 NE	021
		081	60 S	103	15 NE	013
		084	60 S	095	14 N	005
		073	64 SE	135	14 NE	045
		080	66 S	118	9 NE	028
		084	44 S	093	10 N	003
		091	61 S	068	15 NW	338
		095	63 S	052	16 NW	325
		097	65 S	046	16 NW	316
		089	64 S	073	15 NW	343
		091	67 S	062	12 NW	332
		088	65 S	070	10 NW	340
		088	65 S	070	10 NW	340
		089	87 S	055	9 NW	325
		091	67 S	054	10 NW	324

Locality: Section T1, Truchas
Stratigraphic position: 130 - 133 m within R3 Member
Plunge of fold axes: F1 = 219 52; F2 = 262 9
Paleocurrent indicator: Tabular-planar cross beds
Number of readings: n(total)=39 n=22 n=17
Vector mean: Bimodal 186 327

Bedding		Unrotated		Rotated		Current Direction
Strike	Dip	Strike	Dip	Strike	Dip	Azimuth
083	73 S	085	52 S	092	22 N	002
		085	55 S	090	20 N	000
		085	56 S	092	12 N	002
		090	55 S	077	20 NW	347
		096	56 S	065	22 NW	335
		103	54 SW	056	27 NW	326
		108	55 SW	050	28 NW	320
		110	55 SW	049	31 NW	319
		091	62 S	070	15 NW	340
		102	64 SW	040	20 NW	310
		084	68 S	091	7 N	001
		090	66 S	061	10 NW	331
		096	68 S	036	14 NW	306
		098	69 S	026	16 NW	296
		093	69 S	035	10 NW	305
		094	71 S	022	11 NW	292
		092	72 S	017	8 NW	286
		075	83 SE	057	13 SE	147
		075	85 SE	067	12 SE	157
		078	83 SE	063	14 SE	153
		081	82 S	088	9 S	178
		081	83 S	089	10 S	179
		083	83 S	096	10 S	186
		085	81 S	117	8 SW	207
		087	80 S	134	8 SW	224
		089	83 S	135	12 SW	225
		090	84 S	138	13 SW	228
		089	84 S	129	13 SW	219
		082	85 S	092	12 S	182
		079	85 SE	081	12 S	171
		082	87 S	092	14 S	182
		081	87 S	089	14 S	179
		078	88 SE	079	15 SE	169
		078	89 SE	076	17 SE	166
		084	87 S	101	13 SW	191
		085	88 S	104	14 SW	194
		087	87 S	113	13 SW	203
		079	87 NW	088	20 S	178
		078	87 NW	081	20 S	173

Locality: Section P1, Picuris
Stratigraphic position: Middle R3 Member
Plunge of fold axis: 267 15
Paleocurrent indicator: Tabular-planar cross beds
Number of readings: n(total)=35 n=25 n=10
Vector mean: Bimodal 142 326

Bedding		Unrotated		Rotated		Current Direction
Strike	Dip	Strike	Dip	Strike	Dip	Azimuth
290	35 S	245	60 SE	206	51 SE	116
		227	49 SE	227	24 SE	137
		266	54 SE	232	28 SE	142
		279	48 S	261	15 S	171
		340	35 SW	228	29 NW	318
		269	50 S	235	22 SE	145
		253	49 SE	207	34 SE	117
		316	25 SW	248	17 NW	338
		319	32 SW	228	17 NW	318
		252	72 SE	218	61 SE	128
		339	30 SW	237	27 NW	327
		262	44 S	211	23 SE	121
		275	49 S	252	18 SE	162
		285	40 SW	267	7 S	177
		286	50 SW	233	24 SE	143
		249	58 SE	209	45 SE	119
		325	28 SW	240	20 NW	330
		322	30 SW	234	19 NW	324
		275	48 S	248	18 SE	158
		270	55 S	245	26 SE	155
		260	57 S	225	35 SE	135
		248	61 SE	210	50 SE	120
		336	28 SW	240	25 NW	330
		286	52 SW	292	19 SW	202
		265	48 S	224	24 SE	134
		255	55 SE	216	37 SE	126
		256	50 SE	212	33 SE	122
		275	53 S	258	22 SE	168
		265	51 S	228	27 SE	138
		330	29 SW	236	22 NW	325
		258	52 SE	217	33 SE	127
		334	27 SW	242	23 NW	332
		270	50 S	239	22 SE	149
		268	45 S	225	20 SE	135
		331	32 SW	230	24 NW	320

Locality: Section P2, Picuris
Stratigraphic position: Lower R3 Member
Plunge of fold axis: 267 15
Paleocurrent indicator: Tabular-planar cross beds
Number of readings: n(total)=29 n=14 n=15
Vector mean: Bimodal 104 292

Bedding		Unrotated		Rotated		Current Direction
Strike	Dip	Strike	Dip	Strike	Dip	Azimuth
265	46 S	241	58 SE	183	34 E	093
		306	28 SW	236	31 NW	326
		301	42 SW	207	29 NW	297
		255	53 SE	202	12 SE	112
		302	44 SW	204	30 NW	294
		289	45 SW	196	23 NW	286
		321	44 SW	215	41 NW	305
		305	39 SW	214	32 NW	304
		240	50 SE	170	30 E	080
		286	50 SW	182	22 W	272
		272	55 S	142	16 SW	231
		288	45 SW	192	22 NW	283
		305	36 SW	219	31 NW	309
		243	60 SE	189	34 E	098
		250	52 SE	187	18 E	097
		307	34 SW	222	33 NW	312
		309	34 SW	222	34 NW	312
		248	58 SE	195	25 SE	105
		250	49 SE	179	17 E	089
		259	63 SE	259	18 SE	165
		258	55 SE	231	10 SE	141
		300	44 NW	202	29 NW	292
		248	63 SE	205	28 SE	115
		242	49 SE	171	26 E	081
		289	58 SW	170	34 W	260
		240	58 SE	181	36 E	091
		243	55 SE	182	29 E	092
		300	40 SW	212	28 NW	302
		241	64 SE	189	42 E	099

Locality: Section P3, Picuris
Stratigraphic position: Lower R3 Member
Plunge of fold axis: 267 15

Paleocurrent indicator: Tabular-planar cross beds
Number of readings: n(total)=23 n=20 n=3
Vector mean: Bimodal 254 084

Bedding		Unrotated		Current Direction
Strike	Dip	Pitch	Transport	Azimuth
252	78 SE (ot.)	14 W	W	250
		17 W	W	252
		19 W	W	254
		20 W	W	255
		20 W	W	255
		22 W	W	258
		09 W	W	244
		24 W	W	259
		27 W	W	263
		31 W	SW	204
		09 W	W	244
		22 W	E	078
		27 W	W	263
		30 W	E	086
		32 W	W	267
		34 W	W	269
		34 W	E	089
		38 W	W	273
		39 W	W	274
		41 W	W	275
		42 W	W	276
		04 E	W	231
		18 E	W	215

Paleocurrent indicator: Trough cross beds
Number of readings: n=16
Vector mean: 154

	71 E	S	165
	74 E	S	162
	76 E	S	161
	77 E	S	159
	77 E	S	159
	78 E	S	158
	79 E	S	156
	79 E	S	156
	80 E	S	154
	82 E	S	153
	83 E	S	152
	84 E	S	151
	84 E	S	151
	86 E	S	149
	88 E	S	147
	71 W	S	130

Locality: Section P4, Picuris
Stratigraphic position: R3 Member
Plunge of fold axis: Horizontal
Paleocurrent indicator: Tabular-planar cross beds
Number of readings: n(total)=14 n=12 n=2
Vector mean: Bimodal 183 343

Bedding		Unrotated		Rotated		Current Direction
Strike	Dip	Strike	Dip	Strike	Dip	Azimuth
292	32 SW	279	52 S	266	22 S	176
		282	49 SW	270	18 S	180
		284	60 SW	278	29 S	188
		288	42 SW	286	11 SW	196
		288	52 SW	286	21 SW	196
		292	56 SW	294	24 SW	204
		295	81 SW	296	48 SW	206
		305	20 SW	268	14 N	358
282	38 SW	263	53 S	234	20 SE	144
		265	46 S	221	14 SE	131
		268	40 S	241	15 SE	151
		285	55 SW	291	17 SW	201
		289	49 SW	307	13 SW	217
		333	26 SW	237	28 NW	327

Locality: Section P5, Picuris
Stratigraphic position: Upper R3 Member
Plunge of fold axis: Horizontal
Paleocurrent indicator: Tabular-planar cross beds
Number of readings: n(total)=14 n=11 n=3
Vector mean: Bimodal 147 321

Bedding		Unrotated		Rotated		Current Direction
Strike	Dip	Strike	Dip	Strike	Dip	Azimuth
256	38 SE	239	66 SE	225	31 SE	135
		240	63 SE	224	28 SE	134
		240	61 SE	223	25 SE	133
		244	70 SE	235	33 SE	145
		246	63 SE	237	28 SE	147
		248	62 SE	240	24 SE	150
		249	68 SE	243	30 SE	153
		256	65 SE	257	26 SE	167
		265	58 S	279	21 S	189
		265	26 S	236	15 NW	326
		273	20 S	235	20 NW	325
		282	23 SW	224	21 NW	314
252	53 SE	244	59 SE	214	10 SE	121
		248	61 SE	234	10 SE	144

Locality: Paleocurrent station PS1, Picuris
Stratigraphic position: R3 Member
Plunge of fold axis: 267 15

Paleocurrent indicator: Tabular-planar cross beds
Number of readings: n(total)=19 n=18 n=1
Vector mean: Bimodal 252 062

Bedding		Unrotated		Current Direction
Strike	Dip	Pitch	Transport	Azimuth
084	90	5 E	W	245
		7 E	W	243
		8 E	W	242
		8 E	E	062
		10 E	W	240
		11 E	W	239
		13 W	W	237
		26 W	W	276
		20 W	W	270
		12 W	W	262
		10 W	W	260
		10 W	W	260
		9 W	W	259
		6 W	W	256
		5 W	W	255
		5 W	W	255
		4 W	W	254
		4 W	W	254
		28 E	W	221

Paleocurrent indicator: Trough cross beds
Number of readings: n=8
Vector mean: 174

084	90	59 E	S	157
		69 E	S	167
		70 E	S	168
		75 E	S	171
		76 E	S	172
		77 E	S	173
		82 E	S	181
		88 W	S	192

Paleocurrent indicator: Symmetrical ripples
Number of readings: n=3
Vector mean: 018-198

45 E	204-024
50 E	199-019
60 E	190-010

Locality: Paleocurrent station PS2, Picuris
Stratigraphic position: Upper R3 Member
Plunge of fold axis: Horizontal
Paleocurrent indicator: Tabular-planar cross beds
Number of readings: n(total)=24 n=15 n=9
Vector mean: Bimodal 183 325

Bedding		Unrotated		Rotated		Current Direction
Strike	Dip	Strike	Dip	Strike	Dip	Azimuth
093	60 S (ot.)	067	46 SE	225	24 NW	315
		070	48 SE	224	22 NW	314
		074	52 SE	216	17 NW	306
		075	46 SE	234	20 NW	324
		075	49 SE	218	18 NW	318
		080	50 S	232	15 NW	322
		084	68 S	314	11 SW	224
		085	54 S	237	10 NW	327
		085	70 S	309	12 SW	219
		085	80 S	192	21 SW	202
		086	76 S	192	17 SW	202
		087	70 S	300	11 SW	210
		090	45 S	264	15 N	354
		089	75 S	280	16 SW	190
		090	54 S	256	7 NW	346
		090	70 S	283	10 SW	193
		093	65 S	257	6 SE	167
		093	80 S	267	20 S	177
		095	66 S	247	7 SE	157
		095	75 S	259	15 SE	169
		095	77 S	259	18 SE	169
		095	71 S	255	12 SE	165
		097	70 S	244	12 SE	154
		105	76 SW	230	19 SE	140

Locality: Paleocurrent station PS3, Picuris
Stratigraphic position: R5 Member
Plunge of fold axis: 267 15
Paleocurrent indicator: Small-scale trough cross beds
Number of readings: n=26
Vector mean: 173

Bedding		Unrotated		Current Direction
Strike	Dip	Pitch	Transport	Azimuth
080	90	40 E	S	204
		43 E	S	201
		48 E	S	196
		50 E	S	195
		50 E	S	195
		50 E	S	195
		50 E	S	195
		51 E	S	193
		52 E	S	191
		58 E	S	187
		60 E	S	185
		65 E	S	180
		70 E	S	175
		70 E	S	175
		70 E	S	175
		71 E	S	172
		75 E	S	170
		75 E	S	170
		80 E	S	164
		85 E	SE	159
		87 E	SE	156
		85 W	SE	149
		85 W	SE	149
		70 W	SE	134
		70 W	SE	134
		35 W	SE	100

Locality: Paleocurrent station PS4, Picuris
Stratigraphic position: R3 Member
Plunge of fold axis: 267 15

Paleocurrent indicator: Tabular-planar cross beds
Number of readings: n(total)=28 n=24 n=4
Vector mean: Bimodal 244 031

Bedding		Unrotated		Rotated		Current Direction
Strike	Dip	Strike	Dip	Strike	Dip	Azimuth
067	76 SE (ot.)	049	71 SE	154	28 SW	244
		053	76 SE	138	14 SW	228
		054	76 SE	141	13 SW	231
		055	81 SE	116	13 SW	206
		048	66 SE	163	31 SW	253
		052	67 SE	164	28 SW	254
		047	72 SE	152	30 SW	242
		053	64 SE	173	S7 SW	263
		048	70 SE	156	30 SW	246
		090	75 S	136	23 NE	046
080	71 S (ot.)	049	71 SE	158	30 SW	248
		059	77 SE	139	21 SW	229
		048	74 SE	150	32 SW	240
		045	73 SE	154	34 SW	244
		052	72 SE	155	28 SW	245
		056	71 SE	157	24 SW	247
		059	74 SE	147	21 SW	237
		044	75 SE	152	35 SW	242
		095	66 S	127	15 NE	037
		047	80 SE	141	34 SW	231
065	84 SE (ot.)	052	75 SE	177	16 W	267
		050	70 SE	185	21 W	275
		050	82 SE	148	14 SW	238
		044	85 SE	140	20 SW	230
		045	75 SE	167	22 SW	257
		094	60 S	123	22 NE	033
		086	78 S	097	36 N	007
		052	74 SE	179	17 W	269

Paleocurrent indicator: Trough cross beds
Number of readings: n=12
Vector mean: 171

Bedding		Unrotated		Current Direction
Strike	Dip	Pitch	Transport	Azimuth
085	65 S (ot.)	65 E	S	186
		70 E	S	180
		70 E	S	180
		75 E	S	176
		75 E	S	176
		80 E	S	170
		80 E	S	170
		80 E	S	170
		85 E	S	166
		90	S	160
		90	S	160
		90	S	160

Locality: Section JB1, Tusas
Stratigraphic position: Lower Ortega Quartzite
Plunge of fold axis: 283 15
Paleocurrent indicator: Small-scale trough cross beds
Number of readings: n=19
Vector mean: 185

Bedding		Unrotated		Current Direction
Strike	Dip	Pitch	Transport	Azimuth
107	65 SW	88 E	S	204
		85 E	S	201
		83 E	S	199
		83 E	S	199
		80 E	S	196
		78 E	S	194
		78 E	S	194
		72 E	S	189
		71 E	S	187
		69 E	S	186
		68 E	S	184
		68 E	S	184
		62 E	S	178
		62 E	S	178
		60 E	S	176
		58 E	S	174
		55 E	S	172
		50 E	S	167
		47 E	S	162

Locality: Section JB1, Tusas
Stratigraphic position: Basal Ortega Quartzite
Plunge of fold axis: 283 15
Paleocurrent indicator: Large-scale trough cross beds
Number of readings: n=15
Vector mean: 193

Bedding		Unrotated		Current Direction
Strike	Dip	Pitch	Transport	Azimuth
110	60 S	87 E	S	205
		86 E	S	204
		84 E	S	202
		82 E	S	200
		80 E	S	198
		80 E	S	198
		75 E	S	193
		74 E	S	191
		74 E	S	191
		73 E	S	190
		70 E	S	188
		69 E	S	187
		67 E	S	185
		67 E	S	185
		60 E	S	178

Locality: Section JB1, Tusas
Stratigraphic position: Upper Ortega Quartzite
Plunge of fold axis: 283 15

Paleocurrent indicator: Tabular-planar cross beds
Number of readings: n=18
Vector mean: 139

Bedding		Unrotated		Rotated		Current Direction
Strike	Dip	Strike	Dip	Strike	Dip	Azimuth
118	52 SW	087	53 S	025	26 SE	115
		082	60 S	036	31 SE	126
		089	58 S	036	25 SE	126
		097	57 S	039	19 SE	129
		090	60 S	041	25 SE	131
		092	60 S	041	24 SE	131
		101	58 SW	045	16 SE	135
		098	59 S	045	19 SE	135
		083	66 S	046	33 SE	136
		088	63 S	047	28 SE	137
		100	62 S	055	19 SE	145
		098	63 S	055	21 SE	145
		096	66 S	059	24 SE	149
		100	65 S	060	20 SE	150
		093	69 S	061	28 SE	151
		095	68 S	063	26 SE	153
		101	65 SW	065	20 SE	155
		103	64 SW	067	18 SE	157

Paleocurrent indicator: Trough cross beds
Number of readings: n=25
Vector mean: 192

Bedding		Unrotated		Current Direction
Strike	Dip	Pitch	Transport	Azimuth
118	52 SW	78 W	SW	228
		82 E	S	207
		81 E	S	206
		77 E	S	203
		75 E	S	200
		75 E	S	200
		74 E	S	199
		72 E	S	198
		72 E	S	198
		72 E	S	198
		70 E	S	196
		70 E	S	196
		69 E	S	195
		67 E	S	193
		67 E	S	193
		65 E	S	192
		64 E	S	190
		62 E	S	188
		59 E	S	185
		56 E	S	182
		56 E	S	182
		54 E	S	181
		54 E	S	181
		52 E	S	177
		39 E	S	165

Locality: Paleocurrent station JB2, Tusas
Stratigraphic Position: Upper Ortega Quartzite
Plunge of fold axis: 283 15

Paleocurrent indicator: Tabular-planar cross beds
Number of readings: n=8
Vector mean: 218

Bedding		Unrotated		Rotated		Current Direction
Strike	Dip	Strike	Dip	Strike	Dip	Azimuth
076	45 NW	029	37 NW	125	28 SW	215
070	46 NW	046	29 NW	101	20 SW	191
070	48 NW	044	49 NW	119	18 SW	209
076	45 NW	038	38 NW	119	22 SW	209
071	44 NW	032	37 NW	121	26 SW	211
070	46 NW	036	42 NW	128	24 SW	218
066	43 NW	042	52 NW	154	21 SW	244
070	46 NW	046	49 NW	156	17 SW	246

Paleocurrent indicator: Trough cross beds
Number of readings: n=13
Vector mean: 209

Bedding		Unrotated		Current Direction
Strike	Dip	Pitch	Transport	Azimuth
076	45 NW	16 E	SW	235
		24 E	SW	227
064	50 NW	30 E	SW	220
076	45 NW	33 E	SW	218
		47 E	S	205
064	50 NW	50 E	S	201
070	53 NW	55 E	S	196
076	45 NW	55 E	S	196
		56 E	S	194
		60 E	S	191
070	53 NW	65 E	S	186
076	45 NW	74 E	S	177
		19 W	S	268

Locality: Paleocurrent station JB3, Tusas
Stratigraphic position: Upper Ortega Quartzite
Plunge of fold axis: 283 15

Paleocurrent indicator: Tabular-planar cross beds
Number of readings: n=14
Vector mean: 119

Bedding		Unrotated		Rotated		Current Direction
Strike	Dip	Strike	Dip	Strike	Dip	Azimuth
151	25 SW	120	46 SW	101	26 SW	191
		124	40 SW	099	20 S	189
		131	32 SW	093	11 S	183
		131	48 SW	119	25 SW	209
		133	49 SW	123	26 SW	213
		138	40 SW	127	17 SW	217
		146	44 SW	148	20 SW	238
164	33 SW	140	47 SW	102	21 SW	192
		140	50 SW	107	24 SW	197
		163	45 SW	158	12 SW	248
135	25 SW	115	45 SW	098	23 S	188
131	22 SW	090	40 S	060	26 SE	150
		100	38 S	074	21 SE	164
140	27 SW	129	45 SW	119	19 2W	209

Paleocurrent indicator: Trough cross beds
Number of readings: n=6
Vector mean: 243

Bedding		Unrotated		Current Direction
Strike	Dip	Pitch	Transport	Azimuth
153	23 SW	87 W	SW	249
		87 E	SW	243
		82 E	SW	237
		82 W	W	254
		73 W	W	263
140	27 SW	70 E	SW	213

Locality: Paleocurrent station JB4, Tusas
Stratigraphic position: Upper Ortega Quartzite
Plunge of fold axis: 283 15

Paleocurrent indicator: Tabular-planar cross beds
Number of readings: n=25
Vector mean: 179

Bedding		Unrotated		Rotated		Current Direction
Strike	Dip	Strike	Dip	Strike	Dip	Azimuth
125	45 SW	090	60 S	057	32 SE	147
		090	65 S	064	35 SE	154
		100	65 S	077	29 SE	167
		105	60 SW	079	22 SE	169
		105	60 SW	079	22 SE	169
		105	65 SW	086	26 S	176
		105	70 SW	090	30 S	180
		105	70 SW	090	30 S	180
		110	70 SW	103	27 SW	193
		175	35 SW	257	33 NW	347
120	40 SW	095	70 S	084	35 SE	174
		095	70 S	084	35 SE	174
		095	75 S	088	40 SE	178
		100	65 S	087	30 SE	177
115	45 SW	090	65 S	066	29 SE	156
		100	65 S	084	23 SE	174
		100	65 S	084	23 SE	174
		100	65 S	084	23 SE	174
		100	70 S	090	28 S	180
		100	75 S	093	32 S	183
		105	65 SW	096	21 S	186
		110	70 SW	110	25 SW	200
		120	65 SW	135	21 SW	225
		120	75 SW	131	30 SW	221
		140	60 SW	181	24 SW	271

Paleocurrent indicator: Trough cross beds
Number of readings: n=12
Vector mean: 204

Bedding		Unrotated		Current Direction
Strike	Dip	Pitch	Transport	Azimuth
115	45 SW	90	SW	211
		90	SW	211
		90	SW	211
		85 E	S	206
110	45 SW	80 W	SW	216
		80 W	SW	216
		85 W	SW	211
		90	SW	206
		85 E	S	204
		73 E	S	190
		73 E	S	190
		65 E	S	181

Locality: Paleocurrent station JB5, Tusas
Stratigraphic position: Upper Ortega Quartzite
Plunge of fold axis: 283 15

Paleocurrent indicator: Tabular-planar cross beds
Number of readings: n=25
Vector mean: 183

Bedding		Unrotated		Rotated		Current Direction
Strike	Dip	Strike	Dip	Strike	Dip	Azimuth
110	50 SW	085	65 S	053	25 SE	143
		110	80 SW	117	32 SW	207
		090	75 S	075	30 SE	165
		095	80 S	088	32 S	178
		110	80 SW	117	32 SW	207
		120	75 SW	139	26 SW	229
		120	75 SW	139	26 SW	229
		090	70 S	068	26 SE	158
		095	70 S	079	23 SE	169
110	60 SW	100	65 S	059	10 SE	149
		095	80 S	080	24 S	170
		090	70 S	052	20 SE	142
		100	80 S	092	21 S	182
		120	75 SW	158	17 SW	248
		105	75 SW	106	15 SE	196
		095	70 S	162	17 SE	152
		100	80 S	092	21 S	182
		095	75 S	074	20 SE	164
115	55 SW	100	90	101	36 SW	191
		125	75 SW	149	23 SW	239
		120	80 SW	137	25 SW	227
		095	70 S	067	23 SE	157
		090	80 S	075	33 SE	165
		095	70 S	076	27 SE	166
		100	70 S	079	20 SE	169

Paleocurrent indicator: Trough cross beds
Number of readings: n=8
Vector mean: 208

Bedding		Unrotated		Current Direction
Strike	Dip	Pitch	Transport	Azimuth
110	50 SW	85 W	SW	212
		85 W	SW	212
		90	S	207
		90	S	207
		75 E	S	191
110	60 SW	85 W	SW	214
115	55 SW	90	SW	213
		85 E	S	208

Locality: Section MQ1, Picuris
Stratigraphic position: Middle Marquenas Quartzite
Plunge of fold axis: 100 20

Paleocurrent indicator: Trough cross beds
Number of readings: n=25
Vector mean: 027

Bedding		Unrotated		Current Direction
Strike	Dip	Pitch	Transport	Azimuth
275	80 S (ot.)	55 W	N	353
		65 W	N	003
		65 W	N	003
		65 W	N	003
		69 W	N	007
		75 W	N	013
		75 W	N	013
		75 W	N	013
		85 W	N	023
		90	N	028
		90	N	028
		90	N	028
		80 W	N	018
		84 E	NW	033
		82 E	NW	036
		81 E	NW	037
		80 E	NW	038
		80 E	NW	038
		80 E	NW	038
		75 E	NW	042
		75 E	NW	042
		70 E	NW	048
		70 E	NW	048
		70 E	NW	048
		65 E	NW	053

Paleocurrent indicator: Primary current lineations
Number of readings: n=22
Vector mean: 146-326

	60 W	174-354
	25 W	139-319
	40 W	153-333
	45 W	159-339
	40 W	153-333
	40 W	153-333
	52 W	166-346
	50 W	165-345
	46 W	161-341
	49 W	164-344
	50 W	165-345
	62 W	177-357
	38 W	151-331
	10 W	124-304
	15 W	129-309
	15 W	129-309
	25 W	139-319
	10 W	124-304
	10 W	124-304
	5 W	118-299
	0	115-295
	25 W	139-319

Appendix D

PETROGRAPHY OF PEBBLES FROM MARQUENAS CONGLOMERATE CONTRASTED WITH PETROGRAPHY OF SELECTED ORTEGA AND VADITO GROUP

Lithologies of boulders, cobbles and pebbles in the Marquenas conglomerate are analogous to rock types in the Ortega and Vadito Groups. It has been concluded from this study that the Marquenas conglomerates were derived from both the Ortega and Vadito Groups. In this section similarities and differences between pebble-parent pairs are contrasted petrographically.

Ortega Group and Marquenas Pebble Lithology Pairs

Quartz Arenite: More than 90 percent of pebbles in the Marquenas conglomerate consist of grey quartzite. In the Ortega Group grey and white quartzites also dominate, and are present in the Ortega Quartzite, R3 and R5 Members. Quartz grains within quartzite pebbles and in the Ortega quartzite units are totally recrystallized and abut oneanother at 120 degree triple junctions (Fig. 39). Well-rounded detrital tourmaline grains (Figs. 39 and 40), in some cases with authigenic overgrowths (Fig. 39b), and detrital zircon grains in both pebbles and parent rock (Figs. 41) imply that the protolith to the quartzites was quartz arenite.

Figure 39: Well-rounded detrital tourmaline grain within recrystallized quartzite pebble from Marquenas conglomerate. Note 120 degree angle between grain boundaries of recrystallized quartz (arrow). Crossed nicols. Horizontal field of view is 2 mm.

Figure 40: Well-rounded detrital tourmaline grain with authigenic overgrowth from R3 Member, Rinconada Formation in southern Picuris range. Width of plate is 1 mm.

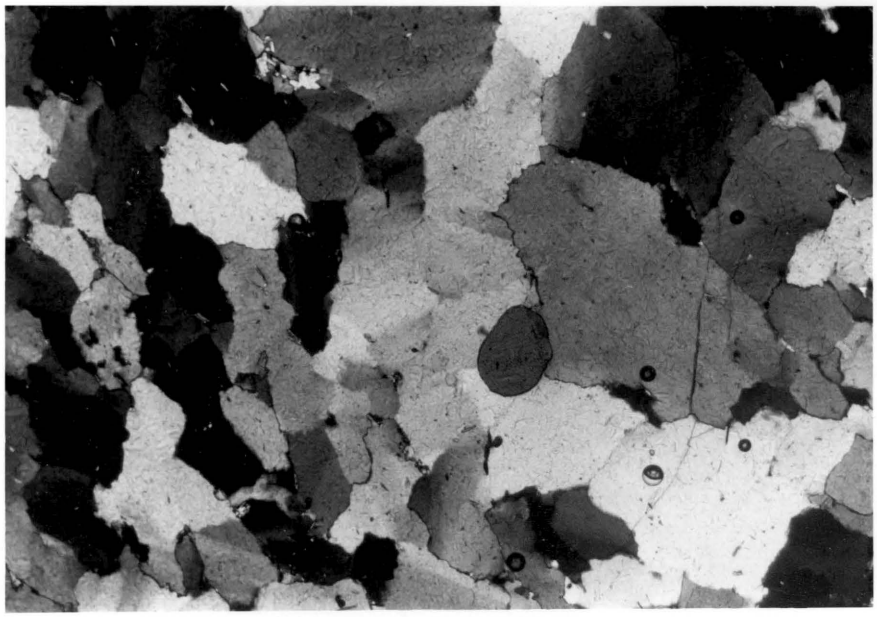

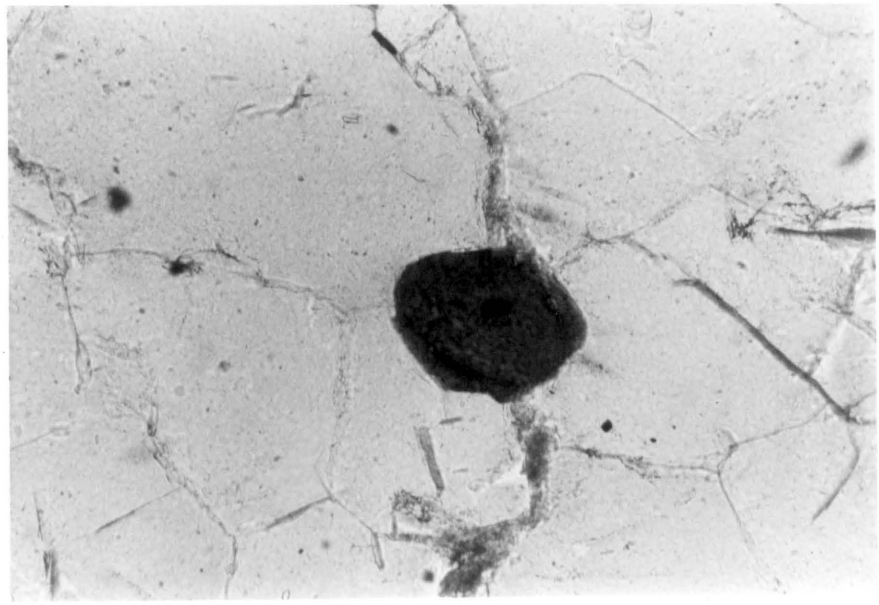

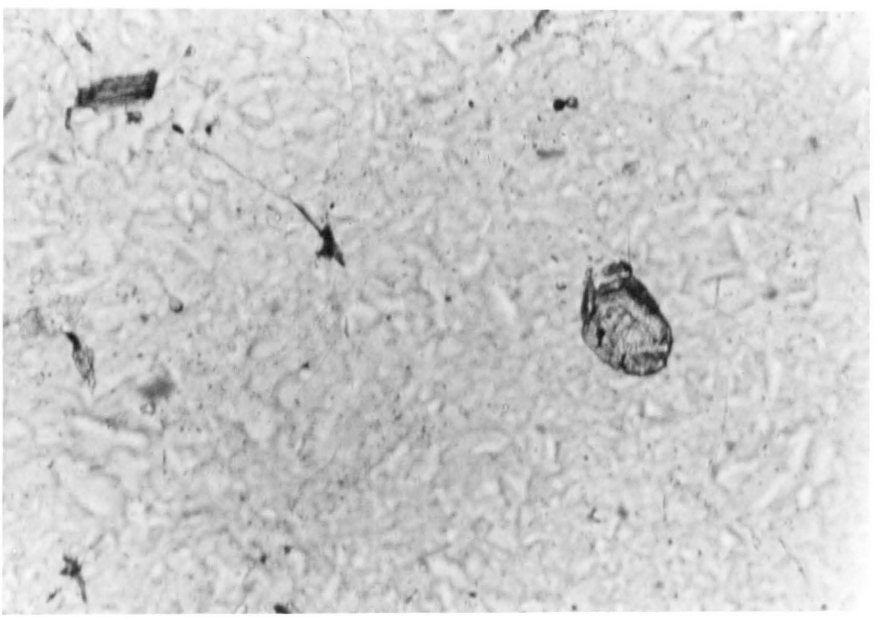

Figure 41: Well-rounded detrital zircon grain within recrystallized quartzite pebble from Marquenas conglomerate.

Quartz Arenite with Heavy Mineral Banding: Metamorphosed quartz arenite pebbles in the Marquenas Quartzite display rare magnetite enriched laminations. Magnetite is similarly concentrated along foresets of cross beds in the Ortega Group.

Black Quartzite: Black quartzite pebbles are common in the Marquenas conglomerate and are paired with black quartzite beds at the top of the R3 Member, within and at the top of the R5 Member and at the boundary between the R6 Member and Pilar Slate. These quartzites owe their black coloration to fine-grained disseminated hematite and subordinate magnetite. The black quartzite pebbles and parent rock contain detrital tourmaline and zircon indicating a sedimentary origin for the quartzites.

Garnet-Biotite Quartzite: Garnet- and biotite-bearing quartzite pebbles in the Marquenas conglomerate are identical to garnet- and biotite-bearing quartzites at the contact between the R6 Member and Pilar Slate in the southern Picuris range. In both pebble and parent rocks, garnet and biotite is poikiloblastic surrounding earlier microcrystalline quartz. Biotite in both quartzites is partially retrograded to chlorite. In Marquenas pebbles the poikiloblastic garnets are idioblastic whereas these garnets are xenoblastic in the R6 Member. Abundant fine-grained disseminated hematite exists in the R6 quartzite but is absent in garnet-biotite quartzite pebbles in the Marquenas Quartzite.

Biotite-Garnet-Quartz-Muscovite Schist: Pelitic schists are abundant in the Ortega Group, in the R1, R2, R4 and R6 Members of the Rinconada Formation and in the Piedra Lumbre Formation. Rare pelitis schist pebbles exist in the Marquenas conglomerate. The Rinconada schists contain variable amounts of biotite, garnet, quartz, staurolite and muscovite with minor tourmaline, plagioclase, graphite, ilmenite, andalusite, kyanite and sillimanite (Holdaway, 1978). Pelitic schist pebbles could not be extracted from the Marquenas metaconglomerates due to the friable nature of the pebbles. However, based on field observations, pelitic pebbles in the Marquenas Quartzite are comprised of biotite, garnet, quartz and muscovite and are analogous to the pelitic schists in the Ortega Group. A notable difference between schist pebbles and Rinconada schists is the absence of staurolite porphyroblasts in the pebbles. The protolith to the pelitic schists was mudstone. The low abundance of pelitic pebbles in the Marquenas Quartzite is due to the low preservation potential of mudstone pebbles during transportation within braided alluvial systems, as those present during deposition of the Marquenas Quartzite.

Calc-silicate: Calc-silicate pebbles in the Marquenas conglomerate are lithologically identical to calc-silicate beds in the Piedra Lumbre Formation. Large xenoblastic garnet, green hornblende porphyroblasts and accessory plagioclase are imbedded within a microcrystalline quartzite matrix, and comprise a primary metamorphic mineral assemblage (Figs. 42 and 43). A retrograde metamorphic event resulted in chlorite (from hornblende) idioblastic garnet poikiloblasts and

Figure 42: Calc-silicate pebble from Marquenas conglomerate containing poikiloblastic garnet (1) and relict hornblende retrograded to chlorite (2). lateral field of view is 5 mm.

Figure 43: Calc-silicate from Piedra Lumbre Formation in southern Picuris range containing poikiloblastic garnet (1) and relict hornblende retrograded to chlorite (2). Plate width is 5 mm.

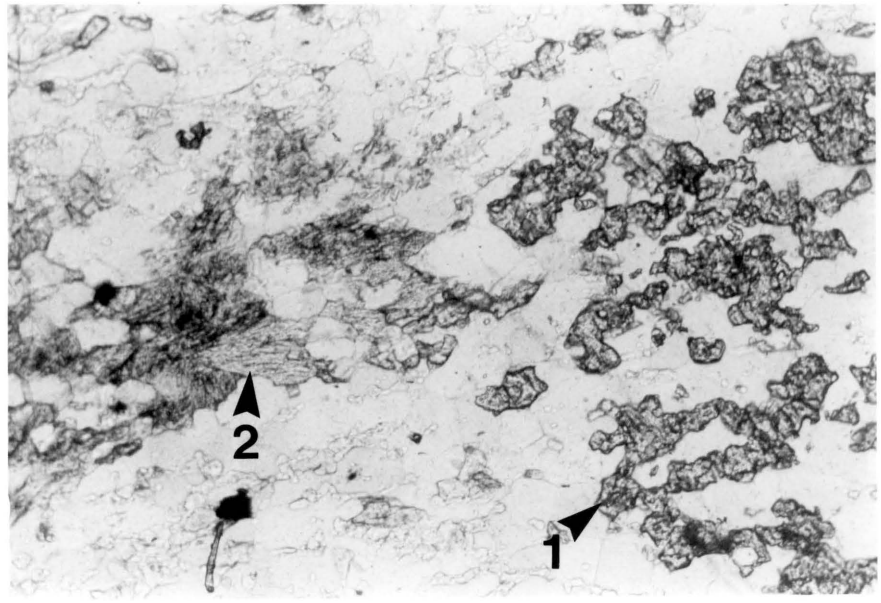
2
1

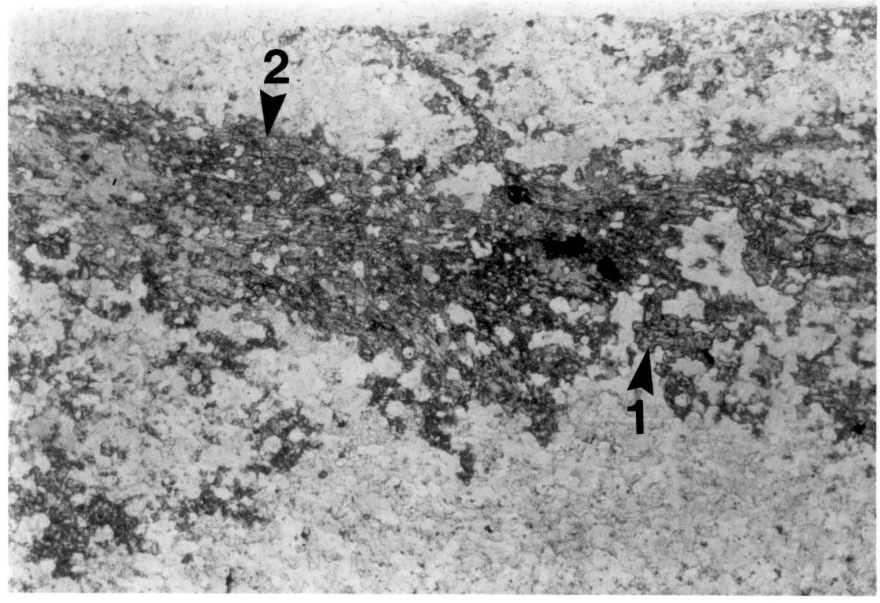
2
1

accessory epidote, muscovite, tourmaline and zircon (Figs. 42 and 43). Pebble samples contain up to 5 percent calcite whereas calc-silicate layers in the Piedra Lumbre Formation include accessory amounts of brown retrograde biotite. The protolith to the calc-silicates contained mainly silica with some carbonate and kaolinite.

Vadito Group and Marquenas Pebble Lithology Pairs

Porphyritic Rhyolite: White and pink porphyritic metarhyolite pebbles with large quartz phenocrysts are common in the Marquenas conglomerate. Quartz phenocrysts are euhedral and exhibit well developed embayments (Fig. 44). Rare feldspar phenocrysts are also present but are highly weathered. Porphyritic metarhyolites analogous to those in the Marquenas conglomerate exist in the Burned Mountain Metarhyolite in the Tusas mountains. The Burned Mountain Metarhyolite also has a characteristic pink coloration and contains large euhedral quartz phenocrysts.

Amphibolite: Rare amphibolite pebbles in the Marquenas Quartzite are matched with amphibolites in the Vadito Group. A petrographic analysis of amphibolite pebbles has not been possible since the pebbles are friable and cannot be extracted from the conglomerate. Based on field observations, hornblende is the dominant mineral phase in both the pebbbles and parent rocks in the Vadito Group with subordinate feldspar. Protoliths to the pebble and Vadito amphibolites were mafic volcanic rocks.

Figure 44: Embayed euhedral quartz phenocryst within rhyolite pebble from Marquenas conglomerate. Width of plate is 5 mm.

The vita has been removed from the scanned document